Curtin University, School of Mines: Minerals, Energy and Chemical Engineering,
26 Dick Perry Avenue,
Kensington, WA 6151, WA, Australia

Novel Approach to Predict and Model Asphaltene Precipitation and Deposition in Multiphase Flow

Sherif Elkahky

This thesis is presented for the Degree of Master of Philosophy
of
Curtin University
2021

DECLARATION OF ACADEMIC INTEGRITY

To the best of my knowledge and belief this thesis contains no material previously published by any other person except where due acknowledgment has been made.
This thesis contains no material which has been accepted for the award of any other degree or diploma in any university.

Signature:
(Sherif Elkahky)
Date:

COPYRIGHT

Signature:
(Sherif Elkahky)
Date:

DEDICATION

First of all, I would like to thank Professor Ahmed Barifcani for his guidance, great support and his kind advice throughout my research. It was real privilege and an honour for me to share of his exceptional scientific knowledge but also of his extraordinary human qualities.

I also would like to thank my co-supervisors Doctor Christopher Lagat and Doctor Mohamed Sarmadivaleh for their constant support, availability, and constructive suggestions, which were determinant for the accomplishment of the work presented in this thesis.

I would like to dedicate my thesis to my Parents for their great support and patience.

To my brother, family, and friends for their prayers and encouragement.

ABSTRACT

One of the well-known problems encountered in oil flow lines, oil reservoirs and completion strings, causing flow assurance issues, is the deposition of asphaltenes in these areas. The complications due to asphaltenes deposition include, but are not limited to, permeability reduction, wettability reversal, pipeline and well plugging, increased pressure drop and an overall reduction in oil production. The problem is not only severe, but it can occur abruptly and damage the reservoir formation in a few days. The tendency for deposition of asphaltene from a given oil can be measured using highly technical and expensive laboratory equipment. In a multiphase flow environment this process involves added complexity and additional costs. The physical and chemical properties of asphaltenes, and the parameters that affect their behaviour, are detailed from an extensive literature research. Despite the extensive historical research material, uncertainties remain concerning the complex nature and controls of asphaltene formation, precipitation and deposition. This research presents multiple mathematical modelling approaches for the prediction of asphaltene deposition and precipitation in crude oil in multiphase flow by the use of governing equations calculated by applying finite difference discretization methods. These numerical models belong to the family of front-capturing-models which permit the capture of the depositing front on a fixed mesh. This research also presents a model for studying the effect of CO_2 on asphaltenes precipitation during enhanced oil recovery operations in a reservoir. The numerical models are validated against each other. Parametric effects on asphaltene deposition from crude oil was modeled and studied against previous experimental values. The numerical models and resulting simulations were in good agreement with the steady-state solution of the asphaltenes onset curve.

PUBLISHED AND ACCEPTED PAPERS:

Publications

1- Sherif Elkahky, Christopher Lagat, Mohammad Sarmadivaleh, Ahmed Barifcani
A comparative study of density estimation of asphaltene structures using group contribution methods and molecular dynamic simulations for an Australian oil field.
The Journal of Petroleum Exploration and Production Technology
https://link.springer.com/article/10.1007/s13202-019-0641-x

2- Sherif Elkahky, Christopher Lagat, Mohammad Sarmadivaleh, Ahmed Barifcani
Prediction of Asphaltenes Deposition in Multiphase Flow Systems Through the Use of Novel Numerical Modelling. Global Journal of Science Frontier Research
https://globaljournals.org/GJSFR_Volume19/E-Journal_GJSFR_(A)_Vol_19_Issue_4.pdf
https://globaljournals.org/GJSFR_Volume19/3-Prediction-of-Asphaltenes-Deposition.pdf

3- Sherif Elkahky, Christopher Lagat, Mohammad Sarmadivaleh, Ahmed Barifcani
A Novel Perception for Scaling Equations of Asphaltene Precipitation within an Australian Crude Oil Field. Industrial Engineering Letters.
https://www.iiste.org/Journals/index.php/IEL

Manuscript Submitted:

4- Sherif Elkahky, Christopher Lagat, Mohammad Sarmadivaleh, Ahmed Barifcani
An Alternate Approach to Asphaltene Precipitation and Deposition Prediction and Mitigation Through the Use of Neural Network
The Journal of Petroleum Exploration and Production Technology
https://link.springer.com/journal/13202

TABLE OF CONTENTS

LIST OF FIGURES

LIST OF TABLES

ABBREVIATIONS

Abbreviation	Description
AAD	Average Absolute Deviation
APE	Asphaltene Phase Envelope
API	American Petroleum Institute gravity
ATM	American Society for Testing and Materials
BBL	Barrel = 158.98 L
CII	Colloidal Instability Index
CMC	Critical Micellar Concentration
CNAC	Critical Nano-Aggregate Concentration
CPA	Cubic Plus Association
DSC	Differential Scanning Calorimetry
EOR	Enhanced Oil Recovery
EOS	Equation of State
FOT	Flocculation Onset Titration
FTIR	Fourier Transform Infrared Spectroscopy
GLR	Gas Liquid Ratio
GPC	Gel Permeation Chromatography
HP	High Pressure
HT	High Temperature
ITC	Isothermal Titration Calorimetry
LLE	Liquid-liquid equilibrium
MAB	Methanol-Acetone-Benzene mixtures
PPM	Parts Per Million (1 ppm = 1 mg/L)
PR	Peng-Robinson
RI	Refractive Index
SAGD	Steam Assisted Gravity Drainage
SANS	Small Angle Neutron Scattering
SARA	Saturates-Aromatics-Resins-Asphaltenes
SAXS	Small Angle X-ray Scattering
SDS	Solid Detection System
SDS	Sodium Dodecyl Sulphate
SEC	Size Exclusion Chromatography
SLE	Solid-Liquid Equilibrium
SRK	Soave-Redlich-Kwong
SPE	Society of Petroleum Engineers
SPECS	In-house PVT software
STO	Stock Tank Oil
TOAM	Thermo Optical Analysis by Microscopy
VAPEX	Vapour Extraction Process
VLE	Vapour-liquid equilibrium

DEFINITIONS

API: American Petroleum Institute, refers to a density scale used in the oil industry to describe the gravity of an oil and helps describing it (from "light" to "heavy").

Asphalt: asphalt is a type of bitumen, a highly viscous liquid that occurs naturally in most crude petroleum. Asphalt can be separated from the other components in crude oil (such as naphtha, gasoline and diesel) by the process of fractional distillation, usually under vacuum conditions.

Asphaltenes: wax-free material found in crude oil, bitumen and coal, operationally defined as being insoluble in n-heptane but soluble in hot benzene.

Bitumen: fraction extractable from a sedimentary rock with organic solvents (Tissot & Welte, 1984). Bitumen is a category of organic liquids which are highly viscous, black, sticky and wholly soluble in carbon disulfide. Asphalt and tar are the most common forms of bitumen.

Component: set of substances or cuts grouped for simulation purposes(Montel, 1994).

Constituent: pure substance which has been identified and subjected to quantitative analysis(Montel, 1994).

Cut: set of substances subjected to global quantitative analysis and presenting identical behaviour in relation to an analysis method(Montel, 1994).

First order transition: a transition in which the molar Gibbs energies or molar Helmholtz energies of the two phases (or chemical potentials of all components in the two phases) are equal at the transition temperature, but their first derivatives with respect to temperature and pressure (for example, specific enthalpy of transition and specific volume) are discontinuous at the transition point, as for two dissimilar phases that coexist and that can be transformed into one another by a change in a field variable such as pressure, temperature, magnetic or electric field(Clark, Hastie, Kihlborg, Metselaar, & Thackeray, 1994).

Flocculation: the process of adding reagents to facilitate the removal of suspended solids and colloidal particles (less than 1 micron). It is used in the final stage of solids liquids separation for large water treatment systems, either via settling, flotation or filtration. The coagulant is the reagent that destabilized the solids and causes them to flocculate (come together and grow till they are heavy enough to sink).

Glass transition: a second-order transition in which a supercooled melt yields, on cooling, a glassy structure. Below the glass-transition temperature the physical properties vary in a manner similar to those of the crystalline phase(Clark et al., 1994).

kerogen: designates the organic constituent of the sedimentary rocks that is neither soluble in aqueous alkaline solvents nor in the common organic solvents. Sometimes, it is used for the total organic matter of sedimentary rocks, but it seems to be a misuse(Tissot & Welte, 1984).

Lyophilic: solvent attraction

Lyophobic: solvent aversion

Maltenes: mixture of the resins and oils obtained as filtrates from the asphaltene precipitation(Simon I Andersen & Speight, 2001).

Oligomer: in chemistry, an oligomer consists of a finite number of monomer units ("oligo" is Greek for "a few"), in contrast to a polymer which, at least in principle, consists of a large number of monomers.

Order-disorder transition: A transition in which the degree of order of the system changes. Three principal types of disordering transitions may be distinguished: (i) positional disordering in a solid, (ii) orientational disordering which may be static or dynamic and (iii) disordering associated with electronic and nuclear spin states (Clark et al., 1994).

Petrology: a field of geology which focuses on the study of rocks and the conditions by which they form. There are three branches of petrology, corresponding to the three types of rocks: igneous, metamorphic, and sedimentary.

Porphyrines: a porphyrin is a heterocyclic macrocycle made from 3 pyrrole subunits and one pyrroline subunit and linked on opposite sides through 4 methine bridges.

Precipitation: the formation of a solid phase within a liquid phase (Clark et al., 1994).

Pyridine: Pyridine C_5H_5N is a simple heterocyclic aromatic organic compound that is structurally related to benzene, with one CH group in the six-membered ring replaced by a nitrogen atom.

Pyrrole: Pyrrole, or pyrrol, is a heterocyclic aromatic organic compound, a five membered ring with the formula C_4H_5N.

Second-order transition: a transition in which a crystal structure undergoes a continuous change and in which the first derivatives of the Gibbs energies (or chemical potentials) are continuous but the second derivatives with respect to temperature and pressure (i.e. heat capacity, thermal expansion, compressibility) are discontinuous (Clark et al., 1994).

Sedimentation: a process by which solid material settles out of a suspension in a liquid medium under the opposing forces of gravitation and buoyancy.

Solvation: when specific chemical forces act between molecules, there is a possibility of complex formation. The complexes cannot be isolated usually but their existence is certain from measurements such as spectroscopic studies. Hydrogen bonding is an example as well as Lewis acid/base interactions. When complexation occurs between molecules that are all from the same component, the phenomenon is called association. When complexation occurs between molecules that are from different components, the phenomenon is called solvation(Elliott & Lira, 1999).

Stacking: in supramolecular chemistry refers to a stacked arrangement of aromatic molecules, which interact through aromatic interactions. The most popular example of a stacked system is found from consecutive base pairs in DNA.

Thiophene: it (C_4H_4S) is a heterocyclic aromatic organic compound. It is aromatic because one of the two lone electron pairs of the sulphur atom contribute to the delocalized pi electron system.

Wax: paraffinic waxes are n-alkanes with n greater than 17.

CHAPTER 1 *Introduction*

There are challenges to flow assurance presented by asphaltene deposition in oil wells producing under multiphase flow conditions. Multiphase flow refers to flow of the fluid in two or more thermodynamic phases. Asphaltene deposition phenomena can commonly occur during oil production in various sections of an oil field's production system, from within the reservoir and inside facilities, such as wellbore tubulars, surface flow lines and processing equipment. Major operational problems can be caused by the sudden precipitation and deposition of asphaltenes. These problems can lead to very adverse economic outcomes.

An understanding of the mechanisms controlling the precipitation and deposition of asphaltenes is, therefore, of great importance in the management of oilfield operations. This research addresses some aspects of these phenomena through computer modelling of well flow conditions within an oil well's production tubing. Extensive literature research was performed to identify the key parameters that impact on and define the behaviour of asphaltenes that occur in petroleum products, viz crude oil. Various operational conditions commonly practiced in the industry are considered.

This research is aimed at providing some remedial solutions through the development of a robust simulation model, having the ability to incorporate multiple key parameters, for the prediction of flow restrictions through the precipitation and subsequent deposition of asphaltenes in the production tubulars.

The literature survey has revealed that very few models have been developed that can predict the asphaltene precipitation in a unified framework and with the flexibility to analyse the flow assurance problems. Most of the currently existing models cannot work in a standalone mode or in combination with a reliable reservoir simulator, for example the ECLIPSE simulator, developed by Schlumberger.

1.1 Research Objectives

The aim of this research project is to discuss and develop simulation methodologies based on actual data obtained from an Australian oil field. Following are some of the important objectives of this dissertation:

- The development of multiphase flow simulation models for pipelines and wellbores with the comprehensive numerical performance analysis of the models.

- Density estimation of flow restrictors, i.e., asphaltenes deposits, by comparative study of molecular dynamic simulation and group contribution models for the specified oil field.

- Prediction of asphaltenes deposition in multiphase flow systems through the use of Novel Numerical Modelling.

- The use and optimization of scaling equations for precipitation of asphaltenes.

- A novel approach to prediction of asphaltenes precipitation and mitigation through the use of neural networks –an innovative technique to genetic algorithm applications.

- Mass percentage predictions of asphaltene under variable conditions and investigation of the impact of CO_2 on asphaltene precipitation in an Australian oil well.

- Development of a fully compositional wellbore numerical model with predicting capabilities to mitigate potential flow assurance problems.

- Comprehensive system analysis of the phase behavior and modelling of asphaltene precipitation.

1.2 Methodology and significance

A significant amount of research has been performed by many researchers into phase behaviour of asphaltene precipitation. The studies also explored the dynamic behaviour of asphaltene depositions under thermodynamic conditions in the oil well. The researchers developed models that are more specific to certain oil field. Opportunities exist for the development of comprehensive asphaltene precipitation models by the use of integrated methods in the simulation of fluid behaviour within reservoirs and wellbores. An aim of this dissertation is to provide a means to reduce the risk of flow reduction of the crude oil, due to asphaltene deposition, through the application of predictive modelling.
The development of the simulation models will incorporate multicomponent, multiphase flow behaviour of crude oil in wellbores while having the capability to integrate with compositional reservoir simulators.
Another significant feature will be the prediction of formation of flow barriers in multiphase flow near the wellbore area. It will also be able to model the well behaviour under different condition such as for enhanced oil recovery by CO_2 flooding.

1.3 Thesis outline and organization

This thesis comprises of ten chapters and one Appendix.

Chapter 1 — Introduction
This chapter provides an introduction of the history, general problems encountered, and proposed solutions regarding asphaltene precipitation and deposition and prevention. This chapter also covers the research objectives and the thesis' structural organisation.

Chapter 2 — Literature review
A comprehensive review and summary of the many aspects of asphaltene precipitation and deposition, structure and formation mechanisms, characterization, solubility parameter, elemental composition, asphaltene molecules, asphaltenes in petroleum, molecular weight, and thermo-physical properties.

Chapter 3 — Existing modelling of asphaltene precipitation
Discussions detail existing simulation models for asphaltene prediction. It presents the models for asphaltene precipitation using cubic equations of state in liquid-liquid equilibrium. Other models include thermodynamic and steric-stabilization model.

Chapter 4 — Wellbore modelling - numerical solutions
Boundary conditions; mathematical solution methods; the fully implicit approach; numerical convergence and robustness of solutions.

Chapter 5 — Prediction of asphaltenes deposition in multiphase flow systems
Materials and methods; assumptions and the development of the mathematical model; effects of CO_2 injection; development of the computational model; effects of CO_2 on asphaltene deposition

Chapter 6 — A comparative study of density estimation of asphaltene structures: using group contribution methods and molecular dynamic simulations for a specific oil field.
Simulations of molecular dynamics conducted to assess the average structure densities representing different asphaltenes in a specific oil field. These simulations assist in predicting the formation of asphaltene structural model.

Chapter 7 — A Novel perception for Scaling Equations of Asphaltene Precipitation within an Australian crude oil Field
This chapter presents the asphaltene precipitation using scaling equations technique. The advantage of scaling equation is its predictive capabilities and simple mathematical formulations that do not need extensive asphaltene properties.

Chapter 8 — Mass percentage predictions of asphaltene under variable conditions and investigation of impact of CO_2 injection on asphaltene precipitation in an Australian oil well
The chapter discusses the the development of computational model based on the Flory–Huggins polymer arrangement hypothesis and solubility concept of Hildebrand. This chapter shows how the calibrated model was able to predict the weight percent of asphaltenes in several different conditions. The predictions were used to recognize the conditions which leads to the precipitation of asphaltene.

Chapter 9 — Novel Approach to Asphaltene Precipitation and Deposition Prediction and Mitigation Through the Use of Neural Network – Innovative Technique to Genetic Algorithm Application
An Alternate Approach to Asphaltene Precipitation and Deposition Prediction and Mitigation Through the Use of Neural Network. Using the fuzzy based neural network technique, asphaltene flocculation in the oil formations during CO_2 flooding was analyzed and simulated.

Chapter 10— Conclusions and future works
The final chapter presents the concluding remarks for the research and development of simulation model.

CHAPTER 2 *Literature review*

The literature review focusses on and highlights important properties and parameters impacting on the understanding of the existence of asphaltenes in crude oil, many of which are input to computer modelling and prediction of their behaviour, which is the objective of this research.

2.1 Definitions for asphaltenes

Asphaltene definition (Montel, 1994): Asphaltenes are non-waxy components found in crude oil, bitumen and coal which are operationally defined (Elliott & Lira, 1999) as being insoluble in n-heptane (n-C_7)while soluble in hot benzene.. This definition (Elliott & Lira, 1999) is well established but researchers (Aquino-Olivos, Andersen, & Lira-Galeana, 2003) have proposed several other definitions. The effect of n-heptane and n-pentane (n-C_5) on asphaltene is shown in the following schematic (after Speight, 1994). Figure 2.1 shows that the n-pentane asphaltenes are less heavy than n-heptane ones.

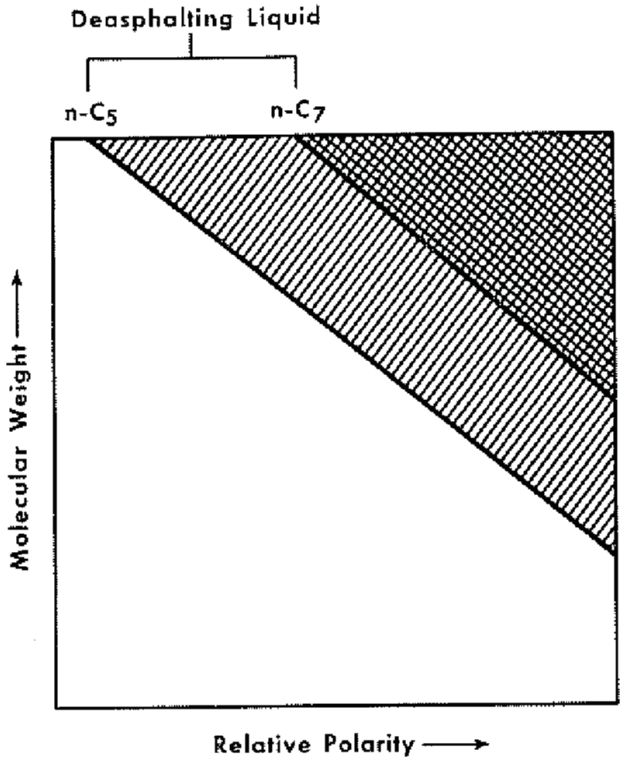

*Figure 2-1: An asphaltene composition representation in terms of polarity and its molecular weight(*J. G. Speight, 1994*).*

Additional to the asphaltenes definition (Montel, 1994), it is also appropriate to define asphaltenes precipitated by n-alkanes under temperature and pressure variations. Studies have shown the differences among the asphaltenes precipitated due to pressure depletion and n-heptane asphaltenes. One such study conducted by Klein et al. (Klein et al., 2006) presented that n-heptane asphaltenes contain lesser oxygen and sulfur concentrations in their structure than n heptane asphaltene formed by pressure depletion. The n-heptane asphaltenes were found to have high concentrations of nitrogen in their networks. The aromaticity of n-heptane asphaltenes was also higher.

Research carried out by Aquino-Olivos et al. (Aquino-Olivos, Andersen, & Lira-Galeana, 2003) showed some differences in asphaltenes. One crude oil sample was selected for size exclusion chromatography (SEC) of standard asphaltenes and live-oil derived asphaltenes precipitated during atmospheric titration. The results showed that standard asphaltenes had larger hydrodynamic volume and broader

distribution than live oil asphaltenes. The Fourier Transform Infrared Spectroscopy (FTIR) tests showed significant differences in the structure of asphaltenes obtained at high-pressure filter and standard asphaltenes. The latter was found comprising of less functional groups and be more saturated.
Conclusively, the literature survey evaluated the composition of asphaltene changes by varying the precipitation method. However, the initial definition provided in this dissertation remains widely prevalent. Appendix-A describes the n-heptane asphaltenes obtained from dead-oils. These are also used for the present research.
Researchers have worked on the fractional separation of crude oil. The conventional SARA (Saturates, Aromatics, Resins, Asphaltenes) separation, the preliminary de-asphalting of crude oil is done while separating the soluble portion into resins, saturates and aromatics. During SARA separation, problems arises due to two factors , the inherent cross-contamination and the non-standardization of reported results from different laboratories(Bissada, Szymczyk, & Nolte, 2003). In one of the studies conducted by Andersen et al.(Simon I Andersen & Speight, 2001), it was found that there are large differences in the results for asphaltene yields and other analysis for the set of crude oil under consideration. The results show a deviation factor as high as 254. Such variations in laboratory results make it difficult to confidently model the asphaltene precipitation even if the experimental data is available. The reliability of the results is still in question whether the asphaltenes are formed under depressurization, or due to the injection of gases such as CO_2, for enhanced oil recovery.

2.2 Asphaltene origin and formation

The origin of asphaltenes in crude oil was initially suggested by Tissot and Welte (Tissot & Welte, 1984). A more recent study was carried out by Craddock et al. (Craddock, Bake, & Pomerantz, 2018) where they evaluated the chemical, molecular and microstructural evolution of kerogen during thermal maturation. In a similar study, a detailed description of the structure of kerogen was discussed which reveals the formation of these compounds (Burnham, 2017). It is proposed that structural formation of kerogen (part of naturally occurring organic matter that is insoluble in organic solvents) was due to burial of the organic material in sedimentary rocks under elevated temperature and pressure conditions. The increased temperature in absence of air leads to the formation of several hydrocarbons along with an initial formation of bitumen. The authors, mentioned above, proposed the molecular structure of kerogen as the alkyl chain attached with cyclic nuclei which are linked with aliphatic chains by hetero-atomic bonds. The thermodynamic conditions underground changes with time, thus the initial structure that was once in equilibrium with the oil, moves out of equilibrium. The structural rearrangement of the molecules produces a more ordered carbon structure and increased aromaticity. Under such conditions, theoretically the most stable structure is graphite, however, it is not formed in non-metamorphosed sediments. The progressive development of building blocks of kerogen results in parallel sheets aromatic compounds.
The second stage is termed as diagenesis, where the bonds between heteroatoms, particularly oxygen, are broken to produce volatile components such as carbon dioxide and water. As a result of this breakdown, other smaller structures comprise aliphatic chains and bound nuclei. Other compounds have larger networks, while lesser molecular weights become soluble in oil with increased temperature and pressure. These soluble compounds are asphaltenes. Tissot and Welte (Tissot & Welte, 1984) termed the Acetone-Methanol-Benzene mixtures as asphaltene compounds. These compounds have certain properties: they are more polar, and heavier compared to the asphaltenes recovered from certain solvents such as chloroform. There are relatively greater amounts of asphaltenes and resins (heteroatoms) in the crude oil in the diagenesis stage.

The third stage of formation is termed catagenesis, where the temperature is higher, and bonds like esters and some carbon-to-carbon start to break. The breaking of bonds occurs within the kerogen and other smaller fragments generated during the diagenesis stage. Oxygen is liberated during the bond breakages, and the resultant compounds lack oxygen. Hydrocarbons start forming, which is the first stage of crude oil formation leading to wet gas and the generation of condensates (Kontorovich et al., 2019).

During the final stages, the liquefied product produces seeps down through the sedimentary rocks and reaches the bottom part of the sedimentary basin. At this depth, the hydrocarbons are subjected to a further increase in temperature and pressure. This results in the cracking of larger carbon chains in bitumen and kerogen. Furthermore, the aliphatic compounds disappear in this stage, leading to the formation of dry gas.

In these stages, the poly-condensation and aromatization of the remaining kerogen occur. Further changes in temperature pressure conditions do not affect the structure, and no new hydrocarbons are formed. This stage is known as metagenesis. Some non-hydrocarbon gases are also produced. These gases can include hydrogen sulfide and nitrogen. These gases are mostly associated with light hydrocarbons and methane. Large amounts of hydrogen sulfides may be producing due to the thermal cracking of sulfur compounds in crude oil and the trapped molecules within kerogen. Both nitrogen and hydrogen sulfide gases have been related to asphaltene instability and thus have an important research value.

Figure 2.2 depicts of crude oil and hydrocarbon development during different stages.

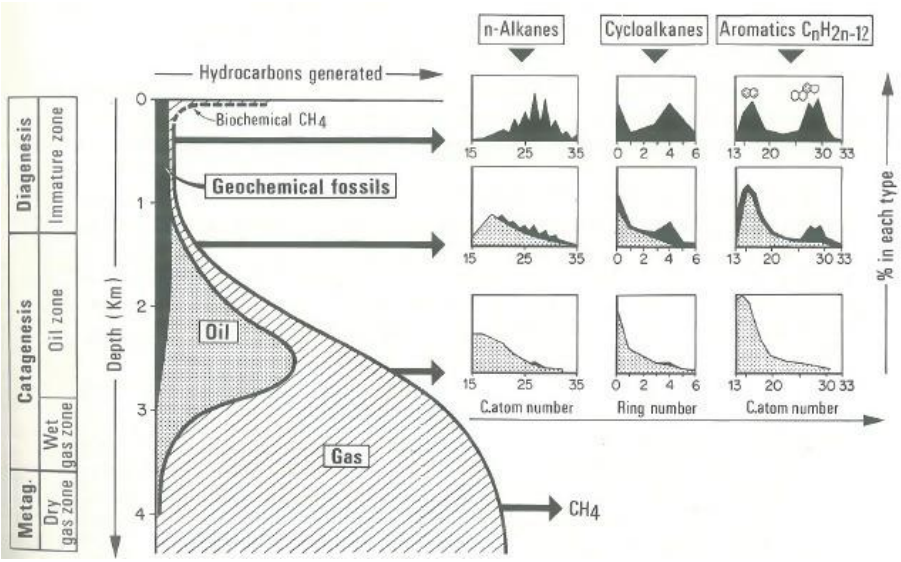

*Figure 2-2: Crude oil and hydrocarbon development under three different stages(*Tissot & Welte, 1984*)*

A question can be raised as to which of the oils may contain asphaltenes? The researchers have developed the ternary diagram, which shows the composition of six division of crude oils. The diagram indicates that degraded crude oils have a greater tendency to contain asphaltene fractions. In the first stage, the biodegradation results in the removal of alkanes. As a result of this process the composition of aromatic compounds increases. Heavily degraded oil may comprise 20% to 60% of asphaltene fractions. The paraffinic oils are higher quality and may contain only 10% or less asphaltenes. The aromatic intermediate oil may have 10 to 40% of asphaltene fractions. The details are shown in Figure 2.3

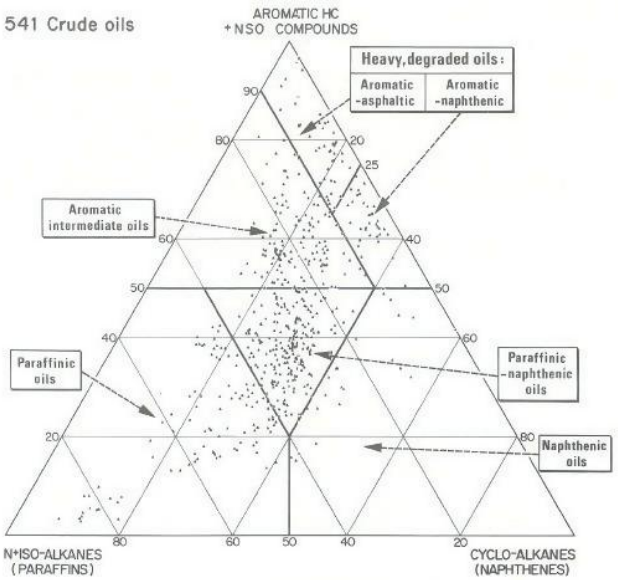

*Figure 2-3 The "Ternary diagram" depicting the six divisions of crude oils based on their composition from 541 oil fields(*Tissot & Welte, 1984*)*

Asphaltene problems have been found in some cases where there was zero asphaltene present initially in the crude oil. This phenomenon was reported by Andersen et al. (Simon I Andersen & Speight, 2001). The initial presence of asphaltenes in crude oils may not be the confirmation of asphaltene formation during oil drilling and extraction. Some asphaltene rich oils are found to be very stable and no asphaltene precipitation occurs. In some cases, the concentration of mere 20 to 50 ppm of asphaltenes in the crude oil caused the flow assurance problems. These apparent anomalies lead to the need for further studying of the characteristics of asphaltenes.

2.3 Asphaltene characterization

Characterization of asphaltenes is problematic due to the change in composition during extraction with changes in temperature, pressure and other thermodynamic conditions. The validity of results is subjective. Researchers have proposed that reliable results about asphaltene prediction behaviors can only be obtained if the samples are subjected and analyzed under the conditions identical to that inside the formation. The following sections describe properties of asphaltenes :

2.3.1 Solubility parameter of asphaltenes

Asphaltenes are the compounds which show solubility in certain solvents. This property places them under different solubility classes where the compounds with similar solubility parameters are miscible in each other. Figure 2.4 represents the distribution of asphaltenes in terms of its solubility in different solvents.

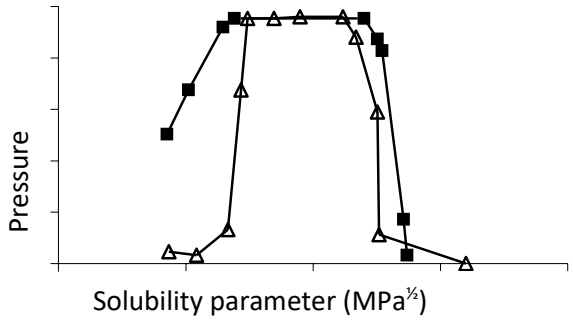

*Figure 2-4: Solubility limit graph from an asphalt (▪) and its related asphaltenes (Δ)(*Chilingarian & Yen, 1994*).*

In order to measure the solubility parameters of asphaltenes in the solvents, it is necessary to extract it from the crude oil at laboratory conditions. The literature places significant importance on the solubility parameter of the asphaltenes. The phase behaviour of asphaltenes is studied and modelled under the regular solution theory.

The solubility parameters of asphaltenes are between 19 to 22 $MPa^{1/2}$ (Simon I Andersen & Speight, 1999). There is a contradiction of these values with the theoretical values found by using a group contribution method. The values depending on molar weight are found to be between 23.1 to 26.4 $MPa^{1/2}$. Further details are disused in subsequent chapters in this dissertation.

2.3.2 Elemental composition of asphaltenes

The elemental composition of asphaltene is important because it provide the details about hydrogen to carbon ratio, and the weight percent of many other elements that affects the asphaltene formation. When determining the elemental composition, the choices of precipitant and procedures are very important. For example, the hydrogen to carbon ratio of pentane precipitate is much higher than the n-heptane. It means that n-heptane has more aromatic structure. The differences in elemental composition and structures is also evident from other ratios such as nitrogen to carbon, sulfur to carbon and oxygen to carbon. It is evident from literature that the asphaltenes contain the largest percentage of organometallic compounds i.e. Fe, V, Ni and heteroatoms i.e. O, N & S.

Table 2. 1 shows the composition of elements and hydrocarbon ratio in n-heptane asphaltenes. In the table J_a is the ratio of aromatic chains to the total number of carbons in the structure.

*Table 2. 1: n-heptane composition table (*Cimino, Correra, Del Bianco, & Lockhart, 1995*)*

Hydrogen to Carbon ratio	N (wt. %)	S (wt. %)	O (wt. %)	j_a
0.8 – 1.4	0.6 – 2.6	0.5 – 10.0	0.3 – 4.8	0.45 – 0.70

The heteroatoms behave like the polar functional groups. In asphaltene molecule sulphur occurs as oxides (Cimino et al., 1995) or in theophanic aliphatic structures. Nitrogen in asphaltenes occurs as pyridinic or pyrrolic form. Oxygen is present in the acidic form as phenolic or carboxylic acid(J. Speight & Plancher, 1991). It also exists as ketones. Asphaltenes contains metals mostly in the form of porphyritic form(Cimino et al., 1995).

2.3.3 Asphaltene molecule structures

Researchers have proposed two structure to depict the asphaltene molecules. Figure 2.5 (A) shows asphaltene molecule that comprises of a large central aromatic area having small alkyl chains near periphery i.e. continental structure. Figure 2.5 (B) shows a structure that consists of smaller aromatic areas connected by bridging alkanes i.e., archipelago structure. The aforementioned types of asphaltenes based on their structure states the nature of asphaltene self-association as following (Yarranton, 2005):

The presence of larger aromatic cores in asphaltene molecules results in π-π bond linkage for the colloidal stacks.

The self-association resemble the polymer structures for the aromatic structures in the asphaltene molecules if they are dispersed and small. Many bonds can be present between such structures including hydrogen bonding, ac-dbase and π-π bond linkages. The cluster structure in this case can be considered as macromolecules. These macromolecules are present in the solution in the disperse form. There is also the possibility that resins present in the solution result in aggregation.

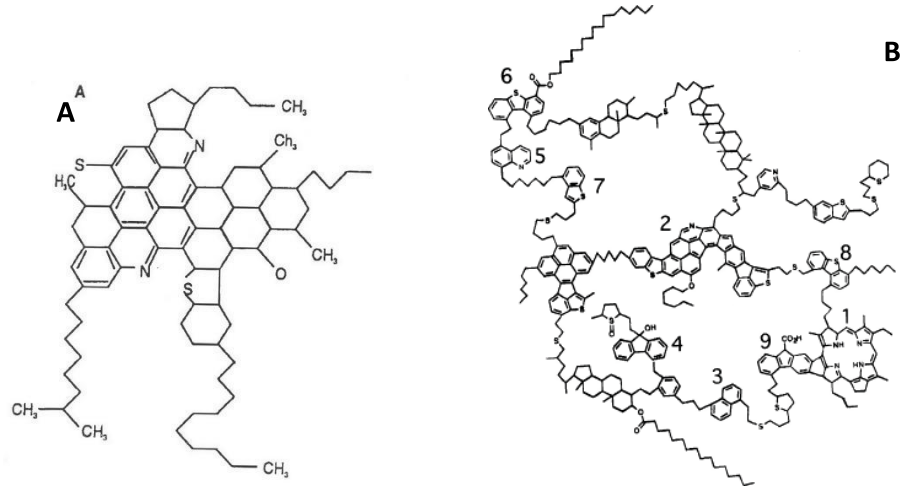

*Figure 2-5: Asphaltene structures: (A) Continental structure (*J. G. Speight & Moschopedis, 1981*) and (B)-Archipelago structure (*Juan Murgich, Abanero, & Strausz, 1999*)*

of asphaltene molecular models requires many approximations. The approximations should be carefully selected, and the models must be fed with the data with great caution. The studies have

found that the molecular mechanics calculations provide semi-quantitative results(J Murgich, 2005).

2.3.4 State of asphaltenes in petroleum

Most of the studies have considered the state of asphaltene in crude oil in the form of colloidal molecules. However, a few studies mentioned two different states for presence of asphaltenes in crude oil. According to one theory it is stated that the asphaltenes are present in the crude oil in dispersed form. While the other theory states that the asphaltenes are dispersed as colloids in the crude oil while stabilized by the presence of resins. The early stages of asphaltene formation is understood by considering colloidal models(Sirota, 2005). The transient concentrations and changing characteristics of multi-component single phase solution explains the scattering data of the asphaltenes during phase separation.

2.3.5 Molecular weight of asphaltenes

The diversity of asphaltene molecular structure has been observed during early periods of research: "the estimation of the molecular weight of asphaltenes gives widely varying results according to the method employed. With the cryoscopic methods value ranging from 2000 to 30,000 g/mol are found"(Eilers, 1949). Recent research, however, has proposed that asphaltene monomers are smaller in size and their molecular weight cannot exceed 1000 g/mol(Porte, Zhou, & Lazzeri, 2003). Most of the studies considered the molecular weights at the aggregation stage, when the molecular weight of colloidal molecules has already increased.

Another method to find the molecular size is based on high resolution mass spectrometry which can provide accurate estimations of composition of fractions as well as mass distribution in the molecule. The data generated from this technique can be used to estimate the size of the asphaltene molecule and its molecular weight. Modelling techniques can further strengthen the accuracy of results.

2.3.6 Thermo physical properties

Thermo physical properties are related to the thermal conductivity, thermal expansion, specific heat capacity, heat of vaporization and coefficient of linear thermal expansion. The literature survey revealed little work done in this field for asphaltenes. Most of the studies considered density and solubility of asphaltenes as the fundamental properties. These properties were found by molecular simulations or by conducting laboratory experiments. Density of asphaltenes is measured using pycnometer (device to measure density of solids and gases). The density of asphaltenes is usually found to be 1.17 to 1.52 Kg/m^3. It was revealed in one of the studies that density of asphaltenes is directly related to the ratio of hydrogen to carbon in the molecule(Rogel & Carbognani, 2003). It was also reported in the study that the unstable crude oils contain asphaltenes with higher aromaticity, lower hydrogen to carbon ratio and higher densities as compared to asphaltenes obtained from stable crude oils.

Thermo-physical properties were found in one of the studies which used molecular dynamic simulations. The study of properties includes heat capacity, molar volumes, thermal expansion and solubility. In one study dielectric properties of asphaltenes were investigated. The author determined the static values of electric conductivity for different asphaltenes. The dielectric constant was found to be in the range of 2.48 to 2.71 at a temperature of 298.15K. The dipole movement were found to be in between 2 to 20D.

.

2.4 Asphaltenes and aggregation

The aggregation properties include interaction of asphaltene with resins, flocculation, self-association and precipitation.
"A most important physical property of colloidal dispersions is the tendency of the particles to aggregate. Encounters between particles dispersed in liquid media occur frequently and the stability of a dispersion is determined by the interaction between the particles during these encounters. The overall situation is often very complicated"(D. Shaw, 1992).
The process of aggregation affects asphaltenes at many levels:
At the first stage, self- association by means of hydrogen bonding takes place among asphaltene monomers, forming "macro-molecules".
Secondly, dispersion force operates between these "macro-molecules" and flocculation and precipitation occur as a result of aggregation of these "macro-molecules".

The process of aggregation begins at quite low concentrations as shown by measurements of "Vapor Pressure Osmometry" (VPO) and "Isothermal Titration Calorimetry" (ITC) (Merino-Garcia & Andersen, 2004; Wiehe, Yarranton, Akbarzadeh, Rahimi, & Teclemariam, 2005). Moreover, the strong driving force of aggregation makes it almost impossible to study monomers. It was also concluded in recent paper by Porte et al.(Porte et al., 2003), stating that "if the aggregation was driven by weak dispersion forces, the aggregates in solution would coexist with a noticeable concentration of free single molecules. […] Aggregation is induced by strong specific interactions (hydrogen bonds, for instance)". Merino-Garcia (Merino-Garcia & Andersen, 2004) performed calorimetry and showed that aggregation of asphaltenes in toluene solutions starts below 34 ppm. Andreatta et al. (Andreatta, Bostrom, & Mullins, 2005)showed that the CNAC value (Critical Nano-Aggregate Concentration) for asphaltenes in toluene was around 100 ppm by performing high-Q ultrasonic measurements. Consequently, the asphaltene properties are actually the properties of aggregates, as it is clearly indicated by VPO measurements that the aggregation starts even below 100 ppm(Wiehe et al., 2005). The standard solutions were prepared and measurements of all the VPO's were taken. The standard solutions were made by using toluene as a solvent instead of crude oil. The reason to use toluene is because the crude oil may contain several compounds that may affect the valuation or detection of any variations. This has previously been observed by Merino-Garcia (Merino-Garcia & Andersen, 2003) who found the energies of interaction by using a step wise crystal growth method. The molecular weight of asphaltene was assumed i.e., 1000g/mol. The energies of interactions found by this method were quite low i.e. -0.6 to -7.5 kJ/mol. Moreover, if the number of compounds is present, they will also affect the detection of self-association phenomenon of asphaltenes. In another study carried out by Merino-Garcia(Merino-Garcia & Andersen, 2004), it was found that some fractions of asphaltenes can be inactive which might be the cause of low energy of interaction. A SEC analysis of toluene-heptane carried out in a study shows that presence of inactive fractions of asphaltene during self-association. The study of Marino-Garcia suggests that asphaltene-asphaltene interaction was highly noticeable compared to the interaction between asphaltene and toluene. This reason was also made the basis for justifying the lower energy of interaction. Conclusively it can be said that the presence of hydrogen bonding even at very low concentrations.

2.4.1 The aggregation phenomenon and Van der Waals forces

It has been determined that the accumulation of asphaltenes in the crude oil was due to the distribution forces acting during changes in temperature and pressure conditions (Juan Murgich,

2002). Others (Moschopedis & Speight, 1976) found that the flocculation and deposition of asphaltenes was caused by self-association forces.

Induction forces:The induction forces account for maximum of only 7% of the total forces present (Kontogeorgis et al., 2006). This is considered very small as the asphaltenes are chargeless particles. A minute fraction present in the asphaltenes might be carrying charge resulting in the detection of induction forces.

Electrostatic forces: Although the asphaltenes are chargeless particles there are several methods which can characterize the molecular charge distribution in the asphaltenes. One such method is known as "multi-polar expansion" (Israelachvili, 1992). This expansion incorporates a single pole which represents the overall charge. This is further supplemented with a dipole, quad-pole and higher multi-poles. The polarity of a molecule can be easily calculated gauging the dipole movements. A study signifies the polar forces for when the movement is higher than 1D(Kontogeorgis et al., 2006). Some other studies signified these values between 2D and 20D for the state of accumulation(Pedersen & Andersen, 2000). Another study suggests that the polar forces are significant for dipole movement between 2.5D to 5D(Paul Maruska & Rao, 1987). The study carried out by Pedersen [34]shows a strong relationship between polarity of toluene solutions and asphaltene production stability. It was found that the polarity of asphaltenes from unstable crude oil was higher than the ones obtained with minimal asphaltene precipitation issue. This leads to the conclusion that not only distribution forces are responsible for the flocculation and deposition of asphaltenes, but the electrostatic forces also have a significant effect on the aforementioned phenomenon.

2.5 The Effect of hydrogen bonding on flocculation and deposition

The effects of the presence of hydrogen bonding has been investigated in number of studies. Moschopedis (Moschopedis & Speight, 1976) found that the asphaltene fractions of a very heavy crude oil formation (Athabasa) involves in the hydrogen bonding interactions. Another study investigated the effect of presence of hydrogen bonding between asphaltenes and resins on flocculation and deposition (Merino-Garcia & Andersen, 2003). This study used chemically modified asphaltenes for testing. A study focused on the enthalpy of interaction of methylated asphaltenes found that enthalpy was reduced up to 46%, also, the self-association of asphaltenes was reduced by methylation of the asphaltene molecules as shown in figure 2.6

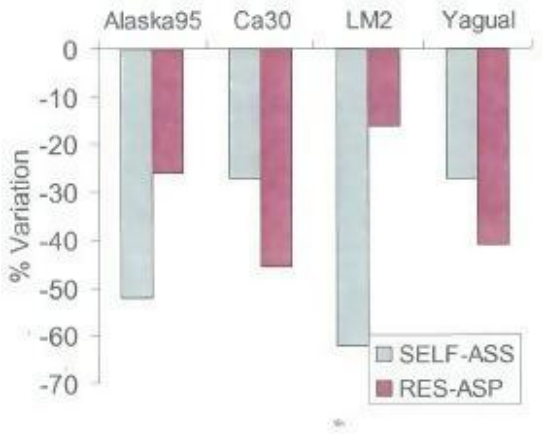

*Figure 22-6: Comparison of asphaltene methylation effects in self-association and interaction with resins(*Merino-Garcia & Andersen, 2003*)*

Initially it was believed that the asphaltene flocculation and deposition is facilitated by the hydrogen bonding because it is a cohesive force which destabilizes the crude oil solution containing asphaltene molecules. However, some studies proposed that removal of hydrogen bonding (by chemically treating the asphaltenes) result in the destabilization of toluene testing solutions (Juyal, Merino-Garcia, & Andersen, 2005; Merino-Garcia & Andersen, 2004). The reason behind this phenomenon is explained by the fact that when hydrogen bonding is removed, the resultant cohesive forces are also removed. As a result, there are less chances of accumulation and deposition of asphaltene molecules. The next question arises is whether the removal of hydrogen bonding has any effect on the asphaltene-resin interaction? This might be the reason for the decreased stability of the solution.

Another kind of charge transfer interaction is the transfer between the aromatic rings and π-orbitals. This interaction between the asphaltene molecules results in the formation of stacks. Yen and Coworkers proposed the model of stacked layers of asphaltene molecules which is yet not fully validated because of the steric effect caused by alkyl branches reducing the probability of stacking asphaltene molecule sheets. In another study, it was found that a very limited interaction takes place between the asphaltene molecules which are stacked between aromatic sheets. It is proposed, after the literature review, that staking is one proposed model for asphaltene accumulation, however, other reliable asphaltene association schemes must be considered to fully understand the flocculation and deposition phenomenon.

In one study, the stability of the solution was linked with the velocity of electron transfer between liquid organic phase and organic solid particles(Siffert, Eleli-Letsango, Jada, & Papirer, 1994). It was concluded in their experimentation that stability of suspension increased with the intense electron transfer i.e. higher charge differences. The electron transfer results in a repulsive interaction which reduces the cohesive forces and bring stability in the solution.

From the reviewed literature it can be concluded that accumulation of asphaltene molecules is mainly caused by interactive forces including hydrogen bonding, stacking polar forces and dispersion forces etc. An important point is that the literature provided qualitative information regarding asphaltene flocculation and deposition. This was stated by Prausnitz et al. (Prausnitz, Lichtenthaler, & de Azevedo, 1999): “we must recognize at the outset that our understanding of intermolecular forces is far from complete and that quantitative results have been obtained for only simple and idealized models of real matters”. In the experimentation and observations, it is clear that asphaltenes are not idealized and simple molecules.

2.6 Investigating Critical Micellar Concentration (CMC) and asphaltene aggregation

A micellar is an agglomerate consisting of simple amphipathic molecules formed at a certain concentration. This concentration is known as critical micellar concentration. This phenomenon was found in the literature related to surface tension (Rogacheva, Rimaev, Gubaidullin, & Khakimov, 1980; Rogel, Leon, Torres, & Espidel, 2000) and calorimetry(Simon Ivar Andersen & Birdi, 1991). The concept of micellar concentration can be used to further elaborate the asphaltene aggregation.

The effect of CMC values on the size of asphaltene aggregate was studied by (Roux, Broseta, & Demé, 2001)where they found a change in aggregate size for asphaltene higher volume fractions above 4%. The CMC value at this change was between 2 to 4 g/L. Similar results were reported by Ravey et al. (Ravey & Stébé, 1989)where small angle neutron scattering data changed with the increase in weight fraction of asphaltenes i.e. above 2.3%. Although the results are similar in magnitude, however, they cannot be attributed to CMC. Another theory proposes that the change in agglomeration size of asphaltene is due to interpenetration of agglomerates themselves. It is obvious that increased concentration will result in reduced spaced between the asphaltene aggregates. The many energies

play their part and makes the reduced distance an unfavorable situation. This results in change in size of agglomerates. The structures under these forces and increased concentration first forms the micelles which are converted to long cylinders and finally into big liposomes. The presence of surfactants further enhances the size enlargement phenomenon of asphaltene molecules.

Reviewing all the relevant literature the question is which the most reliable phenomenon that answers the change in aggregate size at the CMC values of 2 to 4 g/L? Andretta et al. (Andreatta et al., 2005)proposed that in solutions where the values of critical nano-aggregate concentration is much lower than the reported CMC values, asphaltene aggregate sizes are maximum. The following discussion further elaborates the effects of CMC values of asphaltene and thus negates the previous phenomenon.

a. There was no significant change noted in the slope created between log asphaltene concentration and plot of interfacial tension.

b. The presence of water on CMC values was studied by Andersen et al.(Simon I Andersen & Speight, 2001). Water disturbs the self-association of asphaltene molecules by severely affecting the CMC values.

c. The curve assigned to CMC was broken by the addition of resins.

It can be concluded that self-association between the asphaltene molecules is more certain phenomenon when compared to micellization process. Furthermore, the studies conclude that asphaltene is not the sole reason for measured CMC values.

2.7 Infinite self-association

The infinite self-association between the asphaltene molecules was studied by measuring the small-angle neutron scattering measurements using toluene as the solvent and changing the concentration of asphaltenes. The aggregation number of 100 was noted because of the stable molecular weights i.e. 0.3 to 4% volume based near the value of 10^5 g/mol. It was observed that molecular weights start decreasing with the increase in concentration above 4%. Repulsive forces are found accountable for this phenomenon. These repulsive forces exists between the aggregates(Roux et al., 2001).

Prausnitz et al. (Prausnitz et al., 1999) proposed the presence of chemical forces that are causing the self-association behavior. When the saturation levels are increased, the covalent bonds become active. Further saturation starts when two hydrogen atoms comes close to form the hydrogen gas i.e., H_2. The research is supported by the fact that when other elements such as argon atoms comes together, they don't form a molecule.

Further literature survey revealed that it is not only the saturation of chemical forces playing their part in self-association but also the morphological structure of the asphaltene aggregates(Porte et al., 2003). The scattering data initially provides the dimension of asphaltene aggregates. Under such circumstances, it is highly unlikely for a structure to remain stable and fractal because the dimension 2 structure will irreversibly precipitate. The force that inhibits the infinite aggregation is high bending flexibility of single molecular sheets. These bendable sheets cover up the aggregate and thus prevent infinite aggregation of vesicles. The study, however, was not able to prove this theoretical model.

The finite aggregate sizes can be further explained by a phenomenon called steric hindrance. Steric hindrance is the phenomenon that changes the reaction selectivity or speed by altering the shapes and structures of the molecules. Steric hindrance does not involve chemical bonding. This phenomenon, however, is advocated as small factor in size of asphaltene aggregate. Another study proposed that presence of alkyl chains in the crude oil causes the steric hindrance in asphaltene formation. The alkyl chains control the number of sheets for each asphaltene aggregate.

2.8 Presence of resins and their effect on asphaltene formation

Generally, the separation processes distinguish the asphaltenes and resins from each other. However, a number of methods exist by which asphaltenes and resins can be prepared with slight differences in their compositions. Using propane for the precipitation separates the asphaltenes and resins from the crude oil. Further, mutual separation of asphaltene and resins is accomplished by using n-heptane and n-pentane. It has been observed that the size of aromatic rings is smaller in resins. Similarly, the size of alkyl chains is longer. This makes the resins more soluble in aliphatic solvents. The molecular weights of the resins is determined using Vapor phase osmometry methods. The molecular weight results for the resins was found to be in between 650 t0 950 g/mol (J. G. Speight, 1999). The other studies have stated that both the resins and asphaltenes are long chains of poly-aromatic hydrocarbons. The solubility of each poly-aromatic hydrocarbon is different from other depending upon the size and shape of the molecule (Porte et al., 2003).

The effect of presence of resins on the asphaltene was also discovered by Pfeiffer and Saal (Pfeiffer & Saal, 1940)where they found that resins cause the dispersion of asphaltene molecules. The hydrogen bonding has more effect in the interaction between asphaltenes and resins when compared to self-association phenomenon. The presence of these forces keeps the molecules in suspension. The proposed structure is of micellar kind where the central asphaltene molecule is surrounded by several interacting resins. These resins are further surrounded by aromatic hydrocarbon chains. This onion kind of overlapping and wrapping of asphaltene continues throughout the crude oil because of the excess presence of saturated hydrocarbons(Tissot & Welte, 1984).

The earlier discussions have already stated that this kind of model is theoretically limited. However, the experimental results have already demonstrated the stabilizing effect of resins as shown in figure 2.7. It can be seen from the figure that resins are responsible for retardation the initial flocculation point (Al-Sahhaf, Fahim, & Elkilani, 2002; Hammami, Phelps, Monger-McClure, & Little, 2000). The dispersing power of resins is significant. For instance dispersing power of 1 cubic centime of resin is equivalent to 105 cm^3 of benzene (Hotier & Robin, 1983).

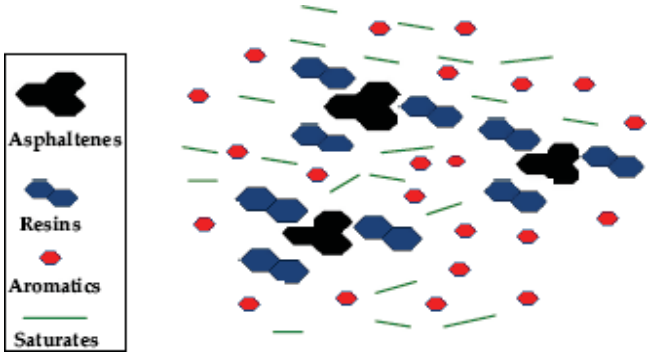

Figure 2-7: Presence of resins and their effect on asphaltenes(Merino-Garcia & Andersen, 2003).

In another set of studies the heat of interaction was studied for different crude oil which was helpful in studying the interaction between asphaltenes and resins(Merino-Garcia & Andersen, 2003). The heat of interactions was different ranging between -1.7 to -3.9 kJ/mol depending upon the concentration of asphaltenes and nature of crude oil. It has been found that heat of interaction is less than that of heat of hydrogen bonding while it is near to that of van der waals forces. It was thus concluded in the study that interactions of resins with asphaltenes is due to van der Waals forces, exchange repulsion forces and charge transfer(Juan Murgich et al., 1999).

The study of methylated asphaltenes inferred that there is lower of heat of interaction due to resins. They methylation causes low heat of interactions because of involvement of hydrogen bonding. Moreover, it is assessed that not all the resin interacts with asphaltenes but a fraction only.

2.9 Colloidal stability, flocculation and precipitation

This section gives a brief discussion on the difference between flocculation and precipitation. It will also cover the fundamental colloid stability theory and properties of asphaltene molecules during precipitation.

Flocculation can be considered as the initial stage where aggregates are formed. These aggregates are molecular in size and forces on attraction and repulsion works on then. The interaction of these aggregates results in the formation of super aggregates. Flocculation cannot be considered as a phase transitioning phenomenon. Instead, it is taken as colloidal stability of colloids. There is no relation with solubility and thermodynamics at this stage. The molecules are in suspended state in the solution.

Precipitation starts when interaction between the asphaltene molecules increases and the size of super aggregates increases. The increase in size of super aggregates make them heavier thus overcoming the Brownian force. These aggregates separate from the solution phase. The phase separation of asphaltenes can now be represented in terms of solubility. The following section is dedicated to phase separation behavior of the asphaltenes

2.9.1 Colloid stability theory

The literature has divided the colloids into two types(Cooper, Dubin, Kayitmazer, & Turksen, 2005):

- *Lyophilic* (solvent attracted)
    - Such colloids can be easily dispersed in the solution by use of a suitable dispersant.
    - The formation of such colloids is negative and are considered stable.
- *Lyophobic*, (solvent repellant)
    - These types of colloids cannot be dispersed using chemical means. They need vigorous mechanical action and shear agitation to properly disperse.
    - These colloids are metastable due to stabilization of charge (result of surface charges). These colloids are thermodynamically unstable.

The colloids are present in a solution. The stability of these colloids is dependent upon the strength of attractive and repulsive forces. If the forces of repulsion are higher the particles will remain in dispersed state. Conversely, if the forces of attraction are stronger, the colliding colloids will stick together to form an aggregate. The literature provided enough evidence about the cause of aggregation i.e., van der Waals forces present between the molecules. These forces can act from considerable molecular distances. In order to neutralize these force and equal and opposite force is required otherwise the colloid stability will be affected resulting in aggregate formation. One study proposed that the electrostatic forces and steric stabilization as to counter the van der Waal forces. Steric stabilization is the method that involves addition of certain water phyllic polymers to inhibit coagulation.

By considering just the electrostatic force as the counter measures to van der Waals force, the sum of attractive forces, potential energy and repulsive forces equates the total interaction energy. Figure 2.8 shows the total interaction energy curve. VR is repulsive force; VA is attractive force.

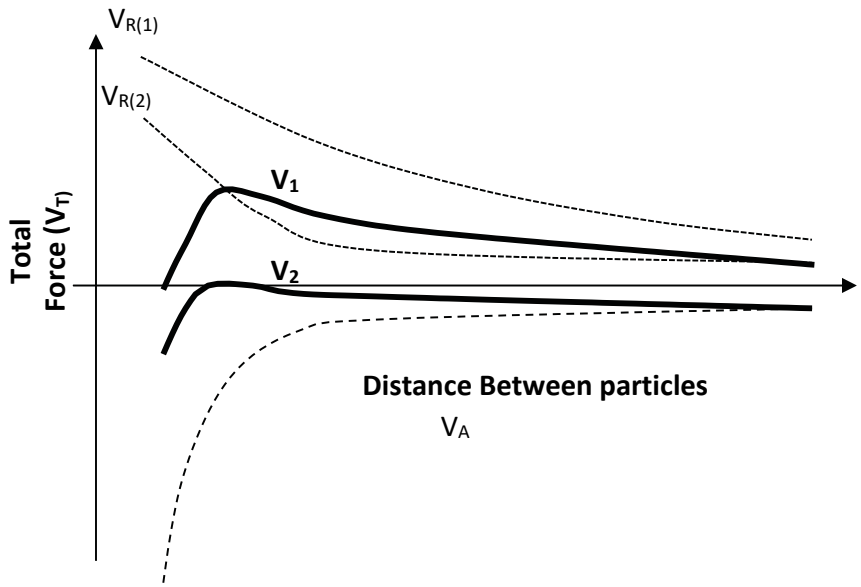

Figure 2-8: Total interaction energy curve (from Shaw,(D. Shaw, 1992; D. J. Shaw, 1980))

2.9.2 Thermal energy

The stability of a system depends upon the relationship between thermal energy and the internal potential energy. For a system to be stable, the thermal energy (kT) must be less than that of internal maximum potential energy. As can be seen from figure 2.8, the curve V_1 represents a stable system in comparison with the curve V_2. As mentioned earlier, the role of steric stabilization cannot be ignored specially when there is an adsorption of bigger molecules. Quoting the author, "The adsorbed layers between the particles may interpenetrate and give a local increase in the concentration of polymer segments. Depending on the balance between polymer-polymer and polymer-dispersion medium interactions, this may lead to either repulsion or attraction. If the dispersion medium is a good solvent for lyophilic moieties of the adsorbed polymer, interpenetration is not favored and interparticle repulsion results. If the dispersion medium is a poor solvent, interpenetration is favored and attraction results. The free energy change which takes place when polymer chains interpenetrate is influenced by factors such as temperature, pressure and solvent composition. The point at which this free energy change is equal to zero and is known at the (theta)-point. If one reads resin" instead of polymers, it becomes quite familiar with the situation of asphaltenes. Therefore, the colloidal view of asphaltenes has been so popular over the years." (D. Shaw, 1992; D. J. Shaw, 1980)

Considering the steric forces along with other forces mentioned in figure 2.8, figure 2.9 is obtained as shown below.

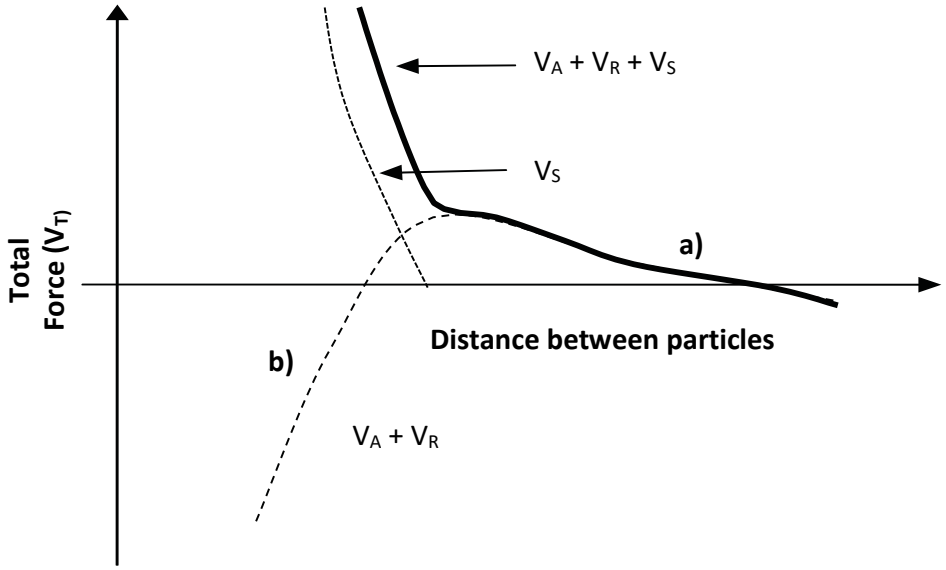

*Figure 22-9: The interaction energy plot for sterically stabilized particles: a) effect of electric double layer repulsion(*D. Shaw, 1992*;* D. J. Shaw, 1980*); b) without presence of electric double layer repulsion*

Gibbs energy provides an easy method to study the effect of temperature on solution stability. According to Gibbs (Merino-Garcia & Andersen, 2003) definition, the enthalpy change on close approach opposes the flocculation while change in entropy promotes it. Because of dominant effect of enthalpy it is called enthalpy-stabilization. It was observed that by increasing the temperature T, the flocculation occurs due to increased entropic effects on the system. Increase in entropy causes flocculation. The relation between enthalpy and entropy is reciprocal. In some cases of crude oil solutions, the flocculation occurs by decrease in temperature this is because of entropic stabilization. Steric stabilization influences two kinds of flocculation in respect to colloidal solution behavior described below:

Bridging Flocculation: This is the kind of flocculation occurs when a relatively higher molecular weight polymer adsorbs on the colloidal molecule. These polymers are present in very minute concentrations i.e., in ppm. When two ends of the polymer attach to two different colloids, they create a bridge. A number of such bridges can be formed in the solution ultimately causing the flocculation.

Depletion Flocculation: This kind of flocculation is different from bridging flocculation because the long chain polymers do not adsorb on the colloids. The colloids are in motion and when they are near to each other an inter-colloidal region is formed. The concentration gradient is high at this point, which is brought to equilibrium by diffusion of solvent molecules thus aggregating the colloidal particles.

2.10 Asphaltene precipitation and flocculation

Flocculation is the first step before precipitation occurs. Flocculation occurs due to many factors. During flocculation asphaltene molecules start aggregating. When the size of agglomerates becomes significant (greater than 1mm) the force of gravity can pull it down, overcoming Brownian forces and this stage is known as asphaltene precipitation or deposition. The Peclet number is used to relate the Brownian force acting within the solution and sedimentation or gravity force

$$Peclet\ Number\ (Pe) = \frac{Gv}{B}$$

Where G is length, v is velocity and B is diffusivity of the particle.

The relation between force of gravity acting on the particle and bouncy force of liquid generates a term known as terminal velocity. It can be expressed as following:

$$fr = m_p \left(\frac{\rho_l}{\rho_p}\right) g$$

Where fr is the frictional coefficient, m_p is mass of the particles, ρ_l and ρ_p represents the density of liquid and density of particles respectively. "g" is acceleration due to gravity.

Gravity force takes over the Brownian force when Pe > 1. The diameter of the particle is easily calculated by assuming the spherical shape of the particle. The diameter is function of changes in density. Density is a function of temperature, as shown in figure 2.10. The approximate diameter of asphaltene molecules can be calculated which is necessary for sedimentation. The density differences between asphaltene particles and liquid rages between 320 to 550 Kg/m^3. However, these values can be further verified during experiments. If it is considered that asphaltene molecules are more or less of the same size, an average diameter of 0.7mm can give a good approximate is obtained which is coherent with the values found by Ferworn.

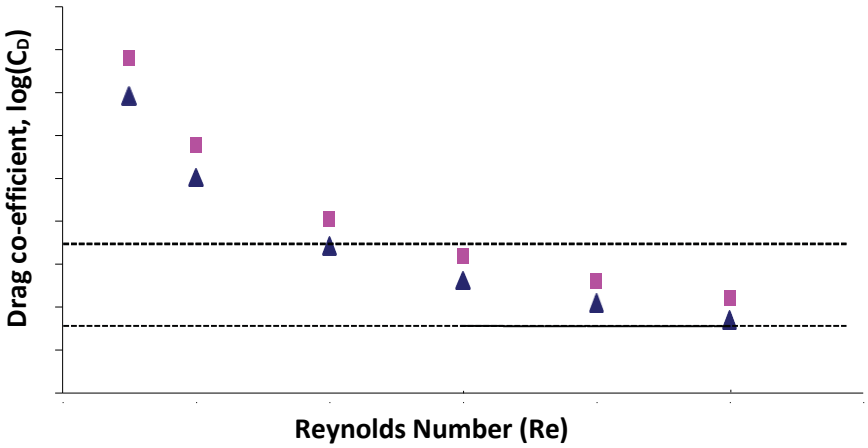

Figure 22-10: Critical Sedimentation Diameter of a spherical particle (K, 300K, 400K)

The values obtained are strictly based on individual calculations, assuming a steady state process with particles in no motion. Moreover, the particles are spherical in size. This case cannot directly be applied on asphaltenes because of differences in size and shape of these particles. They also differ in composition and thus density. The problem can be resolved by using deep learning and computer simulation. One of the example is the study carried out on Brownian forces and hydrodynamic behavior of sedimentation process by Padding and Lousi during 2004(Padding & Louis, 2004). The combined effect of flocculation and sedimentation was simulated by Östlund et al. (Östlund, Löfroth, Holmberg, & Nyden, 2002) which also provide a reference point for starting the asphaltene simulations.

In the literature review it was noted that the terms precipitation and flocculation are used interchangeably. During modelling of these phenomena, they need to be considered separately because they have different hydrodynamic properties. Researchers have modeled flocculation data together with precipitation data using same liquid/liquid or liquid/solid equilibrium. The determination of flocculation or precipitation applies methods such as light transmission and light scattering techniques. The sensitivity of equipment plays an important role in determining whether flocculation or precipitation is taking place. Other experimental techniques to find the flocculation phenomena are by using heat transfer analysis or changes in electrical conductivity. These techniques can provide an estimate of apparent precipitation.

Figure 2.11 shows data for the size of asphaltene molecules from Sky Blue oil. When precipitants are near 25% the average size of aggregates is 0.1 µm but when precipitants increased to 40% the average size increased to 1.0 µm. Similar effects of size were reported for MasrsA12 crude oil. The discussion about this size of aggregate as an initial size is still in progress because there are a number of factors playing between the transition from flocculation and precipitation. These factors include size of

particles, turbulence and presence of other compounds including resins. The studies show that continuous mixing also inhibits uniform settling of particles. Theoretical explanations for the transition between flocculation and precipitation of asphaltenes are widely discussed in the literature. However, there is little study which shows the phenomenon practically. This makes it necessary for the researchers to carefully select the assumptions and experimental results before modelling the data for asphaltene precipitation.

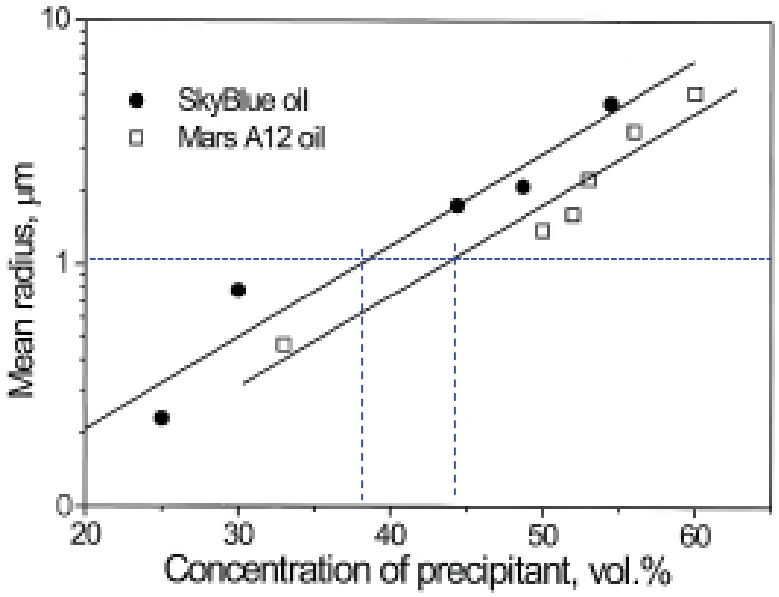

*Figure 2-11: Average size of asphaltenes molecules for different precipitant concentrations (*Burya, Yudin, Dechabo, Kosov, & Anisimov, 2001*).*

A study carried out by Fenistein et al.(Fenistein, Barré, & Frot, 2000) explained the process of asphaltene flocculation as a transition between compaction and aggregation processes. The compact structures were examined using radiation dispersion methods. Question arise concerning the asphaltene is present in solid form in the carrier oil or liquid so are they in equilibrium state? The answer lies in the IUPAC definition (Chung, 1992)of precipitation i.e. "the formation of a solid phase within a liquid phase". Chung (Chung, 1992) modeled the phenomenon in this way. In 2005, Sirota found that the solution theory of molecules describes the asphaltene formation(Sirota, 2005). According to this molecular theory the phase separation of asphaltenes is a liquid-liquid phase separation in the context of thermodynamic principles.

2.11 Conditions at which precipitation of asphaltene take place?

The presence of n-alkanes results in de-peptization of aromatics and resins which are responsible for dispersion of asphaltenes in the solution. This concept is valid only if the colloidal behavior of asphaltene is considered. However, considering the solution, asphaltenes separates out because of higher differential between dispersion solubility of asphaltenes in the solvent. Thus, it was concluded that hydrogen bonding is responsible for aggregation due to strong interaction, while precipitation is caused by non-specific attractions between the aggregates(Porte et al., 2003).

Figure 2.12 shows that when dispersion magnitude of the solubility parameter becomes equal to that of solvent, asphaltene is soluble in such solvent. The behavior testifies the good solvency abilities of some solvents such as decalin, cyclohexane and tetralin. The following section presents explanations for the behavior of solvents, and their effect on precipitation, in the view of molecular theory and thermodynamic properties.

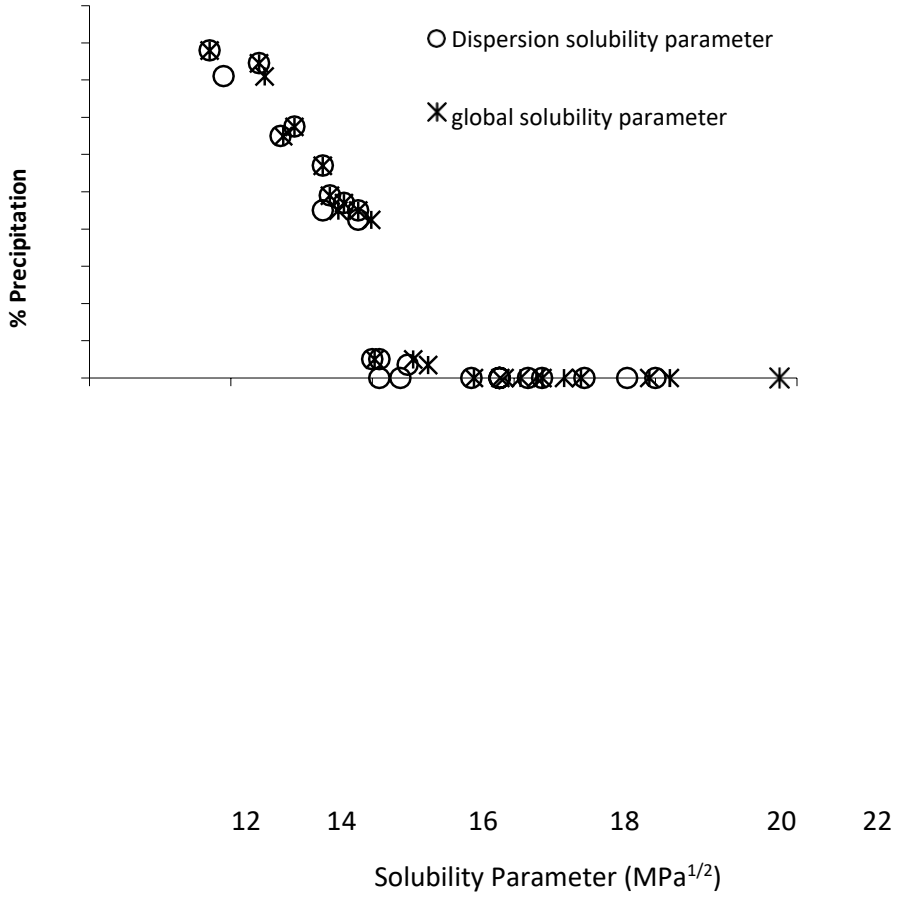

*Figure 22-12: The effect of dispersion forces on magnitude of precipitation (adapted from Mitchell and Speight (*Mitchell & Speight, 1973*))*

The explanations mentioned in previous paragraph, related to sterically stabilized colloids, can be one means to understand the impact of temperature on flocculation. Some studies suggest that there is an effect of thermal expansion differences between asphaltene molecules and solution which causes precipitation (Buenrostro-Gonzalez, Lira-Galeana, Gil-Villegas, & Wu, 2004).

The effect of pressure depletion on asphaltene precipitation has been studied by number of scientists. This phenomenon is more common and scientist are agreed on the effects of pressure depletion (Hammami et al. (Hammami et al., 2000),for gas injection; Akbarzadeh at al. (Akbarzadeh, Alboudwarej, Svrcek, & Yarranton, 2005) for n-alkanes).

2.12 The reversibility of precipitation

The reversibility of precipitation of asphaltene is still one of the most debated topics in crude oil sciences. There are two theories about the presence of asphaltenes in the solution based on experimental evidence. One theory state that asphaltenes are present in the crude oil in the form of dispersed solids. They are stabilized in the solution due to the presence of larger resin molecules. In such case of flocculation, it will be irreversible. The second theory explains asphaltenes as being present in the crude oil in pure liquid state. The changes in thermodynamic properties causes the asphaltene precipitation. This implies that when the thermodynamic conditions are restored, the asphaltenes will become soluble once again. Most of the literature agrees upon the later theory i.e., asphaltene precipitation is reversible under certain conditions.

The solubility of asphaltenes has been observed to increase when the lower critical pressure is higher than the final pressure. Similarly, when upper initial pressure is higher than the final pressure asphaltenes tends to dissolve back into the solution. One study describes the asphaltene precipitation as the reversible process however, the re-dissolution kinetics are dependent on the physical state of

the system(Hammami et al., 2000). Some researcher claims that the reversibility of asphaltenes is also dependent on its composition (K. Leontaritis, Amaefule, & Charles, 1994). However, this postulation is yet not verified. Other studies found that asphaltene precipitation becomes irreversible if the crude oil is subjected to the conditions well beyond those existing when the initial precipitation started.
A number of authors studied the hysteresis between precipitation of asphaltenes and its re-dissolution in crude oils. It was found in the studies that precipitation factors i.e., pressure, temperature and composition etc. play very important roles in the hysteresis behavior. The effect of temperature on these behaviors has been found to be more impactful than that of pressure. Other studies have found that hysteresis is linked with the deposition properties of asphaltenes. Once the asphaltene molecules are deposited on some surface, such as formation rocks or pipelines, their re-dissolution becomes difficult. In such situation the asphaltenes can be re dissolved in the crude oil by sonication process. (Sarma, 2003).

2.13 Empirical tools to predict asphaltene precipitation

Various empirical tools are available to predict the asphaltene precipitation. One such tool (De Boer, Leerlooyer, Eigner, & Van Bergen, 1995) shown in Figure 22-13 The difference between the value of bubble point pressure, Pb and the reservoir pressure, Pr, is plotted against oil density (kg/m^3). The plot gives the relationship for stability of asphaltenes. The diagram shows that when oil is distant from its bubble point, and where the oil is higher in lighter fractions, the chances of asphaltene formation are also high. The diagram is valid only for reservoirs where the assumption of asphaltene saturated crude oil is valid. This graph provides a rough prediction of asphaltene precipitation, but it cannot be used alone due to a number of other factors that are involved, not included with this chart.

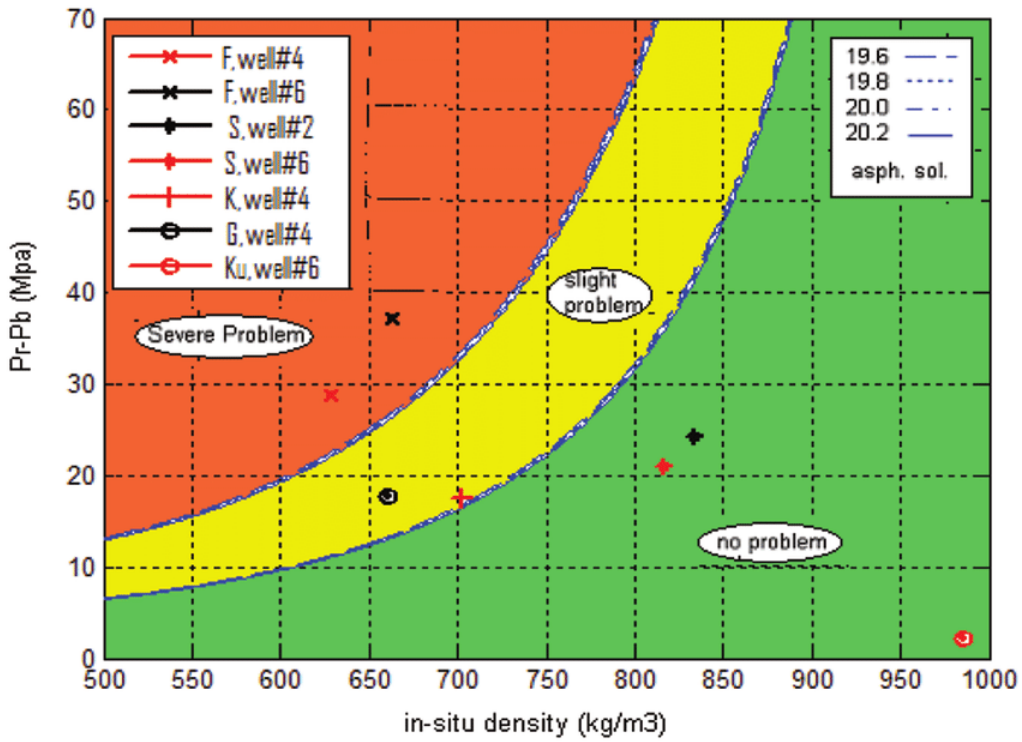

*Figure 22-13: Behavior of various Asphaltene saturated crude oil at their bubble points (*De Boer et al., 1995*).*

2.14 The effects of the presence of resins on asphaltene stability

A number of researchers studied the effects of relative concentrations of resins and asphaltenes and. the ratio of asphaltene and resin is found to be an important factor in asphaltene stabilization. It was

found that crude oil with higher amounts of resin is more stable. The theories suggest that a peptization process is responsible for this behavior, however, only fraction of the resin is involved. A small part of resins forms asphaltene aggregates. Figure 22-14 shows three different methods employed to check the asphaltene stability.

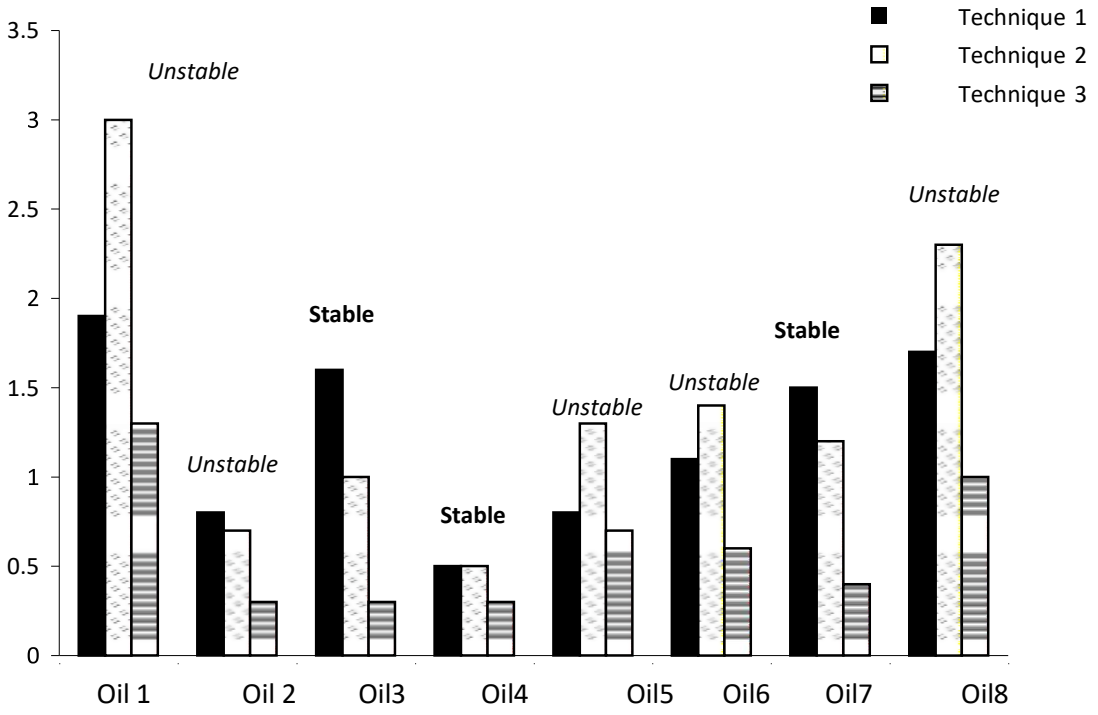

*Figure 22-14: Effect of resin-asphaltene ratio on stability of crude oil (*Guo, Liu, Li, Wu, & Christy, 2006*).*

2.15 Conclusions

Following are the important points that can be concluded from the literature review that have input to the modelling research of this thesis:

- Asphaltene has been identified as a solid mass of polar compounds. It has a higher molecular weight. The exact nature and composition of asphaltene is yet unknown, however there are several methods by which some of their properties can be studied.
- Extraction of asphaltenes from the crude oil in the laboratory can affect their properties significantly.
- The solubility of asphaltenes is limited and it can be used to characterize its composition and other relevant properties.
- The two major types of asphaltene found in the literature are referred to as continental and archipelago.
- Asphaltene can be present in two forms in crude oils i.e. as solutes properly dissolved in the solvent and as colloids suspended in the solvents. Both of these states affect the flocculation and precipitation properties of asphaltene.
- The asphaltene molecules have a higher molecular weight such that a single monomer may be more than 1100 g per mol.
- Hydrogen bonding can cause self-association among the asphaltene molecules at the concentration of 110ppm and above.
- The precipitation of asphaltenes is less affected by other forces present in the solution such as polar dispersion forces.
- Presence of resin in the crude oil affects the destabilizing nature of asphaltenes. Resins helps stabilizing the solution and asphaltenes do not precipitate in their presence.

- The critical micellar concentration in asphaltenes can be explained only by the individual asphaltene structure.

-

CHAPTER 3 *Existing asphaltene modelling- background information*

There are two categories of existing modelling processes:

a) a thermo-dynamic model, and

b) a model that explains mass and energy transport.

For an understanding about the precipitation of dissolved asphaltenes, the thermo-dynamic model is used. Because information related to the physical chemistry that plays its part in the deposition of asphaltenes is meagre, the transport model is used to study the results. The scope of this model is limited as it greatly depends on experimental data.

3.1 The different families of models

Asphaltenes can be studied using two different methods, by peptizing using resins, or by the use of a liquid medium. This is reported in the research literature using two families of models (Cimino et al., 1995):

- The lyophobic models: Asphaltenes that are resistant to solvents are termed lyophobic. The peptization of asphaltenes is by the use of resins. A two-phase system is used in this process. This is referred to as the colloidal model. This has caused a shift in the way scientists are thinking to further this research. Pfeiffer Saal (Buenrostro-Gonzalez et al., 2004; Chapman et al., 1989; David Ting et al., 2003; Li & Firoozabadi, 2010; Ting, 2003; Wu et al., 1998)found that asphaltenes have an insoluble precipitation which is irreversible
- The lyophilic models: Asphaltenes that are lyophilic colloids (solvent-attracted) encircled and solvated by the liquid medium. It involves true solution and it is reversible. This model states that the asphaltenes monomers and aggregates belong to thermodynamic equilibrium. The stabilization effect of resins is because of the solvation power of the liquid medium. Destabilization arises due to the very small solvation power of the liquid medium.

The different versions of these model are explained:

3.2 The steric-stabilization model

Leontarites and Mansorri (K. J. Leontaritis & Mansoori, 1992) introduced this model. They utilized the concept shown by Pfeiffer (Buenrostro-Gonzalez et al., 2004; Chapman et al., 1989; David Ting et al., 2003; Li & Firoozabadi, 2010; Ting, 2003; Wu et al., 1998), i.e, that asphaltenes are insoluble and their solid particles are peptized by resins adsorbed on their surface. According to Leontarites and Mansorri (K. J. Leontaritis & Mansoori, 1992), when the chemical potential of resins, M, are smaller than critical Mcr, then the asphaltenes are soluble. This model is is only utilized for data regression. In addition, the theory behind this model still requires validation: is there a physical presence of resins between the interface of asphaltenes micelles and crude oil? Isolated asphaltenes fractions are inert in some solvents. This shows that there is no need for the presence of resins for the stabilization of the asphaltenes (Cimino et al., 1995)

Victorov and Firoozabai introduced a micellization model. It utilizes the “Pfeiffer assumption “just like the previous model’ (Victorov & Firoozabadi, 1996).Three main activities are involved in micelle formation:

- Lyophobic involvements: These highlight the gain of free energy from the transference of asphaltenes and resin molecules from an indefinitely diluted crude to a micelle.

- Interfacial involvements: Micellar core in the crude is attributed to a positive interfacial tension
- Electrostatic contribution

Properties of the bulk-phase are defined by the Peng-Robinson equation. The model comprises the ability to explain the asphaltenes precipitation, but with a small degree of accuracy. The problem of reversibility was not explained. This appears to be even better than the experimental research. So, attractive as this model might appear, it seems unlikely to be able to explain or evaluate asphaltenes precipitation completely, since it has not been proved so far.

3.3 The thermodynamic models

The initial model, treating asphaltenes as solvated in a liquid medium, was the Flory Theory for polymer solution (Buenrostro-Gonzalez et al., 2004; Chapman et al., 1989; David Ting et al., 2003; Li & Firoozabadi, 2010; Ting, 2003; Wu et al., 1998) . This model is responsible for the decoupling of the vapor-liquid equilibrium from the liquid-solid equilibrium. Initially the vapor-liquid equilibrium is calculated and then the disabilities of the liquid-phase are removed with keeping the vapor phase remain content. Hirschberg (Hirschberg et al., 1984) and co-workers examined asphaltenes as mono-dispersed solvated macromolecules without using resins specifically but only as a component of the solvent. After considerable experimentation it was concluded that the maximum volume fraction of soluble asphaltenes in crude oil was defined as follows:

$$\varphi_a^{\max} = \exp\left[\frac{v_a}{v_l}\left(1-\frac{v_l}{v_a}-\frac{v_l}{RT}\left(\delta_a-\delta_l\right)^2\right)\right]$$

Equation 3.1

where v is the molar volume, φ the solubility parameter, R the gas constant and T the temperature. The subscript and I refer to the asphaltenes and the liquid medium respectively.

SRK EOS (Soave Redlich Kwong Equations of State) are used to evaluate the liquid's solubility parameters when the fluid was characterized. The properties of asphaltenes were studied by titration experiments. The results were quite effective. The effects of pressure, gas injection and temperature were examined.

The progression to maximum solubility with temperature is explained by the following factors:

The difference in thermal expansions: Thermal expansion of a liquid is about 10^{-3} K^{-1} whereas for solids the is lower (10^{-4}-10^{-5} K^{-1}) The thermal expansion of the asphaltenes can be evaluated by using computer assisted software (Diallo, Strachan, Faulon, & Goddard III, 2004). At 300 K, it was calculated to be $1.9*10^{-4}$ K^{-1} . For many oils the thermal expansion was calculated at 303.15 K but such conclusions were not published. The method followed is the same as the method defined by the Verdier and Andersen(Verdier & Andersen, 2003). Thermal expansion range lies between $6.8*10^{-4}$ K^{-1} and $7.8*10^{-4}$ K^{-1} at 303.15 K and 0.1 Mpa.

The molar volumes: The molecular weight is a problematic issue. By assuming no excess of volume, the densities of the asphaltenes can be calculated (Rogel & Carbognani, 2003). The calculated values range between 1.17 and 1.52 g/cm^3. If the molecular weight is assumed to be 1000 g/mol, then the molar volume of the asphaltenes is $7.6*10^4$ m^3/mol. For oil, molar weights range between 200 and 300 g/mol, density ranges between 600 and 800 kg/m^3, then the molar volume is $3.6*10^4$ m^3/mol at room conditions.

Table 3. 1: Characteristics of the oil and asphaltenes

	asphaltene	oil
expansivity (K^{-1})	$2.0\ 10^{-4}$	$7.0\ 10^{-4}$
□ ($MPa^{1/2}$)	21.0	17.0
Molar volume (m3/mol)	$8.3\ 10^{-4}$	$3.3\ 10^{-4}$
m ($MPa^{1/2}.K^{-1}$)	$4.0\ 10^{-3}$	$3.0\ 10^{-2}$
Molar mass (g/mol)	1000	200
density (kg/m3)	1200	600

The influence of the solubility parameter of the asphaltenes is presented in Figure 3-1.

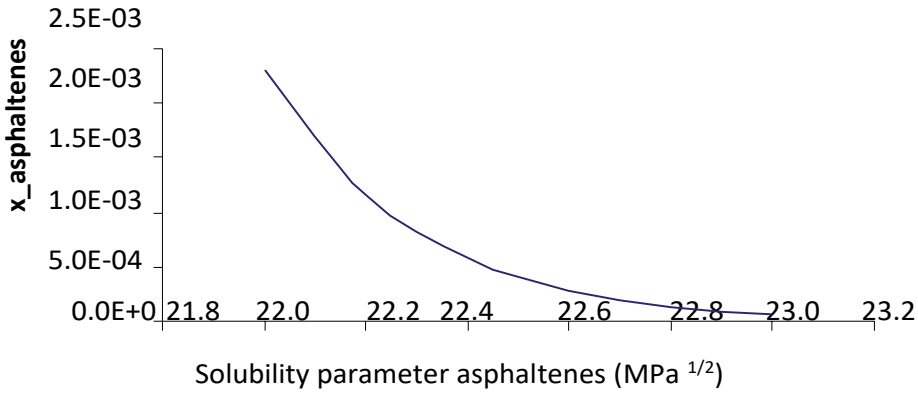

Figure 3-1: Influence of the solubility parameter of the asphaltenes on their solubility

The differences of the solubility are large (4000% deviation for a change of 1 $Mpa^{1/2}$). Solubility parameters cannot be determined directly even for pure compounds. Usually results differ by 0.2 $Mpa^{1/2}$. It is not possible to calculate accurate results for such a sensitive model with any experimental or technical method.

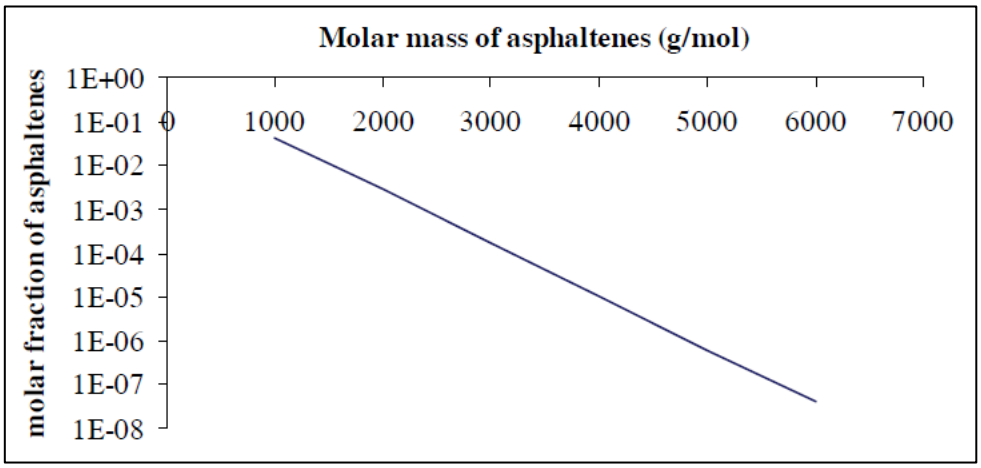

Figure 33-2: Influence of molar mass of asphaltenes on their solubility

Figure 3-2 represents the influence of molar mass as it relates to molar fraction in the model, solubility varies on a logarithmic scale with the aggregation's state. The predictive ability of such a model can be reduced since asphaltenes molar mass has to be assumed or fitted.

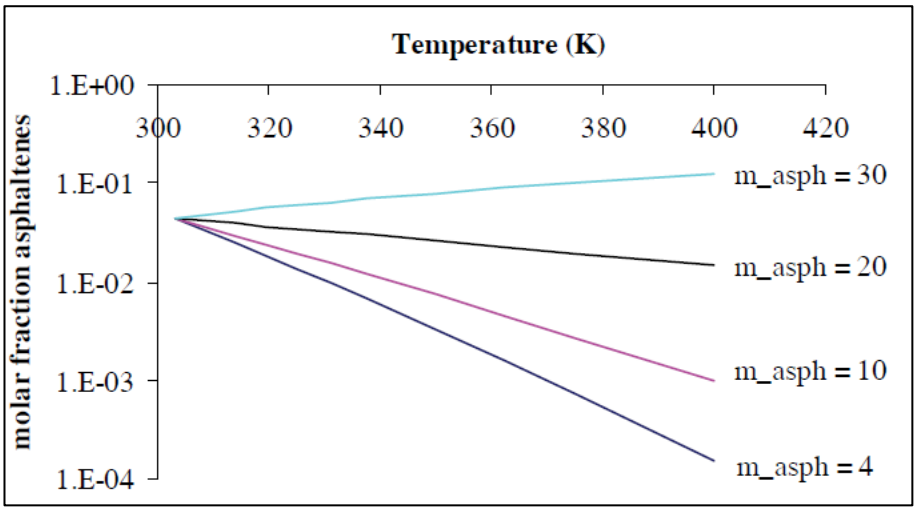

Figure 3-3: Temperature's impact on Asphaltenes solubility (m is in Pa1/2. K-1)

The temperature dependence of asphaltenes: Their solubility can increase or decrease with temperature increase depending on the value of the m_asph factor (Fig 3-3).

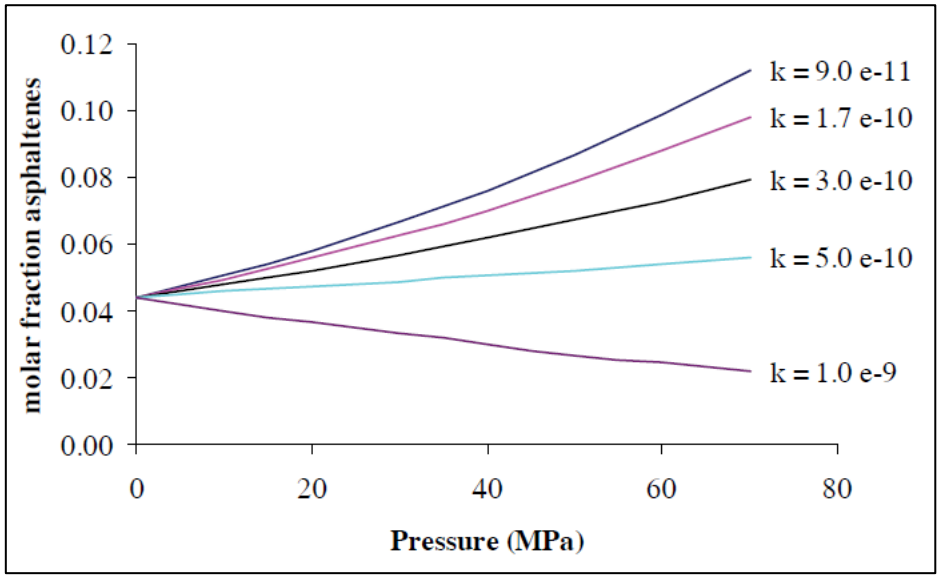

Figure 33-4: Pressure's Impact on asphaltenes solubility

The compressibility of oil was calculated with the use of high pressure, density measurement apparatus for a variety of oils (Verdier & Andersen, 2003). Molar volume values were reported as a function of pressure (Diallo et al., 2004) . Fig 3-4 presents the effects of pressure on the solubility of asphaltenes and it is similar to the function representing compressibility of asphaltenes.

The impact of pressure on asphaltene solubility is very much less than temperature. Experimentally, pressure increases the solubility. However pressure can also decrease the solubility if asphaltenes compressibility is greater than the solvent.

3.4 Cubic equations of state (EOS)

In the oil industry phase equilibrium calculations, the Cubic EOS are very prominent. For oil characterization and critical parameter determinations, (especially the heavy fractions) this method is a good fitting exercise of parameters. More investigations are required on cubic equations of state. . By combining Alexander's correlation using NMR and SRK EOS data the critical parameters can be calculated. Molar weights and content of heteroatoms are crucial, which can lead to misleading results. Key parameters included interactions to obtain proper solubility trends in the model. These parameters need to be fitted during titrations for every n-alkane and regarded as being constant (Simon I Andersen & Speight, 1999).

The formation of a new liquid phase in solutions with high asphaltenic content was described as flocculation by Szewczyk and Behar (Szewczyk & Behar, 1999). They used term flocculation not 'precipitation' to explain phase transition, and the word 'deposit' was applied instead of 'precipitated asphaltenes'. The light fractions, (F11-F20), represent crude oil. The heavy fraction, F20, is subdivided into 4 pseudo-components. The group contribution method is used to predict critical properties whilst the PR EOS is used with specific mixing rules in combination. At atmospheric conditions, a fraction's critical pressure is fitted to density and amount of precipitated asphaltenes are fitted by properties at 303.15 K.

Either as a solid or liquid, precipitated asphaltenes were calculated as a dense phase (Nghiem, Hassam, Nutakki, & George, 1993). Two components are obtained from asphaltene fractions, non-precipitating and a precipitating component. With interaction parameters, the PR EOS was used.

3.5 The association EOS

The most advanced EOS is associating EOS as SAFT. Asphaltenes precipitation analyses use these equations. Many groups applied these equations. (Wu et al., 1998), (Victorov & Firoozabadi, 1996),

For phase envelopes and gas injection, this work is useful for the fitting curves obtained. Many fundamental questions are raised by use of SAFT. Two problems are co-solubilizing effect of resins and dilution effect's absence(Guo et al., 2006).

Figure 3-5 depicts the impact of dilution on pressure from data collected experimentally at point of view and modelled with SAFT(Guo et al., 2006).

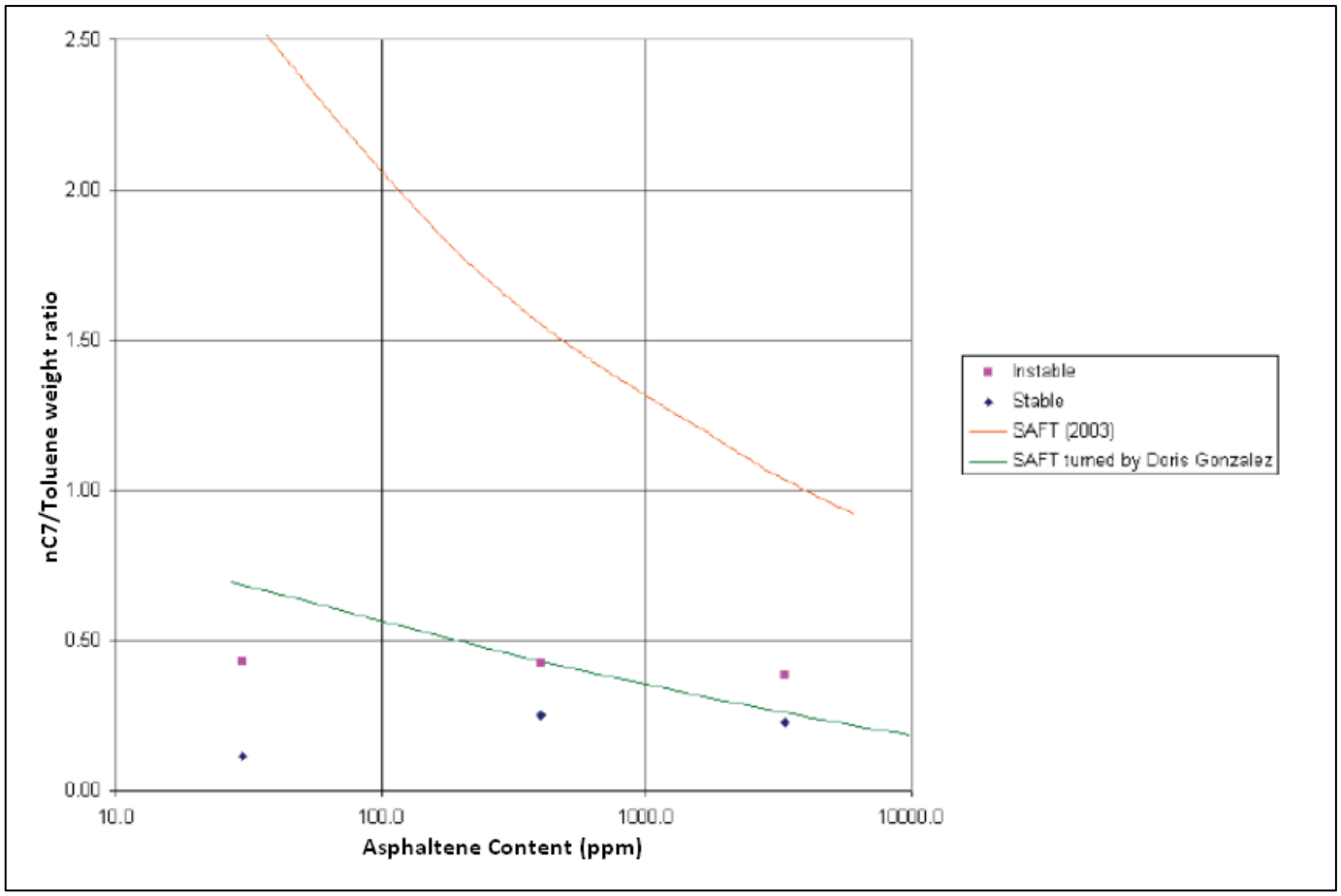

*Figure 33-5: Dilution of asphaltenes modelling (*Guo et al., 2006*)*

The introduction of a minute amount of resins will give a large stabilization to asphaltene that is present in a few ppm(Porte et al., 2003). This amount of resin will not have any large impact on the solvent power in the fluid medium. This can be linked to the co-solubilizing impact generated by resins.

3.6 Scaling equations

Scaling equation that were used in the aggregation and gelation studies(Rassamdana, Dabir, Nematy, Farhani, & Sahimi, 1996). These proposed methods were able to estimate the amount of asphaltenes precipitated depending on the ratio of solvent to crude, and the amount of solvent on a molar basis. The precipitation starting point was also configured by developing a correlation.

3.7 Asphaltene aggregation

Asphaltenes molecules can remain in the crude oil until they aggregate. The aggregates convert into bigger clusters and once this process starts, the precipitation of asphaltenes commences.
The process depends on the two conditions: the concentration of asphaltenes and the elapsed time. If the suspended particles are given a considerable time to collide, then aggregation is more pronounced.
Akbarzadeh et al. (Akbarzadeh et al., 2005) developed similar experimentation results. In the liquid phase, the nano sized asphaltenes particles are completely suspended. When then concentration of the asphaltenes rises, caking occurs at nano size levels and aggregates form. This is depicted in figure 3.6.

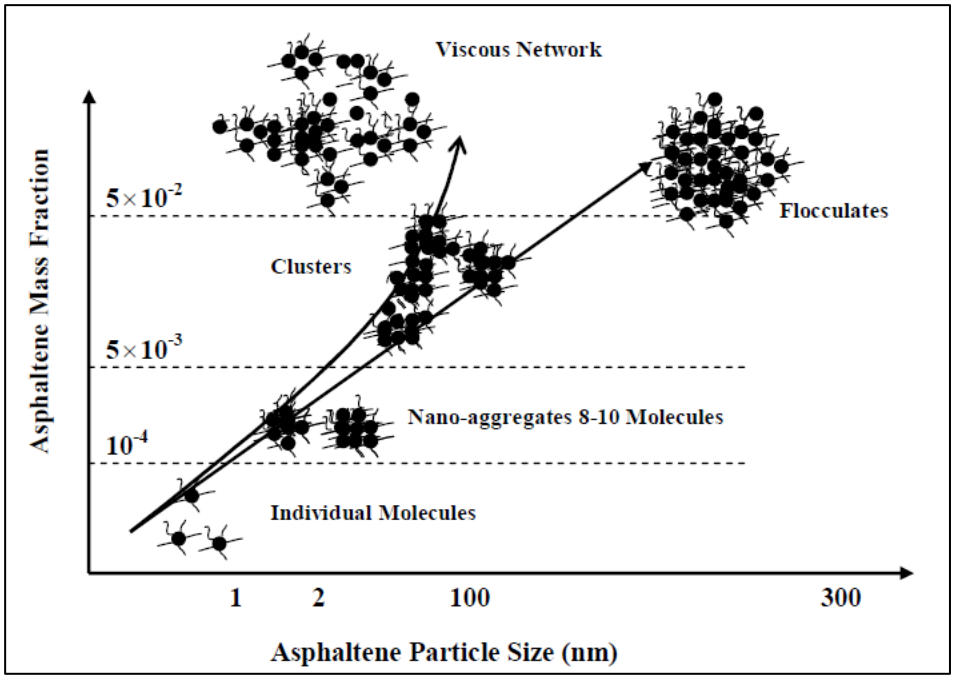

Figure 3-6 Effect of asphaltene concentration on aggregation process

Effect of asphaltene concentration on the aggregation process

Eskin et al. (Eskin et al., 2012) examined the effects of time on particles of asphaltenes. The trend they present shows the amount of particle of asphaltenes increasing with time. The size of these particles is variable, changing from a few nanometres to many multiples in a time as low as 10 hours.

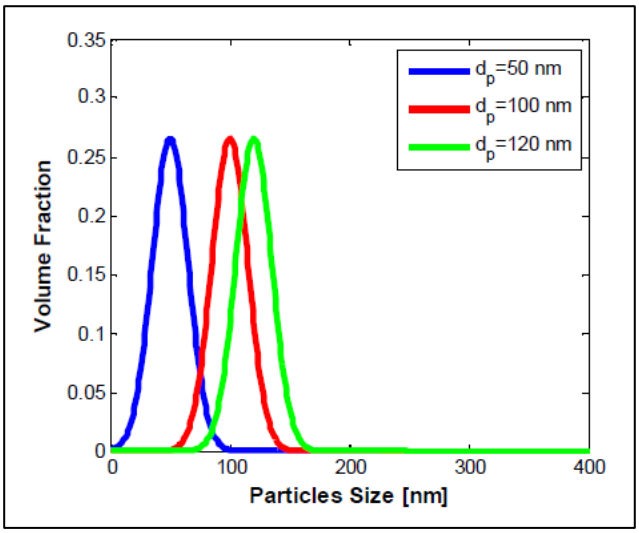

Figure 3-7: Schematic view of asphaltene particles size distribution change with time due to aggregation process.

Asphaltene precipitation modelling was tested in concert with the Burke et al. (Burke, Hobbs, & Kashou, 1990) data driven by experimentations and CMG Winprop (Computer Modelling Group) on real time oil mixture at reservoir temperature.

The model showed the precipitation pressure was 4600 psi at a reservoir temperature of 212°F.

Fig 3.8 also shows the vapour/liquid equilibrium modelling and the onset pressure of asphaltene at both the lower and the upper range. The precipitation shows a maximum value at the saturation point between upper and lower onset pressures.

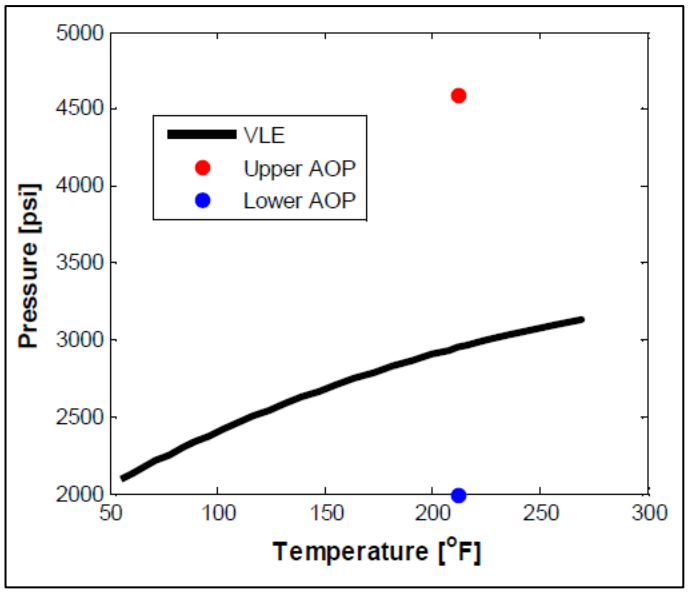

*Figure 3-8: The vapour liquid equilibrium line for fluid with asphaltene(*Burke et al., 1990*)*

CHAPTER 4 *Wellbore modelling - numerical solutions*

Our proposed multiphase flow model solves six field equations to obtain six primary variables defining the state of fluids in the wellbore. The primary variables solved in our model consist of volume fraction of water (Vw), volume fraction of gas (V g), pressure (P), velocity of gas (ug), velocity of liquid (ul) and temperature (T). These variables are used to update the secondary variables from state relations, constitutive relations, and the phasic wall frictions.

This section shows the use of different numerical algorithms following the solution of the field equation. In these equation, finite difference method was applied to discretise the equation system. To find the linearization of the equations, several numerical methods were instigated including implicit, semi and near implicit methods.

4.1 Wellbore boundary conditions

In our model, one can resolve different categories of boundary terms for wellbore. It can present the process of that particular boundary term for transient multiphase flow in pipelines or wellbores . The nodes that can be studied are the following:

Pressure
Mass flow
Mass source
Closed

Except for mass flow all other condition are entered at the outlet or at the inlet node. Temperature, water cut and gas oil ratio, or the mass flow of oil, gas and water are also entered for the inlet node.
To effectively implement the boundary terms we take imaginary nodes at the outlet and inlet and give different the values to those nodes.
Some additional boundary conditions are taken into account in our model with steady-state, multiphase flow and single-phase flow. These limits used some general wellbore conditions to provide either a) constant wellhead flow rate, or b) constant bottom-hole pressure
The well could be controlled at pressures needed at the wellhead to provide a constant wellhead flow rate. For constant bottom hole pressure the wellbore pressure, at the productive zone of the reservoir, is taken as constant and all nodes are assigned.

4.2 Mathematical solution methods

To solve the primary variable the mathematical equation is linearized into different systems of equations. For different flow models (i.e. Drift flux, single or multiphase flow) we use algorithms to initiate linear equation systems.
To resolve two phase modelling, we will use semi-implicit and nearly implicit algorithms to decrease the time limit these methods require.
For the drift flux model we will initiate a full implicit algorithm to resolve the mathematical equation, for the linearization we will use newton techniques. Compensation for non-slip state with analysis of two fluid and drift flux model also give homogenous model.
.The solution technique for steady-state multiphase flow modelling we use a regular algorithm.

4.3 The fully implicit approach

To solve the drift flux flow in our model we will use fully implicit avenue. The mathematical formula for the drift flux model is nonlinear with complete implicit approach. To solve all of the primary variables we will use Newton techniques. Like near-implicit and semi-implicit we decouple momentum and mass from energy equations. If thermal modelling is involved; we will resolve the transport formula and then amend the temperature.

With the Newton techniques we clarify the momentum balance formula and mass balance by setting up a Jacobian matrix, J, and enduring vector, R, with other (primary) variables viz: pressure, water volume fraction, mixture average velocity and liquid volume fraction. As elaborate that we have resolve the equation for f1 as mixture mass balance, f2 as mixture momentum balance, f3 as water mass balance and f4 as liquid mass balance.

4.4 Numerical convergence and robustness of solutions

In this section we will perform different tests on multiphase flow modelling for multiphase flow programs and analytical solutions.

Table 4. 1: Input parameters for gas/oil/ water three-phase flow simulation in our model with different numerical schemes

Well Data		**Reservoir and Fluid Data**	
Well MD	2000 ft	Net pay zone	150 ft
Well TVD	2000 ft	Reservoir pressure	2000 psi
Max grid size	50.0 ft	Reservoir temperature	180 °F
Ambient temperature at top	60 °F	Oil API	30
Ambient temperature at bottom	180 °F	Oil bubble point pressure	2000 psi
Total heat transfer coefficient	1.0 Btu/ft^2-hr-°F	Gas specific gravity	0.6
Tubing ID	0.229 ft	Water specific gravity	1.0
Oil productivity index	0.1 ft^3/psi-ft-day	Gas heat capacity	0.55 Btu/lbm-°F
Water productivity index	0.1 ft^3/psi-ft-day	Oil heat capacity	0.45 Btu/lbm-°F
Gas productivity index	1.0 ft^3/psi-ft-day	Water heat capacity	1.0 Btu/lbm-°F
Wellhead pressure	1000 psi		

Table 4. 2: Input parameters for gas/water two-phase flow simulation in Model and PIPSIM

Well Data		**Fluid Data**	
Well MD	5000 ft	Gas specific gravity	0.7
Well TVD	5000 ft	Water specific gravity	0.98
Max grid size	50 ft	Gas heat capacity	0.55 Btu/lbm-°F
Ambient temperature at top	71 °F	Water heat capacity	1.0 Btu/lbm-°F
Ambient temperature at bottom	141 °F		
Total heat transfer coefficient	0.5 Btu/ft^2-hr-°F		
Tubing ID	0.25 ft		
Water mass injection	1 lb/sec		
Gas mass injection	1 lb/sec		
Wellhead pressure	500 psi		

Table 4. 3: Input parameters for comparison of wellbore temperature calculation between our Model, PIPESIM and analytical model from (Hasan, Kabir, & Sayarpour, 2010)

Well and Reservoir Data		**Fluid Data**	
Well MD	15000 ft	Net pay zone	100 ft
Well TVD	15000 ft	Reservoir pressure	5000 psi
Tubing ID	0.46 ft	Reservoir temperature	250 F
Tubing OD	0.56 ft	Oil API	20.661
Casing ID	0.7 ft	Oil bubble point pressure	14.696 psi
Casing OD	0.8 ft	Gas specific gravity	0.6
Wellbore hole size	1.0 ft	Oil heat capacity	0.40 Btu/lbm-°F
Well productivity index	0.1 STB/ psi-ft-day	Gas heat capacity	0.25 Btu/lbm-°F
Bottom-hole pressure	4071 psi	Oil thermal conductivity	0.45 Btu/hr-ft-°F
Gas injection depth	14900 ft	Gas thermal conductivity	0.55 Btu/hr-ft-°F
Casing head pressure	3500 psi		
Casing head temperature	75 °F		

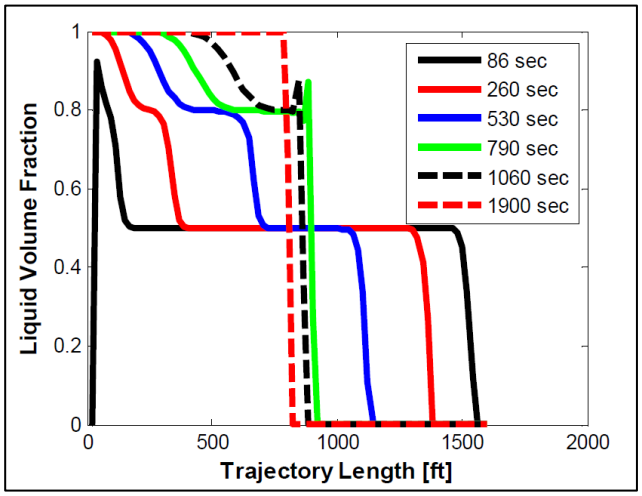

Figure 4-1 Pressure profile results for phase redistribution of a gas-liquid mixture column

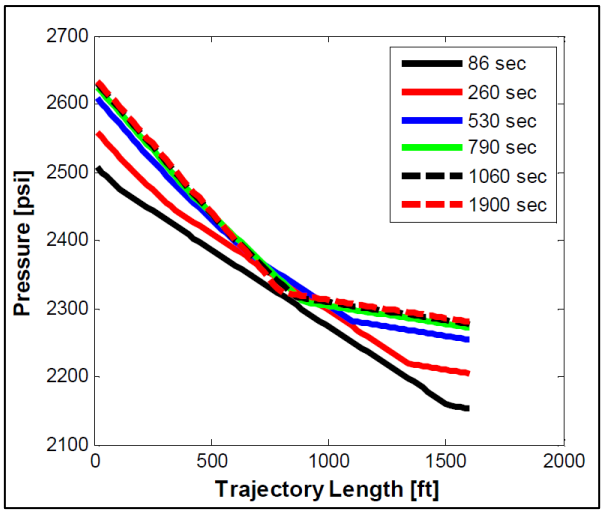

Figure. 4-2: Pressure profile results for phase redistribution of a gas liquid mixture column

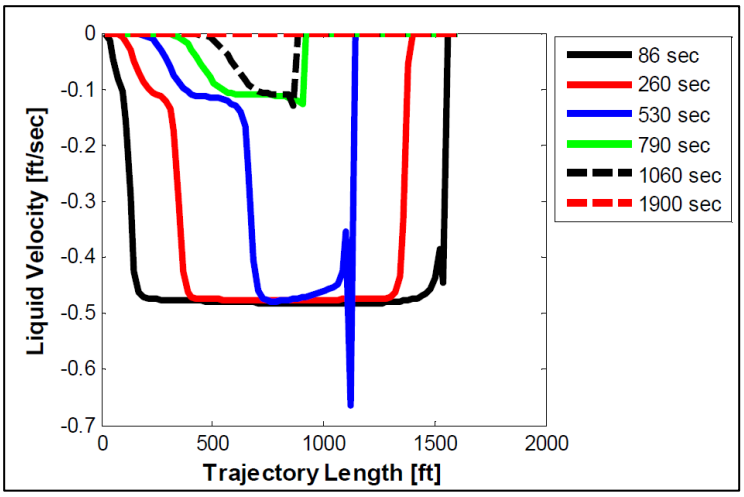

Figure 4-3: Pressure profile results for phase redistribution of a gas liquid mixture column.

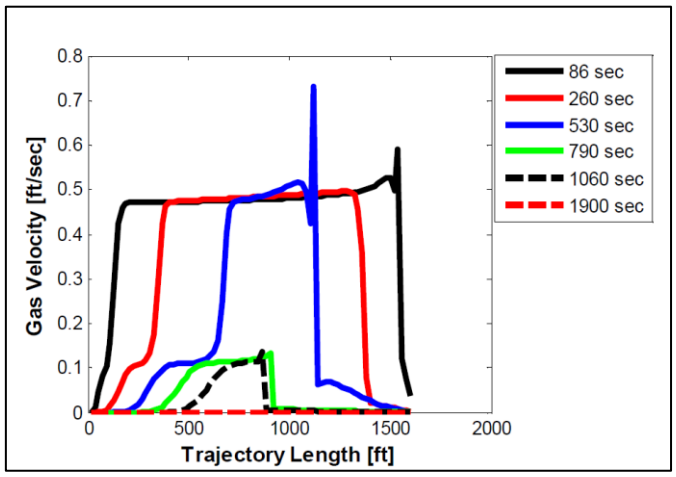

Figure 4. 4-4: Pressure profile results for phase redistribution of a gas liquid mixture column.

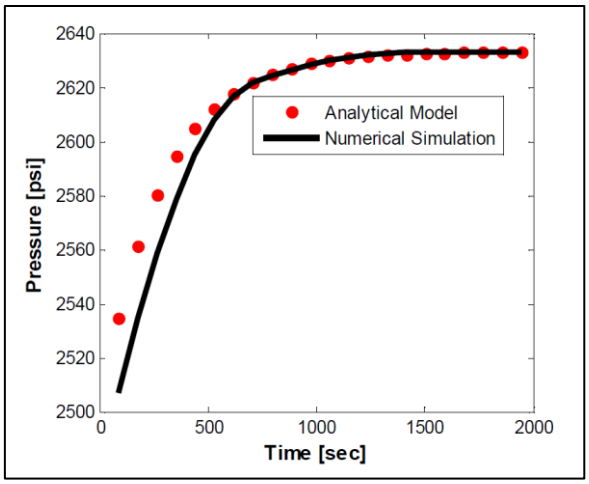

Figure 4-5: Variation of bottom of column pressure versus time for phase redistribution process of a gas liquid mixture.

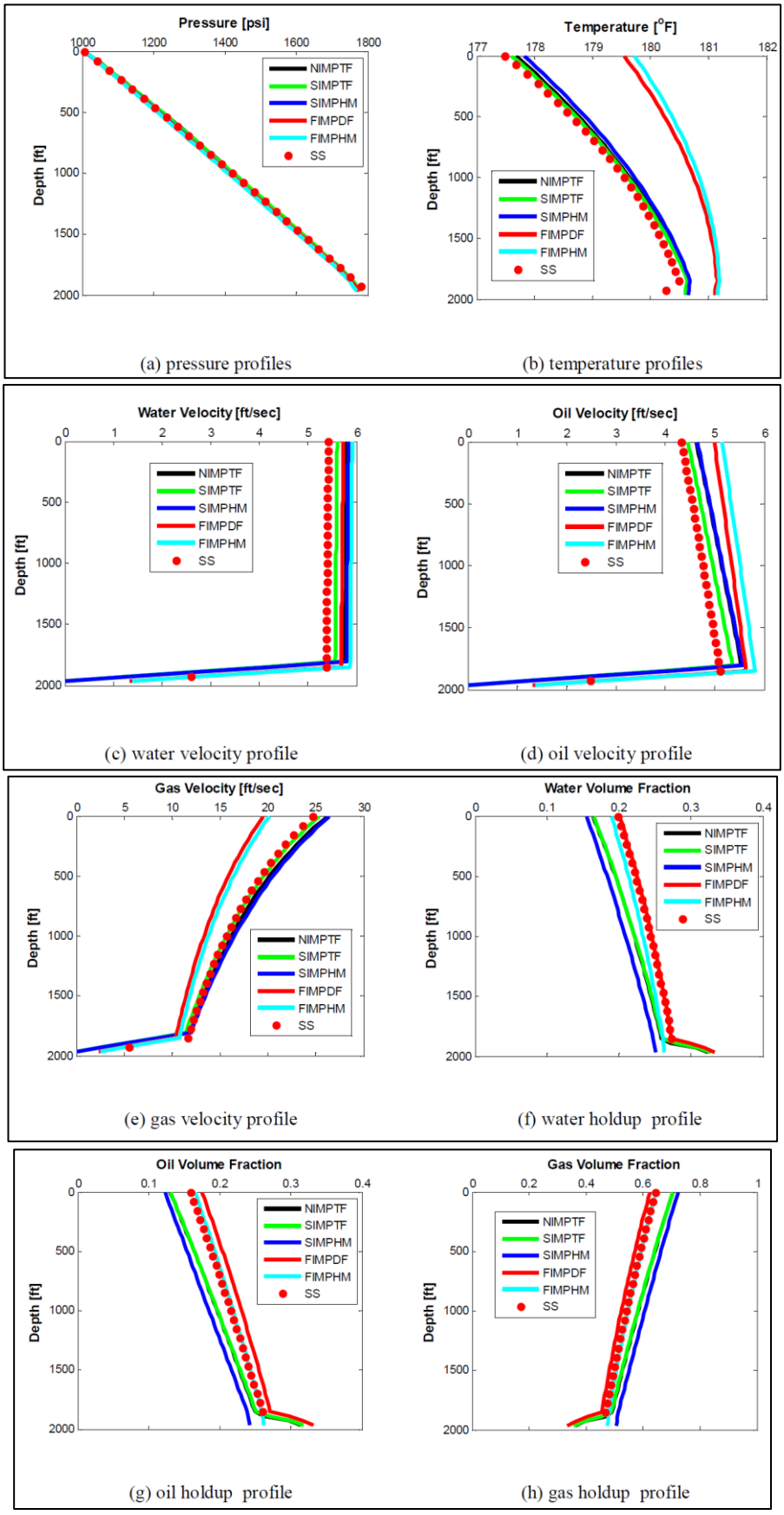

Figure 4 4-6: Comparison of primary variables profiles along the well for different multiphase flow

Figure 4.6 legend*:* two-fluid; drift-flux; homogenous and different numerical methods; Semi-implicit, Nearly implicit, Fully implicit, Steady State Marching Method.

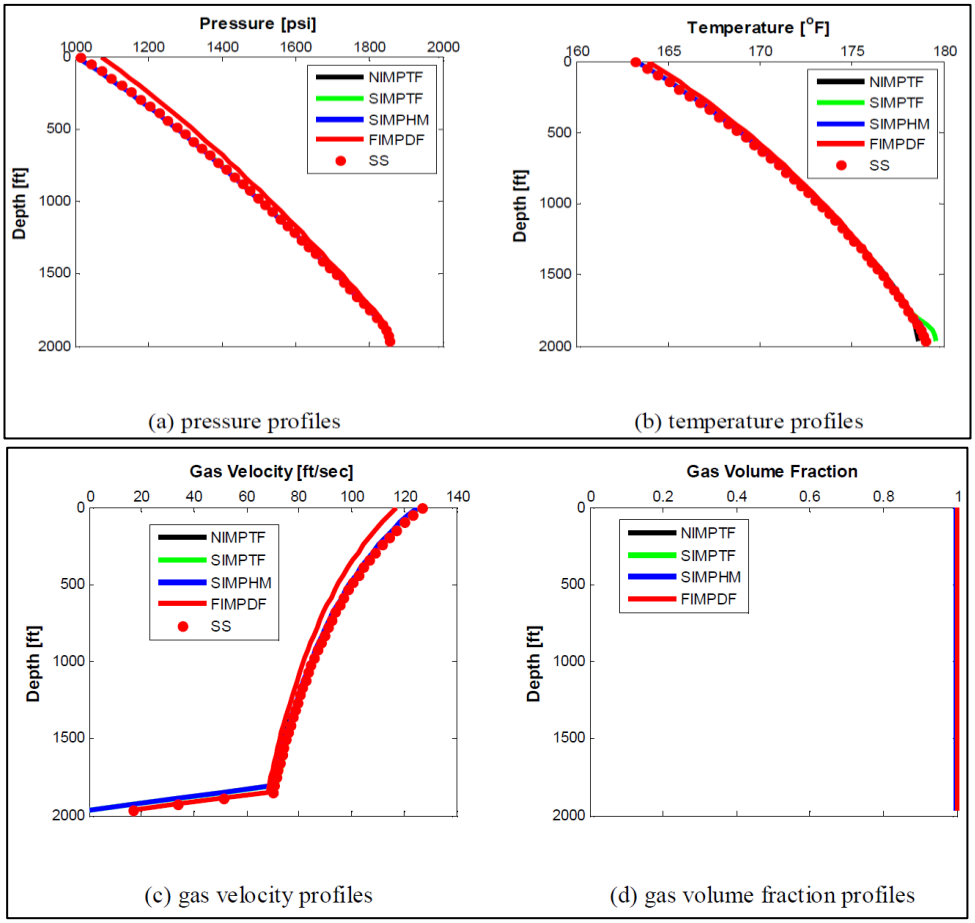

Figure 4 4-7: Comparison of main variables profiles along the well for different multiphase flow models and numerical methods for gas production at the end of steady state solution.

4.5 Conclusion

Methods used to study the precipitation of asphaltenes are models based on thermodynamics. These models are not reliable, consisting of complex and difficult equations and the parameters needed in the modelling consists of large data and experimental values. These models are able to render limited properties but they do not comprehensively explain all features. In the required study, it is an imperative to study all relevant models and parameters.

CHAPTER 5 *Prediction of asphaltenes deposition in multiphase flow systems through the use of Novel Numerical Modelling*

Many studies have been performed on the parameters affecting the deposition of asphaltenes including the impact of molecular weight, the solubility of the phase, temperature and pressure parameters. Some models may prove efficient in the single-phase flow model. However, there is no significant progress in modelling of multiphase flow.

There are some misunderstandings about the deposition of the asphaltenes and whether or not it is a reversible process. This understanding is important in the development of any model related to multiphase flow (Nasrabadi, Moortgat, & Firoozabadi, 2016). One way to study this problem is to apply numerical modelling. This is not only relatively easy and reliable but it is also more economical than other possible solutions(Attar, Sedaghat, Kord, & Mayahi, 2015). The Statistical Associating Fluid Theory (SAFT) was the result of many thermodynamically generated models that made use of solubility indicators. It was determined that the numerical method provided more reliable results then the experimentally determined results (Behbahani, Ghotbi, Taghikhani, & Shahrabadi, 2014).

5.1 Material and methods

The simulation procedure for the study of deposition of asphaltenes in the wellbore was conducted considering a sample of heavy oil. The simulation study showed that the bubble point was achieved in the center of the wellbore. The impact of carbon dioxide on the deposition of asphaltenes was studied by using the same sample and conditions.

In this research, the simulation parameters were taken from a well in an Australian oil field, 2400 meter deep. The well was at the primary stage of production.. The pressure at the initial point in the well is 38 MPa and wellhead pressure is 12.9 MPa. In the analysis of this well by simulation, multiphase flow was used.

Figure 5. 5-1, shows a schematic of the flow in the well. Initially, the crude is flowing at a height given by h. The radius of the pipe is given by r. The composition of the heavy oil is given by a mixture of hydrocarbons denoted by n, i.e. the number of the components. For all phases including gas, liquid and solids, the impact of temperature and pressure is taken for equal mole fractions. The entry point of the oil is the bottom inlet of the pipe. At this point, the inside radius of the pipe is given by r(a). The flow of oil from the pipe is at temperature "T_o" and pressure "P_o". The direction of the flow of oil in the pipe is in upward fashion. While flowing through the pipe, it cools the pipe down resulting into expansion. This expansion results into pressure reduction. The temperature of the crude also changes with the transfer of heat done by the forced convection. Thus, asphaltenes deposition is resulted from the changes in the T/P along the length of the wellbore. The new radius after reduction in the size is denoted by r(w). When the asphaltenes in the pipe increases, it is countered by the shear forces caused by the counter flow of the oil and gas.

As the flow of the crude reaches turbulent range, the asphaltenes layer below the crude layer results into a laminar sub layer. A tri-layered state is resulted that consists of laminar sub layer, the turbulent layer and the transition zone layer.

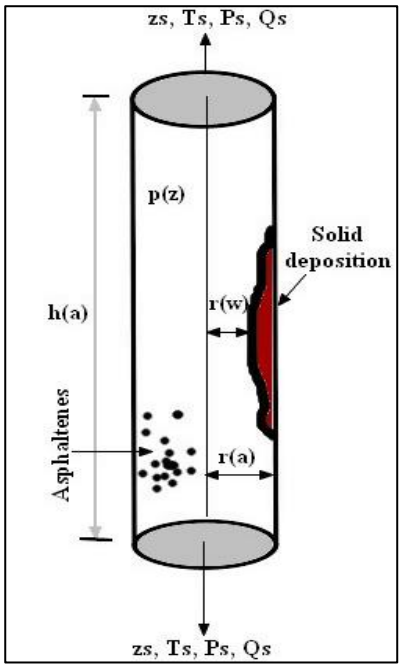

Figure 5. 5-1: Modelling solid deposition in a well bore

The input data for the research is taken from an Australian oil field and shown in the Table 5. 1.

Table 5. 1: Input parameters for simulation of asphaltenes deposition in the wellbore with a specific fluid sample.

Well Data	
Well Height	2400 m
Max. grid size	15.2 m
Top ambient temperature	15.6 °C
Bottom ambient temperature	100 °C
Total heat transfer coefficient	20.4 kJ/m^2.hr.°C
Tubing ID	0.070 m
Wellhead pressure	12.4 MPa
Oil productivity index	2.7 m^3/MPa.m.day
Reservoir & Fluid Data	
Net pay zone	60 m
Reservoir pressure	90 MPa - 922 Kg/cm^2
Reservoir temperature	320°F - 160°C

Table 5.2 shows the fluid composition and the characteristics of the fluid

Table 5. 2: Fluid characterization and composition of the fluid sample.

Component	Pc (MPa)	Tc (R)	VC (m^3/kg.mol)	Mw (kg/kg.mol)	Acentric factor	Parachor	Volume shift	Primary composition
CO_2	7.3780	547.56	0.09408	44.01	0.225	168.17	0	0.0246
Cl-CO_2	4.6092	360.61	0.10258	17.417	0.015127	92.19	0	0.4041
C_3-C_5	3.9517	732.89	0.23784	53.516	0.1793113	195.33	0	0.0755
C_6-C_{19}	2.0092	1135.31	0.85649	164.423	0.655007	512.21	0	0.2719
C_{20}-C_{30}	1.2094	1419.29	1.81247	340.927	1.064023	1016.51	0	0.1064
C_{31+}	0.9871	1682.93	3.53022	665.624	1.371778	1944.21	0	0.0774
Asphaltene	0.9871	1682.93	3.53022	665.6224	1.371778	1944.21	0	0.0401

5.1.1 Assumptions for proposed Multiphase Flow model

In the development of the mass conversation equation, the following conditions were assumed. The assumed data was later practically applied in the wellbore for study of asphaltenes deposition.

a. The direction of the flow was kept one-dimensional along the wellbore length, in vertical and horizontal and along the deviation path. This is only possible in pipes with small diameters.
b. In this research, spacial averaging and Eulerian time was used.
c. For three phase, slippage of the water-oil was made based on the well indices available for each phase.
d. In this research, for all phases, the pressure values were considered to be the same. This is only reliable when the concentration of gas is very small as compared to the other phases.
e. Thermodynamic-equilibrium is considered betweenin all phases. Multiple approaches were considered including black oil and compositional cases to calculate the properties and state of the fluids.

5.1.2 Development of the mathematical model

Based on these assumptions, the flow equations developed for the liquid and gas phases are as follows:

$$\frac{\partial(\rho_O \alpha_O)}{\partial t} + \frac{1}{A}\frac{\partial(A\rho_O \alpha_O u_O)}{\partial x} = \psi_O - \Gamma_g \quad \text{Eq. 5.1}$$

$$\frac{\partial(\rho_g \alpha_g)}{\partial t} + \frac{1}{A}\frac{\partial(A\rho_g \alpha_g \mu_g)}{\partial x} = \psi_g + \Gamma_g \qquad \text{Eq. 5.2}$$

Where ψ_o and ψ_g are the oil and gas mass influx terms, and ρ_g and ρ_o are the oil and gas mass densities. $\alpha_g$represents the coefficient of flow efficiency (dimensionless), $\mu_g$represents the viscosity, ∂ is sign for partial differentiating equation. Along with an appropriate definition of the interphase transfer term, Equations 4.3 and 4.4 result in decreasing the number of primary unknowns. This approach leads to a faster simulation runtime as well as application of the state relations using either compositional phase property calculations or black oil property calculations. The addition of solid particles to the fluid flow results in new sets of mass conservation equations, which are as follows:

$$\frac{\partial(A\hat{\rho}_O \alpha_O x_{nc} + Ac_a \alpha_O)}{\partial t} + \frac{\partial(A\hat{\rho}_O \alpha_O u_O x_{nc} + Au_O c_a)}{\partial x} = A\left(\dot{\hat{\psi}}_{O,nc} + \dot{\gamma}_a - \dot{\hat{m}}_{da}\right) \qquad \text{Eq. 4.3}$$

Where c_a is the asphaltenes concentration in the crude oil, γ is the flocculation of solid particles from the reservoir, and m_d is the deposition rate of the solid particles. Equation 5 is applied to fluids that contain asphaltenes and cause asphaltenes flow assurance problems. Equation 6 is used for fluids with precipitation potentials.

$$\frac{\partial(\sum_{i=1}^{NWAX} A\hat{\rho}_O \alpha_O x_i + Ac_w \alpha_O)}{\partial t} + \frac{\partial(\sum_{i=1}^{NWAX} A\hat{\rho}_O \alpha_O u_O x_i + Au_O c_w)}{\partial x} = A\left(\sum_{i=1}^{NWAX} \dot{\hat{\psi}}_{O,i} + \dot{\gamma}_w - \dot{\hat{m}}_{dw}\right) \qquad \text{Eq. 4.4}$$

Here, c_w is the wax concentration in the crude oil. To solve Equations 5 and 6 for asphaltenes and wax mass conservations, a similar approach for the solution component concentration (mole per volume) at a specific time is considered. Solving the equation in grid block "i" (the goal of gridding is to transform the model into a discrete system to solve the flow equations), we obtain the following equation:

$$N_{k,i}^{n+1} = N_{k,i}^{n} + \frac{\Delta t}{V_b^n} A_{i-1}^n \left[(\hat{\rho}_O \alpha_O u_O)_{i-1}^{n+1} x_{k,i-1}^n + \left(\hat{\rho}_g \alpha_g u_g\right)_{i-1}^{n+1} y_{k,i-1}^n\right]$$

$$-\frac{\Delta t}{V_b^n} A_i^n \left[(\hat{\rho}_O \alpha_O u_O)_i^{n+1} x_{k,i}^n + \left(\hat{\rho}_g \alpha_g u_g\right)_i^{n+1} y_{k,i}^n\right]$$

$$+\Delta t\left[\dot{\hat{\psi}}_{Ok,i}^{n+1} + \dot{\hat{\psi}}_{gk,i}^{n+1} + \dot{\gamma}_{a,i}^{n+1} - \dot{\hat{m}}_{da,i}^{n}\right] \qquad \text{Eq. 5.5}$$

When the number of moles of component k per bulk volume ($NN_{k,i}^{n+1}$) is obtained, the overall mole compositions of the hydrocarbon phases in the grid block i are updated. The next step involves the flash calculations of the concentration of asphaltenes at a new time step. In Equation 6, the solid deposition rate $m_{da,i}^n$ is used for the old-time step. The process can be reiterated using a new deposition rate and new solid concentrations until convergence is achieved. The new concentrations are used for updating the concentrations of fluid species and solid precipitates in grid block i using PHREEQC module, which is a specialized geochemical model(Parkhurst & Wissmeier, 2015) for the reaction among rocks, water and solid precipitates (asphaltenes in our case). The cross-sectional area of well bore pipe decreased due to solid deposition, resulting in production loss. The cross-sectional area at the new time step is calculated as follows:

$$A_i^{n+1} = A_i^n + \frac{V_{s,i}^n}{\Delta_{xi}} \qquad \text{Eq. 5.6}$$

Equation 8 can follow the progress of solid deposition in each wellbore grid block. The model is used for predicting the decline in the flow of crude oil due to solid deposition.

5.2 Effect of CO_2 injection

According to(Darabi, Shirdel, Kalaei, & Sepehrnoori, 2014) , the problems of flow in the wellbore are caused by the injection of carbon dioxide and light HCs in the wellbore. These are injected during the process of enhanced oil recovery. Due to this process, asphaltenes deposition occurs in the wellbore. This is the most troublesome issue related to injection of the carbon dioxide in the wellbore. This needs proper research and studies on this topic. This is clear that the presence of light components can increase the bubble point pressure in the wellbore. Vargas et al.(Vargas, Gonzalez, Hirasaki, & Chapman, 2009) Applied PC-SAFT EOS and studied the effect of light components on the properties of the asphaltenes. The asphaltenes precipitation modelling does not include the effect of composition on asphaltenes onset pressure. In this process, the temperature and pressure and predefined and used as variable in the modelling process. PC-SAFT EOS cannot be used for the entire process of composition as the cubic state equation is not flexible for several composition of the asphaltenes. In order to remove errors from the modelling process, predefined experimentally determined values are used. Table 4.3 shows the onset pressure of the fluid for different molar ratios of carbon dioxide to oil.

Table 5. 3: Asphaltenes onset pressure and temperature for different mixing ratios of CO2

Onset Temperature (°F) – (°C)	**Pressures in PSI for following Compositions**			
	0% CO_2	5% CO_2	10% CO_2	15% CO_2
100 - 37.7778°C	4600	4770	4930	5100
93 - 33.8889°C	5045	5165	5285	5400
88 - 31.1111°C	5450	5545	5640	5735
82 - 27.7778°C	5960	6000	6045	6085
77 - 25°C	6660	6625	6590	6560
71 - 21.6667°C	7580	7445	7310	7170
66 - 18.8889°C	8650	8430	8210	7995
63 - 17.2222°C	9545	9175	8810	8440

Table 5. 4: Reservoir fluid composition for different mixing ratios of CO2

Component	**0% CO_2**	**5% CO_2**	**10% CO_2**	**15% CO_2**
CO_2	0.0246	0.07337	0.12214	0.17091
Cl-C2	0.4041	0.383895	0.36369	0.343485
C3-C5	0.0755	0.071725	0.06795	0.064175
C6-C19	0.2719	0.258305	0.24471	0.231115
C20-C30	0.1064	0.10108	0.09576	0.09044
C31+	0.0774	0.07353	0.06966	0.06579
Asphaltenes	0.0401	0.038095	0.03609	0.034085

5.3 Development of the computational model

A comprehensive computational model is designed for the evaluation and prediction of asphaltenes in wellbores, as shown in Figure-5.1. The model incorporates asphaltenes prediction with and

without injection of CO_2 in the well. The model starts with defining and inputting the variables that affect asphaltenes precipitation. The assumptions are also included in the next step, which defines the flow of the model. The next step is to update the temperature and pressure in the loop for evaluating the asphaltenes precipitation later on. Equations 3.1 and 5.1 are used to calculate the phase equilibria in the next step. All the physical properties, such as the density, viscosity, and temperature of crude oil, are determined in this step, and the diameter of the pipe is updated. Equations 5 and 6 are used for evaluating for asphaltenes precipitation in the next stage. If precipitation doesn't occur under the given conditions, the loop is repeated for changed values of temperature and pressure. If asphaltenes are present, further calculations are made for its verification and are matched with the original data obtained from the Halibut oil field (Australia). If asphaltenes are formed, and the nominal diameter of the pipe decreases to a reduced size, the simulation is stopped, confirming the asphaltenes precipitation. If no asphaltenes are formed, the loop is repeated back for the changing temperature and pressure values. After the initial determination of asphaltenes under the given conditions, the effect of CO_2injection is also studied. This loop can be run or stopped as required. With the injection of CO_2, the asphaltenes mass calculations are made along with changes in the nominal diameter of the wellbore. Upon confirming the asphaltenes precipitation, the loop stops. In the case of no change in pipe diameter, the loop is repeated to change the CO_2 concentration pressure and temperature for a new iteration. Figure-5.1 is the schematic for the computational model used for asphaltenes deposition and precipitation in multiphase flow

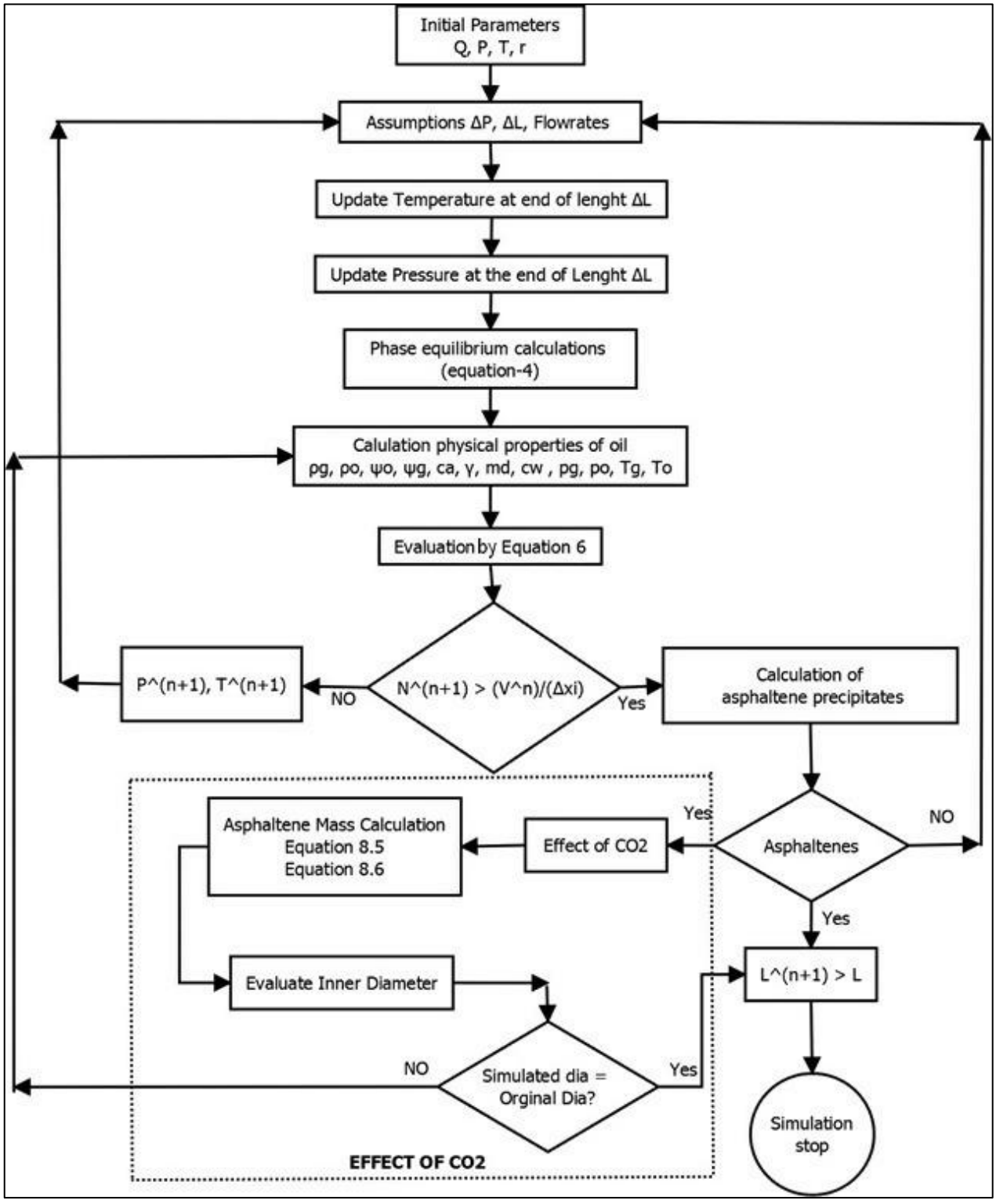

Figure 5. 5-2: Computational model for solid deposition in a well bore for both cases (with and without CO2)

ψ_o and ψ_g : oil and gas mass influx terms

ρ_g and ρ_o: oil and gas mass densities

γ: flocculation of solid particles from the reservoir

m_d : deposition rate of the solid particles

c_w : wax concentration in the crude oil

Ca: Asphaltene concentration in crude

5.4 Results and discussion

This study has considered a working example of an oil field for the analysis of asphaltenes deposition problems. The data of pressure-temperature profiles was available. The natural fractured reservoir has the pressure of 922Kg/cm^2 and temperature of 160 °C. The average oil produced by this well is 32°API and the average bubble point pressure is 132Kg/cm^2. The data of impact of phase behavior on asphaltenes deposition is already available from experiments conducted by the industry. This data includes the extended compositional analysis and asphaltenes phase boundaries. The SARA analysis provides a complete PVT analysis for the fluid. Table-5.4 provides the fluid characterization and composition of the fluid sample. Matlab was used for solving the equations 5.5 and 5.6 for asphaltenes deposition in every grid block. The programming in Matlab has been done according to the developed computational model in figure-5.2. The conditions for simulation are based on the assumptions described in section 4.1. Following are the results from simulations for the developed numerical model.

Figure-5.3 indicates that the maximum asphaltenes precipitation takes place at approximately the bubble point pressure, in which the solubility of asphaltenes is at a minimum. In fact, when gas is released from the crude oil, the asphaltenes components increase their stability and solubility in the oil.

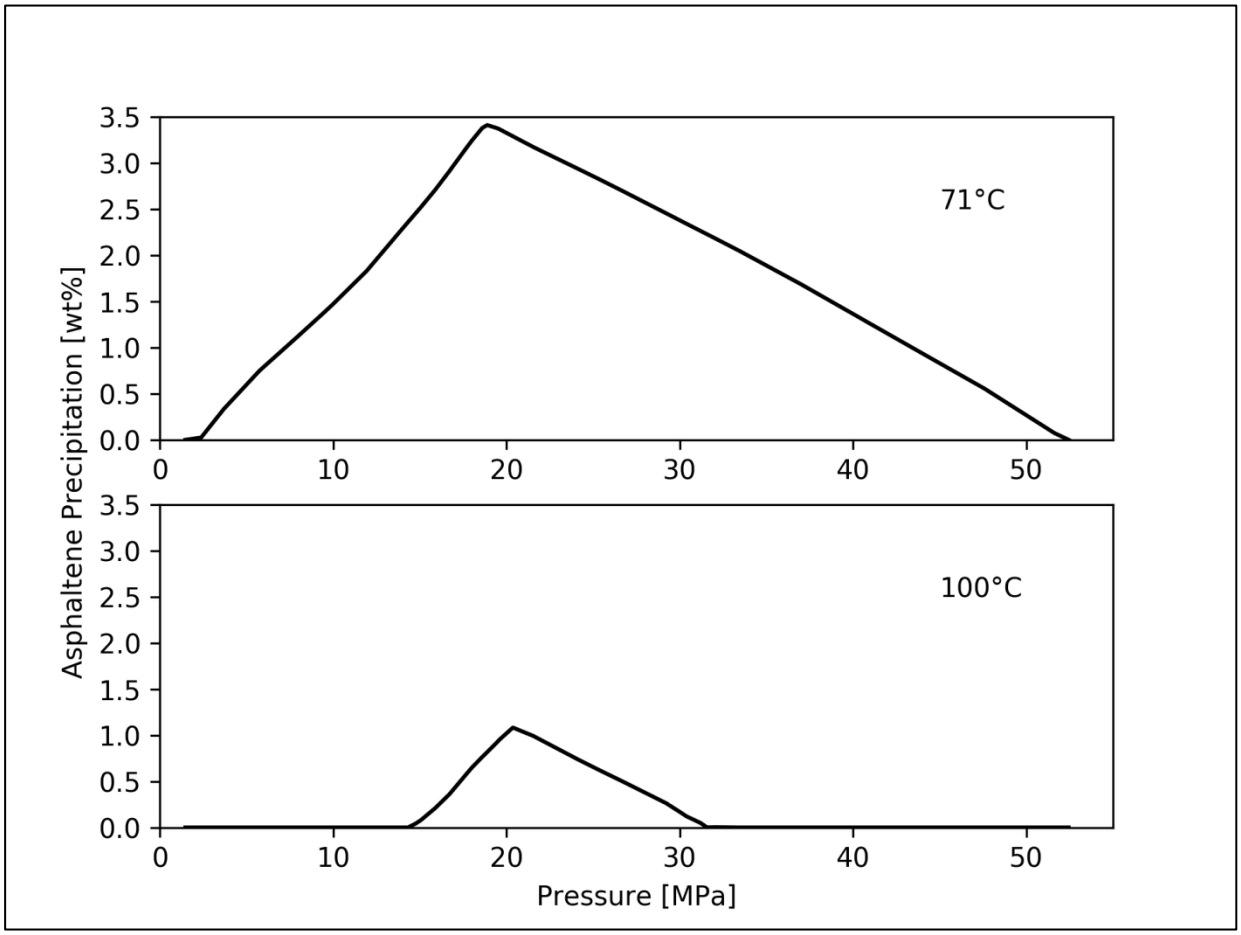

Figure 5-3: Weight percent of asphaltenes precipitation as a function of pressure at different temperatures.

The steady-state solution of the well is obtained at the initial time and then drawn on the vapor/liquid equilibrium and asphaltenes onset curve, as illustrated in Figure 5.4.

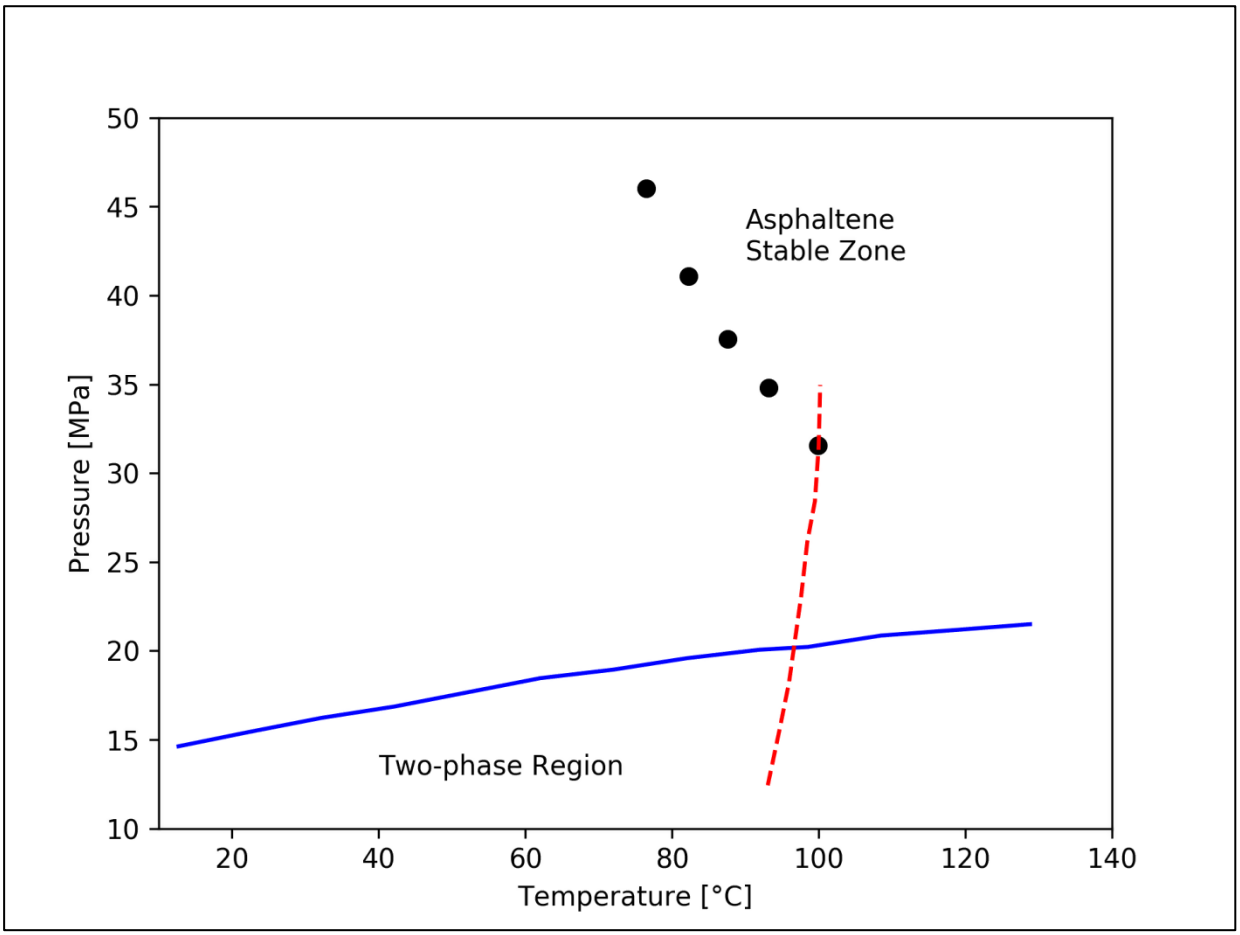

Figure 5 5-4: Pressure and temperature route from the bottom of the well to the surface

In figure 5-4 the pressure and temperature route from the bottom of the well to the surface is shown at at zero time (dashed red line), asphaltenes onset pressure (black dots) and fluid saturation line (solid blue line).

As evident, the pressure-temperature (P-T) path at initial conditions, as indicated by the blue line, shifts from the asphaltenes stable zone towards the asphaltenes unstable zone. At the same time, the blue line shifts towards the two-phase region. Therefore, according to this study, it is understandable that the well can hypothetically experience asphaltenes precipitation. Moreover, the study proceeds with the simulations for calculating the asphaltenes deposition rate and with measuring the quantity of asphaltenes precipitation accumulated in the well. A graph of asphaltenes precipitation as a function of depth is plotted for different temperatures in Figure-5.5.

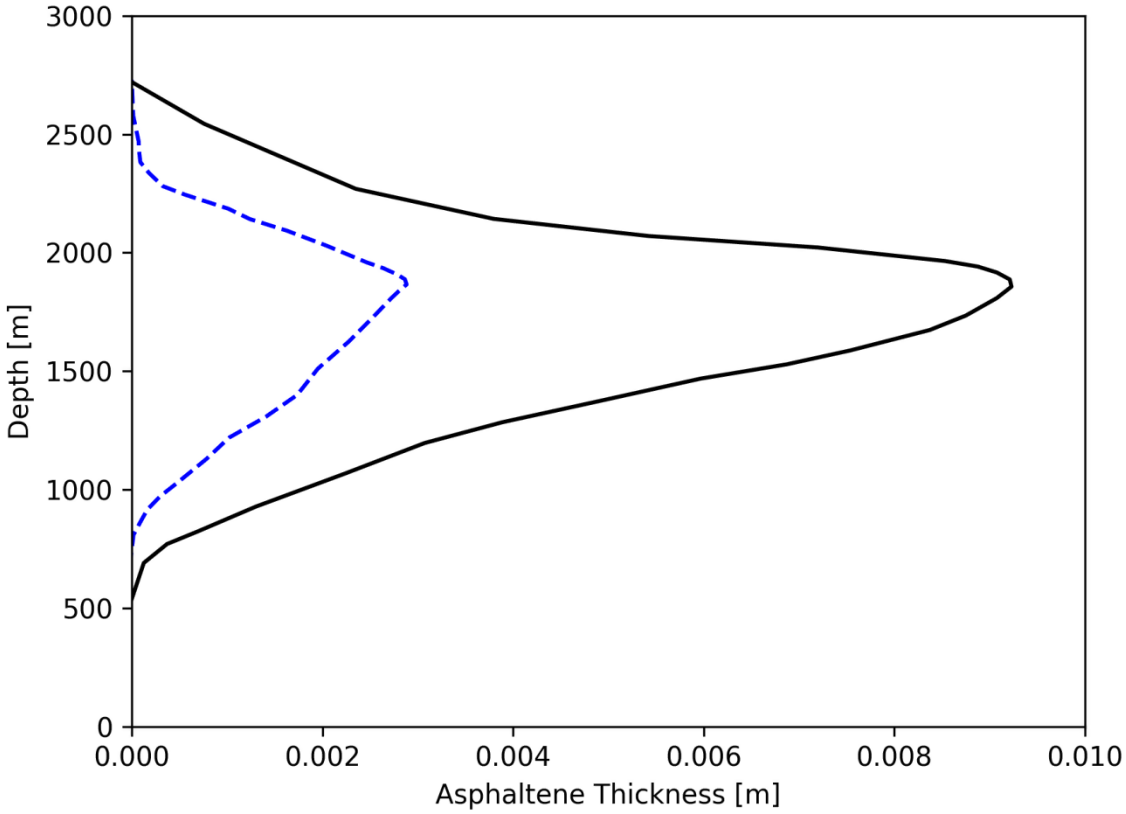

Figure. 5-5: Thickness of asphaltenes deposit on the inner surface of the wellbore at 20 days (dashed blue line) and 90 days (solid black line).

It is expected that more asphaltenes precipitation will be evident in the upper part of the well. This is because of the fact that temperature changes drastically in the wellbore, and the temperature of the wellbore is lower in the upper section. The magnitude of asphaltenes deposition and the rate of deposition in the wellbore can be obtained through conducting simulation runs for the wellbore. The wellbore's cross-sectional area is considerably changed by the asphaltenes deposition within the wellbore, as evident in Figure-5.5, which displays the profile of the inner radius of the well as a function of time. Evidently, the wellbore's cross-sectional area begins to shrink below 2030 m depth, although a minimum asphaltenes thickness is attained at 846 m below the surface. Small dents are observed at the surface of the precipitated asphaltenes as a result of the elimination of asphaltenes by shear forces. The remnant profiles of asphaltenes flocculated in the wellbore are shown in Figure-5.6. Indeed, the concentration of asphaltenes attains a maximum value at 846 m depth, and this behavior substantiates the maximum deposition at that instant.of the asphaltenes on the wall of the wellbore.

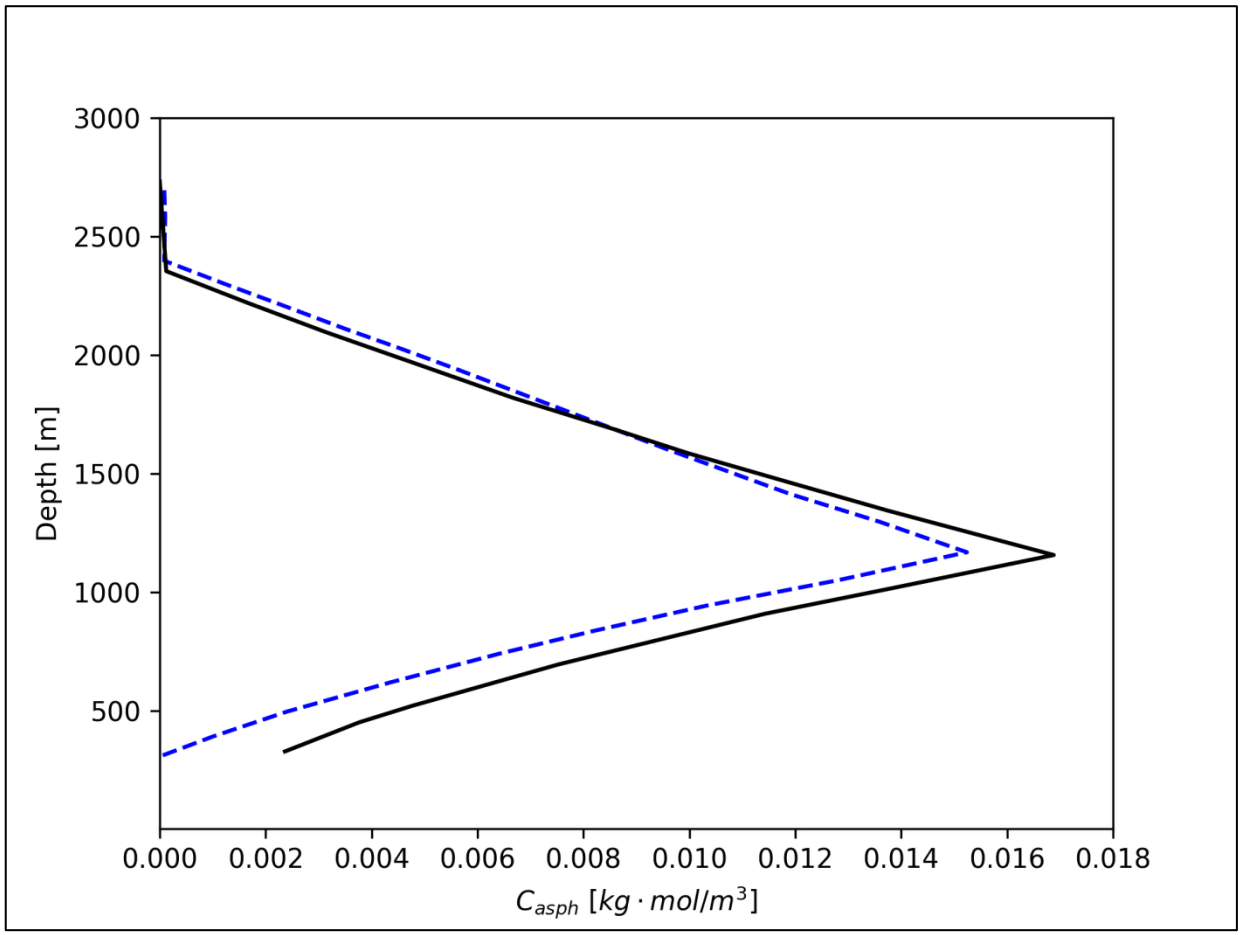

Figure 5-6: Asphaltenes concentration profiles with flocculate in the wellbore at 20 days (dashed blue line) and 90 days (solid black line).

Parameters such as pressure, temperature, and velocity profiles in the wellbore can subsequently change due to the deposition of asphaltenesparticles. For that reason, it also impacts the volume of fluid influx coming from the reservoir. It is important to note that the bottom-hole is pressurized by asphaltenes deposition because of blockage of the wellbore. This pressurization is also contributed to by the rise of frictional forces existing between the surfaces of accumulated asphaltenes and the flowing fluid. As a result, asphaltenes deposition minimizes the influx from the reservoir through the wellbore. Variations in the fluid temperatureinconsistently increase the asphaltenes precipitation while reducing the probability of asphaltenes sticking on the surface of the well. The variation of pressure at bottom-hole as a function of time is shown in Figure 5.7

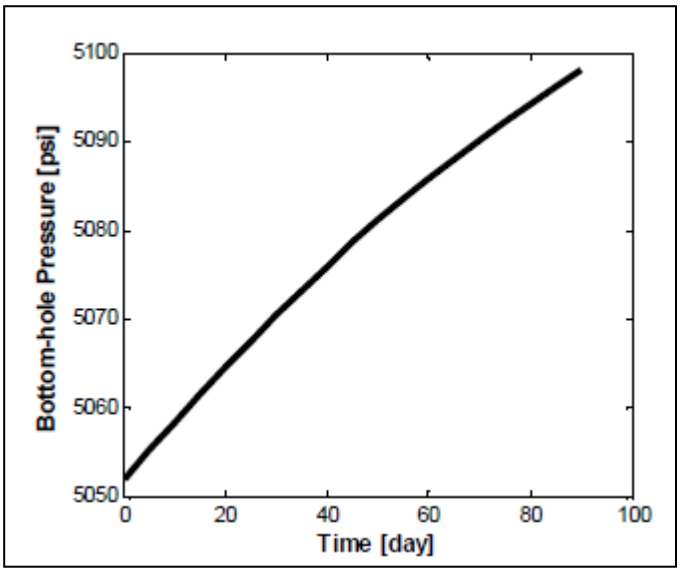

Figure 5 5-7: Variations in bottom-hole pressure due to asphaltenes deposition with time elapsed.

The asphaltenes particle blockage in the wellbore increases the pressure exerted at the bottom-hole as time elapses.

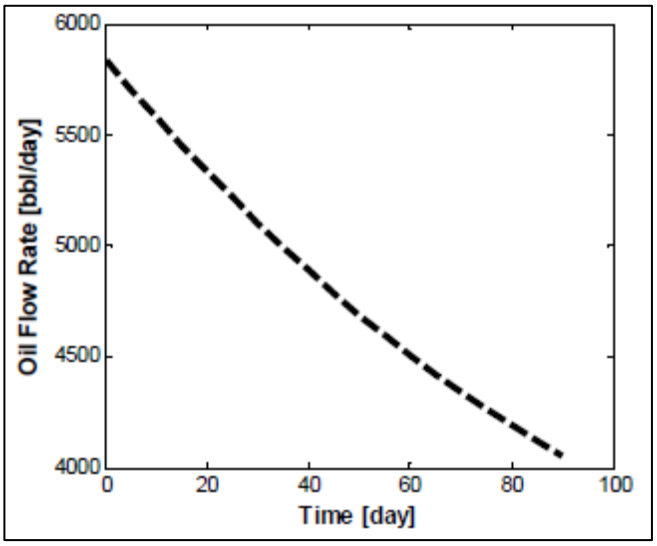

Figure 5-8: Changes of oil flow rate due to asphaltenes deposition with time progression.

5.5 Effect of CO_2 on asphaltenes deposition

This section shows the simulation of the effect of CO_2 on asphaltenes precipitation and deposition in the wellbore in general. Additionally, the simulation process targets capturing the condition where CO2 is extracted in the production well and is combined with the crude oil. In a previous study, Vargas (Vargas et al., 2009) demonstrated that the presence of light components or impurities in crude oil significantly alters the phase behavior of oil. The author has also claimed that asphaltenes lose stability when natural gas or CO_2 is injected with the oil. In Figure-9, it is clear that the results for the effect of CO_2 on the P-T phase are in accordance with Vargas's claims. Additionally, the input onset pressures as shown in Figure-9 (c)follow the same trend as the composition of oil after mixing with CO_2 in Table-5.4.

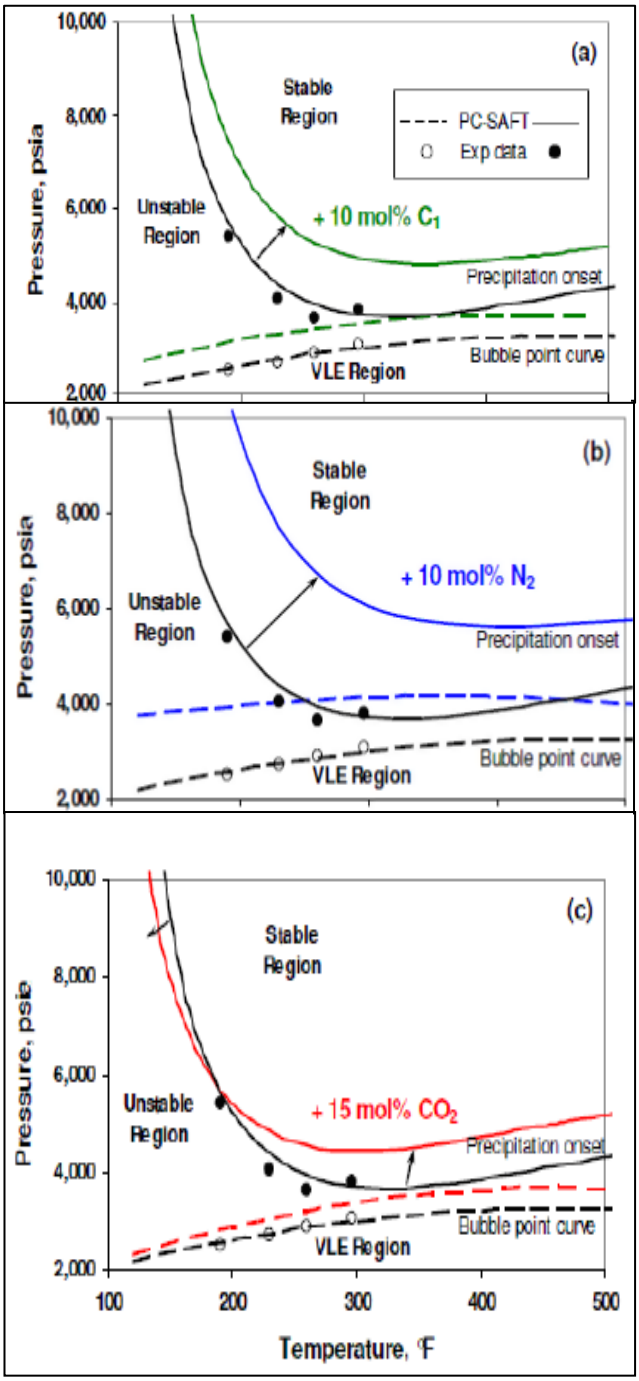

*Figure 5-9: Impact of light hydrocarbons mixing on the stability of asphaltenes in crude oil. A-Effect of methane, b-effect of nitrogen c-effect of carbon dioxide(*Vargas et al., 2009*).*

This section shows the simulation of the effect of CO_2 on asphaltenes precipitation and deposition in the wellbore in general. Additionally, the simulation process targets capturing the condition where CO_2 is extracted in the production well and is combined with the crude oil. In a previous study, Vargas (2009) demonstrated that the presence of light components or impurities in crude oil significantly alters the phase behavior of oil. The author has also claimed that asphaltenes lose stability when natural gas or CO_2 is injected with the oil. In Figure-5.9, it is clear that the results for the effect of CO_2 on the P-T phase are in accordance with Vargas's claims. Additionally, the input onset pressures as shown in Figure-9 (c)follow the same trend as the composition of oil after mixing with CO_2 in Table 4.

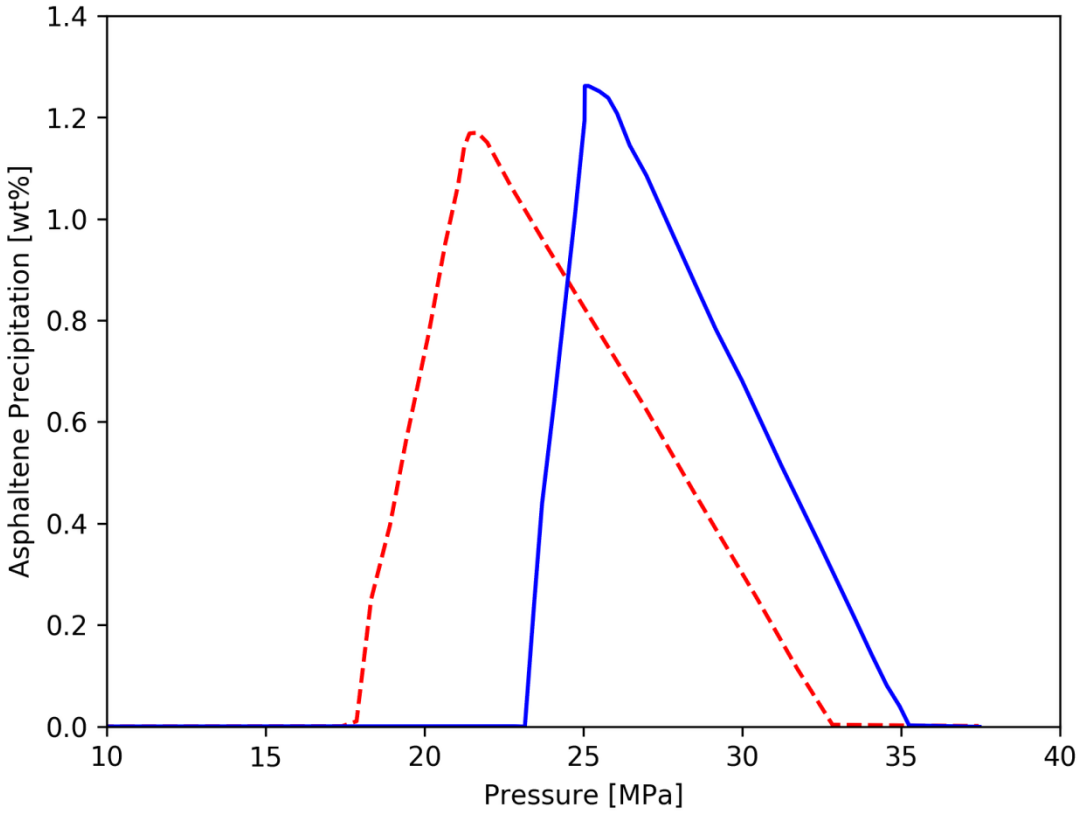

Figure. 5-10: Percentage by weight of asphaltenes precipitation in the presence of CO_2 with 5% of CO_2 (red dashed line) and 15% of CO_2 (blue solid line) at 100 °C

Similar input data were also used for the wellbore and reservoir geometries to ascertain the credibility of the results. The temperature of 100°C, the asphaltenes concentration profiles for different compositions of the reservoir oil were sampled and illustrated, as shown in Figure-11. The asphaltenes concentration is zero at the perforation depth in the well, and it begins to flash out from crude oil at lower temperatures and pressures within the upper sections of the wellbore. It is observed that the presence of higher amounts of CO_2 lowers the point of initial asphaltenes precipitation in the wellbore, as shown in Figure-5.11

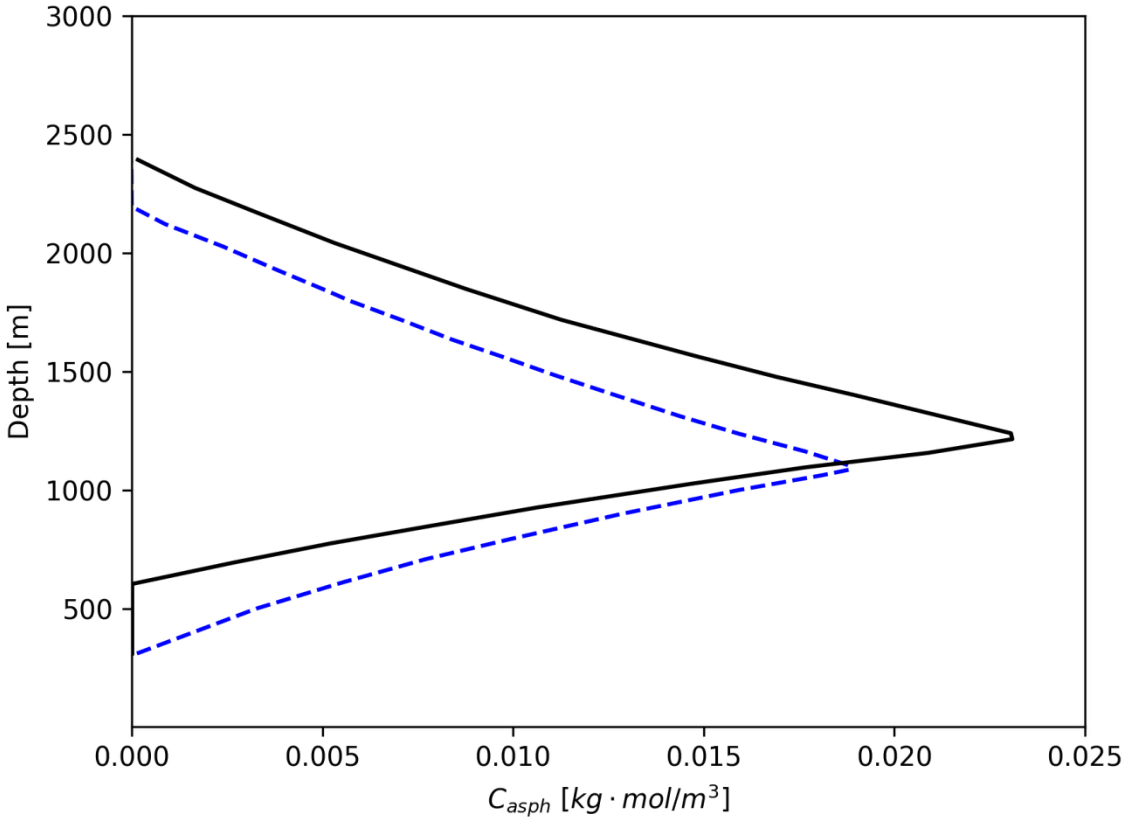

Figure 5. 5-11: The concentration of Asphaltenes with profiles shown at the conclusion of ninety days of production in the wellbore with 5% of the CO2 (blue dashed line) and 15% of the CO2 (black solid line).

Therefore, more asphaltenes accumulated at the bottom of the well when more CO_2 was in the production well. This simulation reveals that CO_2 can indirectly alter the pressure and temperature profiles through varying the velocity fields within the wellbore. As a final point, this section considers the propagation of asphaltenes deposition on the surface of the wellbore as illustrated in Figure-12

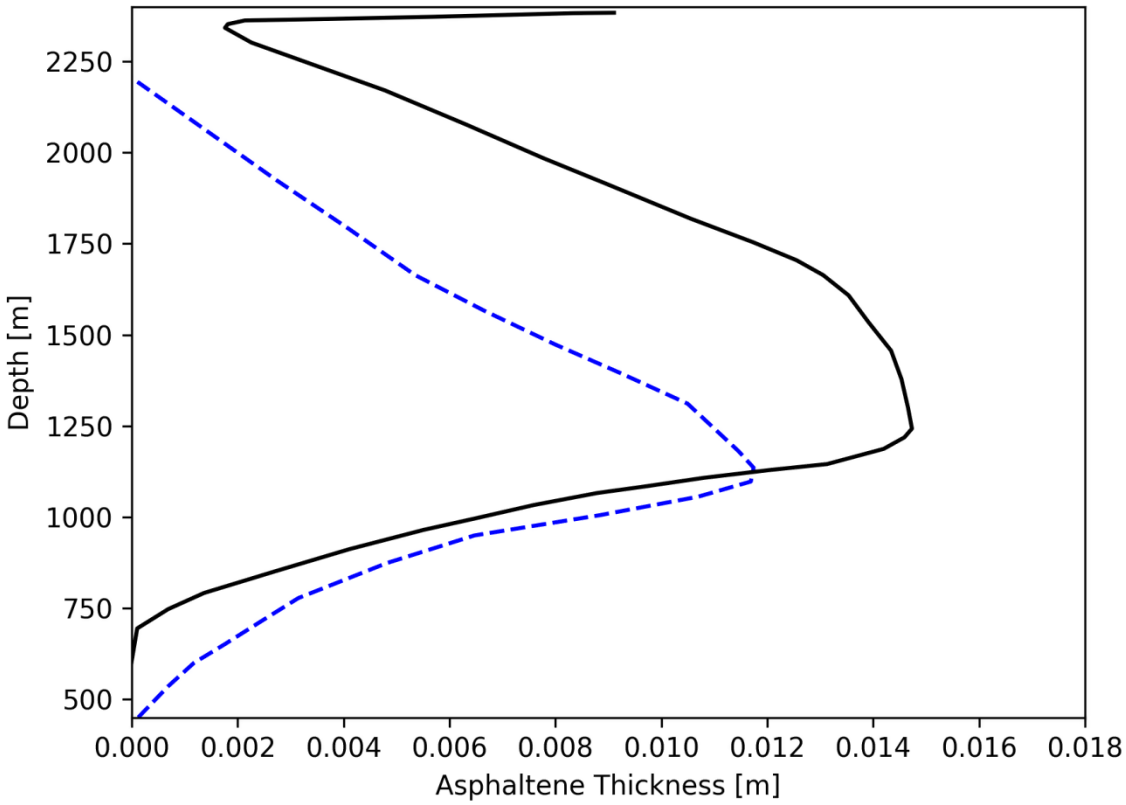

Figure 55-12: Asphaltenes deposition thickness profiles at the end of 90 days of production in the wellbore with 5% carbon dioxide (blue dashed line) and 15% carbon dioxide (black solid line).

The presence of CO_2 can cause plugging of the wellbore to occur at a faster rate than if it is absent, and its presence also moves the maximum plugged cross-section toward the bottom of the well during the deposition process

5.6 Conclusion

The asphaltenes prediction model was developed based on the finite difference method. The deposition problems in wells with proven records were simulated using the developed numerical model. It was observed from the results that the deposited layer of asphaltenes has more thickness at the upper part of the well due to the low temperature and pressure area, favoring the instability of the dissolved asphaltenes. It is noted that the maximum asphaltenes precipitation takes place near the bubble point pressure. The effects of velocity changes, pipe diameter, and pressure variations were investigated in this paper. It is found that a decrease in velocity decreases the heat exchange rates of the wellbore fluid and surroundings. Blockage in the wellbore increases the bottom-hole pressure with time. Additionally, the effect of CO_2 injection for enhanced oil recovery was studied, and it was found that asphaltenes become more unstable in the presence of CO_2.

CHAPTER 6 *Comparative study of density estimation of asphaltene structures*

6.1 Introduction

This comparative study of density estimation of asphaltene structures uses group contribution methods and molecular dynamic simulations for an Australian oil field

Natural asphaltene consists of a mixture of high-molecular-weight hydrocarbons with a chain of up to 150 carbon atoms. The colour of the structure lies between black and black–brown with the properties of a viscous fluid and a distinct smell. There are two kinds of natural asphaltene. One is the solid form which deposits and is mixed with asphalt Rocks (Masson 2008). The other type comes out from the ground because of cracks resulting from the formative movements of the crust of the seismic movements (Yousefi 2008). The natural asphalt has a chemical structure and chemical composition similar to the asphalt of petroleum, but differs in physical properties (Alobaidy 2010). Bad rheological properties of natural asphalt make useless for industrial application. Chemically, the structures of asphalt have two parts (Villaneuva and Zanzolto 2008). The first one is asphaltene which is insoluble in normal heptane or normal hexane, and the other is maltene which soluble in aforementioned. In addition, asphaltene is composed of polyheterogeneous aromatic rings substituted by the nitrogen, oxygen, and sulfur atoms of high molecular weight. It is soluble in carbon disulfide (CS2). The maltene part consists of saturated hydrocarbons, non-polarized aromatics, and the resin (representing polarized aromatics) giving the molecules the properties of high adhesion. These adhesive properties result in force of attraction between the components of asphalt and, thus, affect the behavior of physical properties when used for industrial purposes (Havog 2010).

Asphaltenes are regarded as solids of high molecular weight. Benzene and toluene, being aromatic solvents, are soluble in asphaltene while insoluble in paraffinic solvents (Speight et al. 1985; Eskin et al. 2011). Resins show solubility in less molar mass aliphatic hydrocarbons (n-heptane) and aromatic solvents (benzene and toluene) while insolubility in ethyl acetate (Aguilar et al. 2013). The heavy portion of crude oil is considered to be resins and asphaltene, made up of polar molecules. Both the structures include heteroatoms (nitrogen, sulfur, and oxygen) and metals (iron, vanadium, and nickel). Nevertheless, asphaltene comprises of a greater amount of metals and heteroatoms of larger molar mass and aromaticity (Aguilar et al. 2013; Mullins et al. 2003).

The major problem faced by oil extraction industry is the unstable behaviour of asphaltene formation, yet not fully predictable. The prediction of asphaltene formation depends on small changes in chemical characteristics and composition of the crude oil. Consequently, the study of molecular structure and molecular properties such as density is of a great practical interest. Other properties become very complex to assess when the asphaltene fraction contains 105 different molecules. Average molecular parameters are used to obtain information about asphaltenes. The density of the asphaltenes can easily be calculated and, thus, can be used to evaluate predictive capacities of the average structure. The present work of molecular dynamic simulations was carried out to evaluate the asphaltene densities of an Australian oil field.

6.2 Materials & methods

Two extra-heavy Australian crude oils obtained from two different wells of the same reservoir, named as crude oil A (6.2° API) and crude oil B (7.2°API) with temperatures at 25 °C, were identified as n-C7

asphaltenes source. The n-C7 asphaltene content of crude oil A and B was 12.6 and 11.5 wt%, respectively. The asphaltene fraction was isolated from crude oil as n-heptane (Sigma-Aldrich St. Louis, MO, 99%), as described in the previous studies.

The n-C7 asphaltene samples were named according to the crude oil employed, such as asphaltene A (AspA) and asphaltene B (AspB). The elemental analyses and molecular weight of both n-C7 asphaltene samples are shown in Table 6. 1. For the adsorption experiments, toluene (MerkK GaG, Germany, 99.5%) was used for re-solubilizing n-C7 asphaltenes extract in various mixtures of n-heptane + toluene (Heptol) at 0 (pure toluene), 20 (Heptol 20), and 50 v/v% (Heptol 50). Desorption experiments were conducted using different Heptol mixtures.

Table 6. 1: Properties and experimental densities of asphaltene structures

Asphaltene structure	Crude oil source	H/C	Density(g/cm^3)
BC5	Stable	1.23	1.17
BC6	Stable	1.15	1.16
MG27	Stable	1.11	1.19
MO21	Stable	1.22	1.17
MO29	Stable	1.11	1.19
CN	Stable	1.13	1.18
CO2	Unstable	0.96	1.23
BO7	Unstable	0.99	1.20
VG3	Unstable	1.05	1.22
FU1	Unstable	1.02	1.26
DTJ	Deposit	1.00	1.25
DTQ	Deposit	0.98	1.28
COAL A	Coal	0.55	1.52

6.3 Simulation details

Molecular dynamics and mechanics were performed to calculate the average structural densities of different asphaltenes. The molecular dynamic and mechanic techniques adopted were built in Discover 2.9, an Amorphous Cell of Molecular Simulations and Insight II commercial software programs. The calculations incorporated the consistent valence force field (CVFF). Previously, this field force was used to demonstrate the resin and asphaltene behaviour of aggregation and the amphiphiles activity as asphaltene stabilizers. Atoms charges are designated according to the CVFF database which remained unchanged during calculations.

Figure 6-1 shows the selected average asphaltene structures. These structures relate to asphaltenes separated from crude oil in Australia from various origins while applying the standard technique IP-143. Based on 1 h NMR, these structures were produced according to the previously described procedure. Six structures (CN, MO29, MO21, MG27, BC6, and BC5) of asphaltene were associated with stable crude oil. Four structures (VG3, FU1, BO7, CO2) with unstable crude oil, while rest of the two are associated with asphaltene extracted from deposits of solid taken out from the field, considering that one of the wells was the source of the solids.

Many former studies also reported these structures. Furthermore, ruthenium ion-catalyzed oxidation of the immature asphaltene was carried out to calculate the experimental data about the two different structures and densities. One of the two structures is reported to be Athabasca asphaltene (Azinfar et al. 2017) and the second proposed structure is associated with asphaltene of Arab crude oil structure.

The comparison of these structures with that shown in Figure 6-1 is described by the reduced number of rings per nuclei of aromatic. Moreover, for the structures under consideration, various molecules were utilized to analyze the methodology employed which does not indicate particularly any asphaltene portion, and also the effects of various structural parameters on the density calculations.

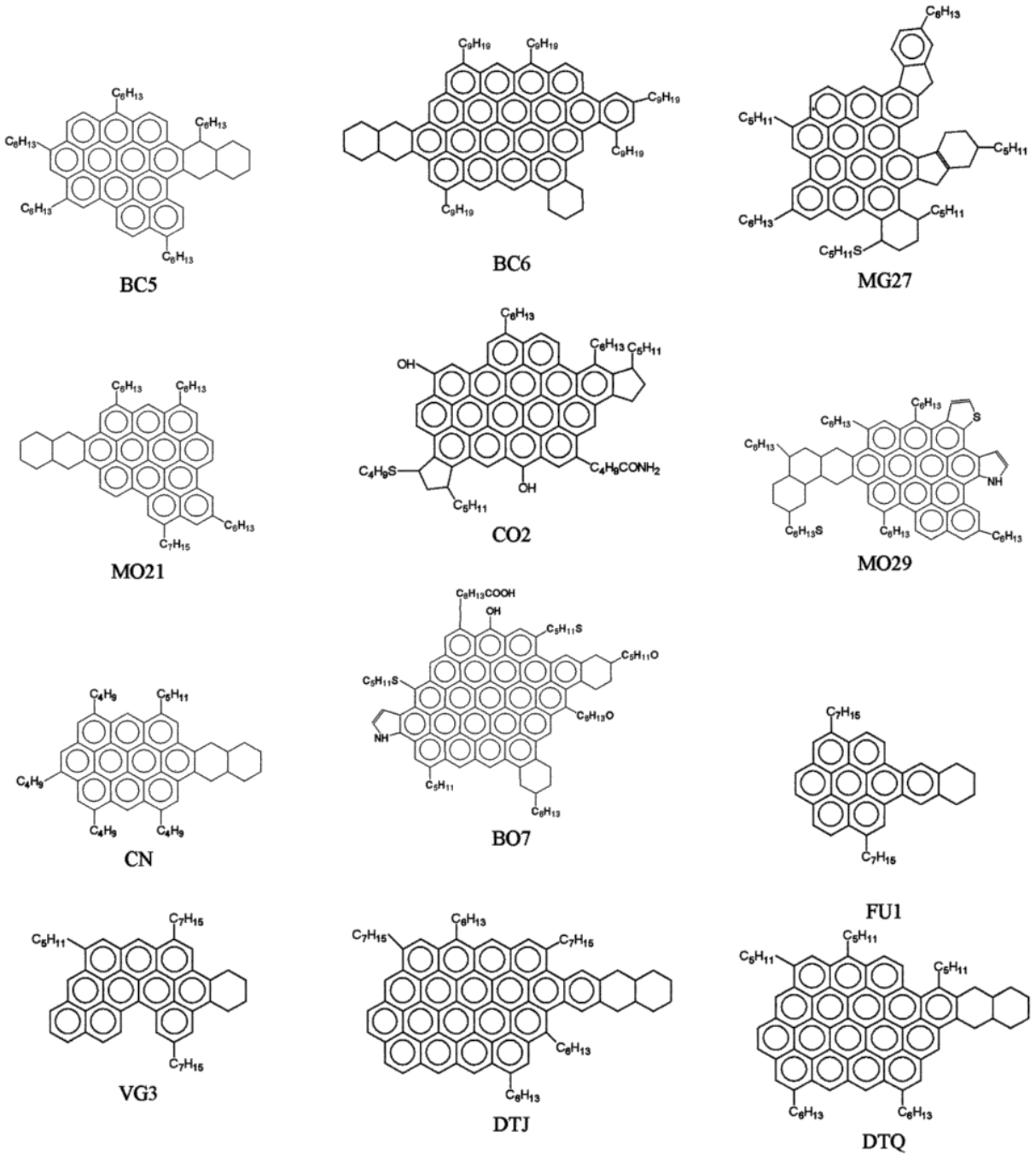

Figure 6-1: Asphaltene samples average structures

The procedure followed to get the optimized average structures for every asphaltene is as follows: minimization of the constructed model potential energy, after that the determination of molecular dynamics constant temperature NVT of 10 ps. The calculation of molecular dynamics used in the setup was in order of five arrangements from lowest energy, followed by the reduction of potential energy so as to decrease the energy even further.

Five amorphous structures were generated using these five molecules based on best five conformers (BC5, MO21, CN, DTJ, and FUI). The hydrogen-to-carbon (H/C) ratio and density (F) correlation established on the experimental data were calculated for the initial density of these structures.
The following is the correlation:

$$\rho = 1.3447\frac{H}{C-0.5396} \qquad r^2 = 0.9666 \qquad \text{Eq. 6-1}$$

This correlation included materials related to crude oil-containing processed and virgin crude oils, achieved using the experimental data.
The former procedure was followed to obtain the five amorphous structures which were further relaxed to reduce energy while exposing these structures to simulated annealing, i.e., 5000 ps cycles repeated five times from 200 to 500 K, adopting the molecular dynamics (NVT). The structure was reduced again at the end of every annealing cycle, aiming to stop the minima of metastable regional high energy. The purpose of this procedure was to stop the metastable local high-energy minima
Molecular dynamics for isothermal-isobaric (NPT) were operated for 300 ps at 298 K. Every NPT operation started along 50 ps of an equilibration phase, i.e., 50,000 steps per time steps (1 fs). Densities' data were compiled along with the final 100 ps. Figure 6-2 shows the calculation procedure of the scheme
.

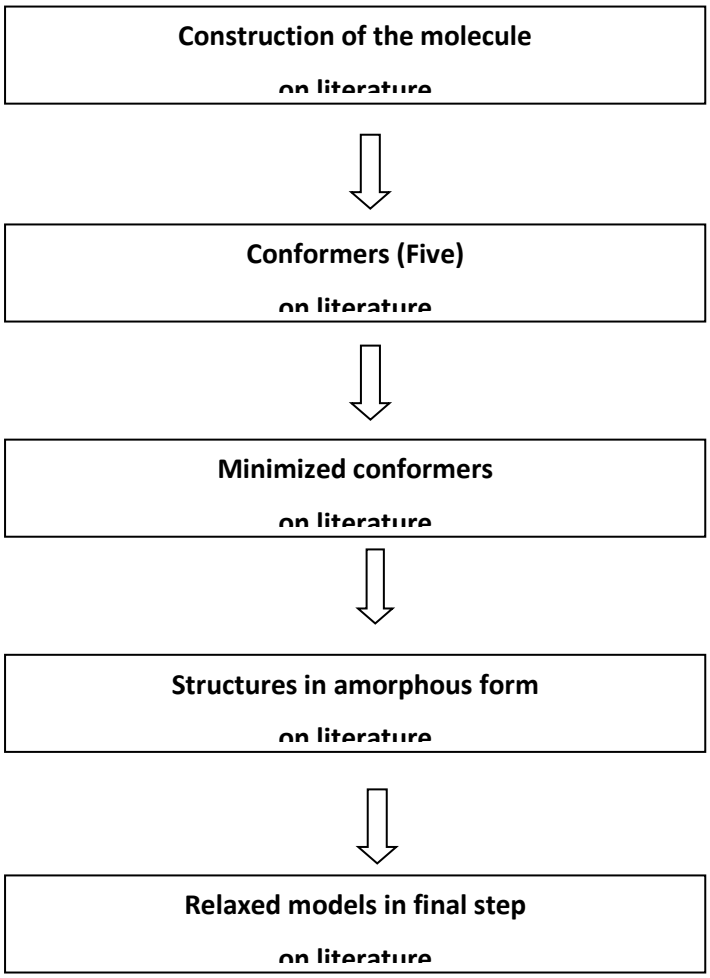

Figure 6-2: Density calculation using simulation

Isothermal and isobaric molecular dynamics were initiated at 300ps and 298 Kelvin. The molecular dynamic process started at 50ps that is 50,000 steps at 1fs. At 100ps, the compilation of density data was done. In figure 2, the schematic information is given for the calculation procedure.
Density measurement:

A standard glass pycnometer was used to measure asphaltene density. To displace the fluid, n-heptane was used, while the capacity of pycnometer was measured as 10 cm^3. The following steps were taken in the procedure: the pycnometer was introduced with a sample weight of 0.50–0.55 g. Afterwards, the addition of 9–9.5 cm^3n-heptane was done while removing the air bubbles trapped by ultra-sonication technique. The n-heptane was filled in the pycnometer followed by immersion and thermostated at 25 °C in a water bath. The stopper is pushed tightly in place. After some time, pycnometer is taken out and weighed before drying. In the next step, the volume of asphaltene is determined. The volume of n-heptane was calculated by determining density and mass at operating temperature reported previously. The ratio of calculated density and mass is used to determine the asphaltene density. The calculations were precise to a figure of the second decimal. The absolute derivations were found to be 0.02 g/cm^3.

Aromaticity Determination: The aromaticity of carbon was calculated using a 13C nuclear magnetic resonance. Spectrometer (Brucker ACP-400) was set at a frequency of 100.614 MHz to determine the

spectra. Afterward, samples were mixed in CD2Cl2 and 0.2M of Cr-III acetylacetonate was added. To suppress the overhauser effect, an opposite gated decouple method was followed.

6.4 Experimental densities

Experimental densities calculated for the chosen asphaltene are shown in Table 6. 1 comprising a Venezuelan coal sample utilized as a reference. A comparison was made between the obtained experimental values to the same values produced by various methods for coal and materials related to crude oil Figure 6.3 The similarity of densities with reported ones was found by this comparison through employing more sophisticated approach, despite being marginally on the lower side. As previously reported, the preferred samples consisted of asphaltene produced from stable/unstable crude oils and deposits. The nC_7 insoluble/toluene and soluble materials are regarded as asphaltenes.

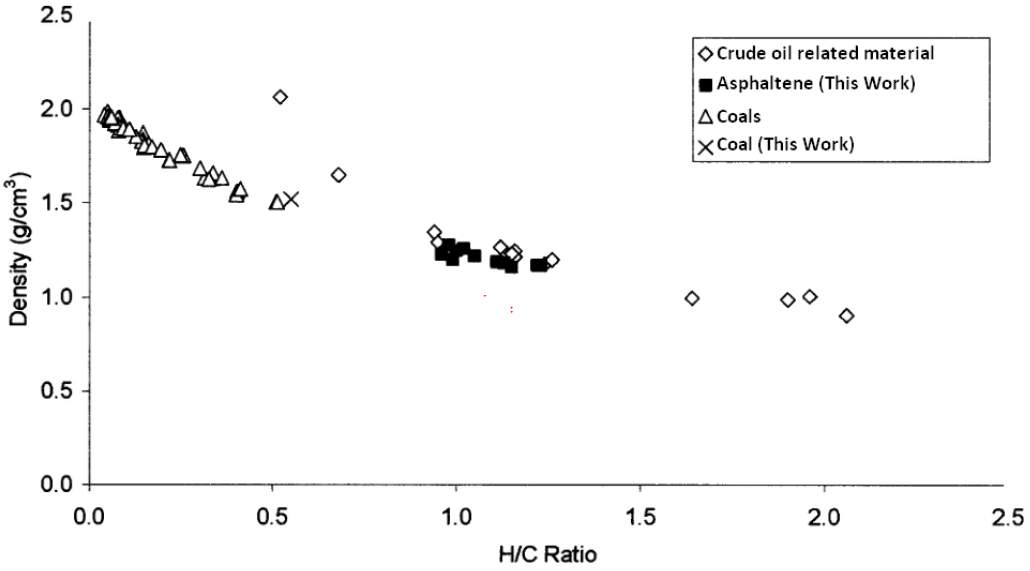

Figure 6-3: Experimental densities comparison

Since polyaromatics density is closely linked to molecular topology, the relationship among the structural characteristics and density of asphaltene is worth evaluating. In Fig. 6.4a the experimental densities are presented as a function of hydrogen-to-carbon ratio, while Fig. 6.4b shows the aromaticity of asphaltene. Asphaltene obtained from stable crude oil is certainly isolated from asphaltene produced from unstable crude oils and solid deposits in these figures. The results show that, by comparing asphaltenes produced from stable and unstable crude oils, the later one exhibited higher density, reduced H/C ratios, and larger aromaticities. This trend has been observed in the previous studies for various samples

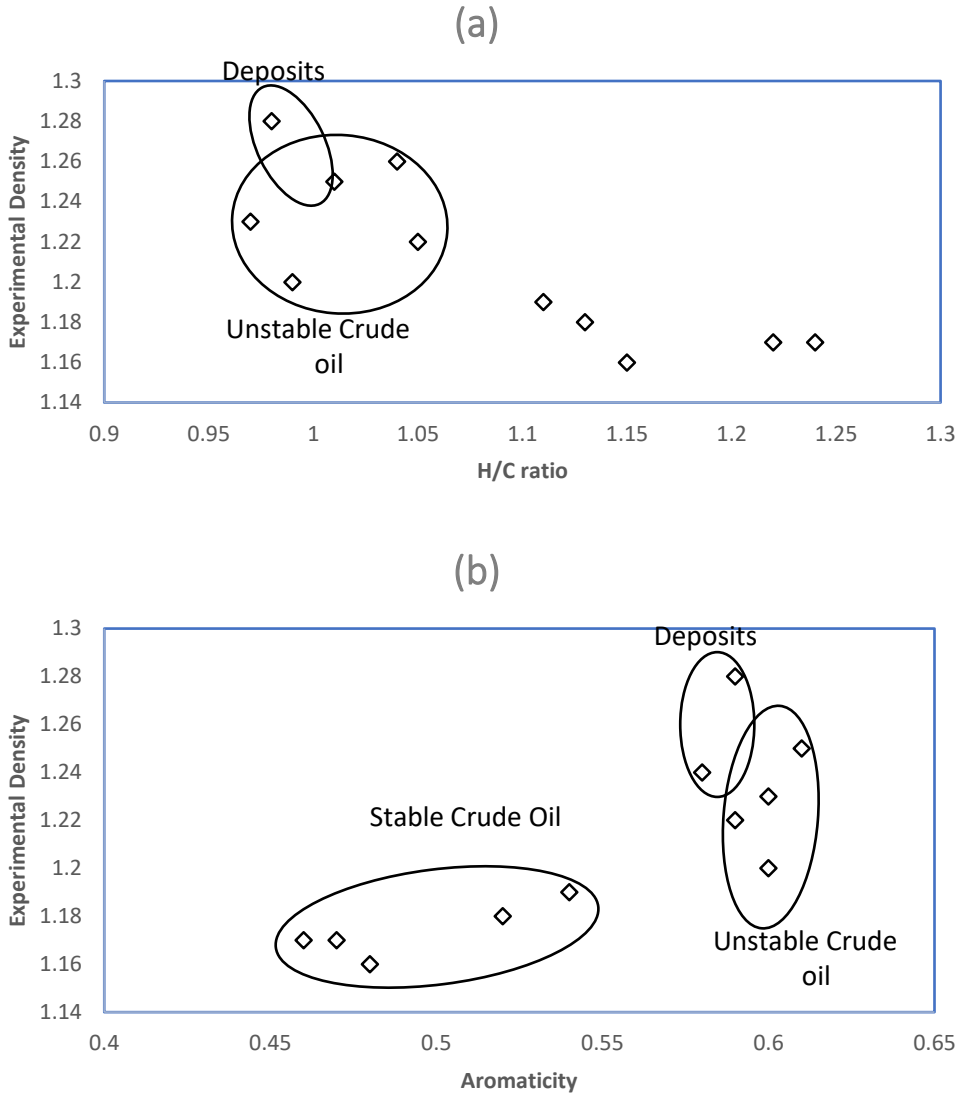

Figure 6-4: Experimental densities as a function of (a) h/c ratio (b) Aromaticity of asphaltene

Since poly-aromatics density is closely linked to molecular topology, the relationship among the structural characteristics and density of asphaltene is worth evaluating. In figure 5(a), the experimental densities are presented as a function of hydrogen to carbon ratio while figure 5(b) shows the aromaticity of asphaltene. Asphaltene obtained from stable crude oil is certainly isolated from asphaltene produced from unstable crude oils and solid deposits in these figures. The results show that by comparing asphaltenes produced from stable and unstable crude oils, the later one exhibited higher density, reduced H/C ratios, and larger aromaticities. This trend has been observed in the previous studies for many samples.

6.5 Calculated densities

Figure 6.1 indicates that, for each average structure, there are five of independent amorphous configuration generated, i.e., BC5, MO21, CN, DTJ, and FUI. This figure was used to estimate the densities according to the procedure previously described.

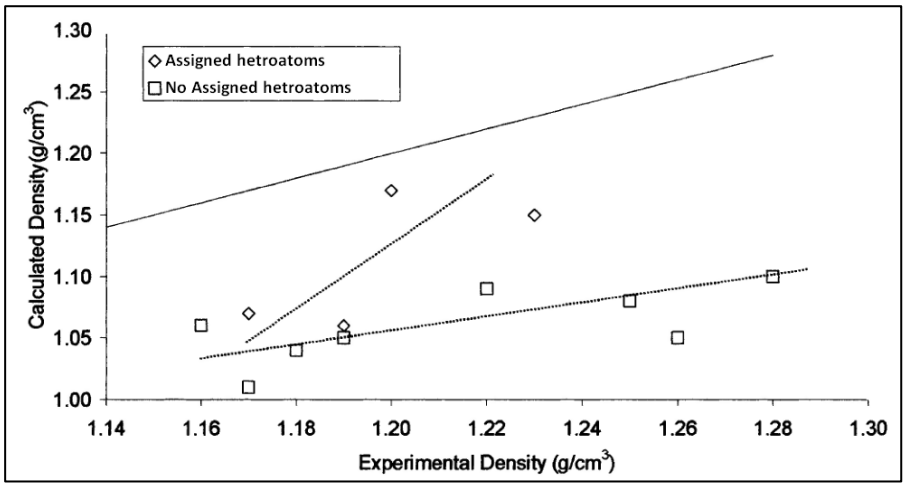

Figure 6-5: Comparison between experimental and calculated densities through molecular modelling

6.6 Effect of hydrogen imperfection

In this section, two different models are being used: an amphoteric fraction representative structure confirmed earlier and a speculative structure of asphaltene with the same H/C ratio and molecular weight. These two molecules were altered to reduce their H/C ratio. To this extent, the structures were gradually eliminated by methylene and methyl groups and after every step and the density was calculated. In addition, the generated structure density was plotted as a function of the hydrogen–carbon ratio at each step. It was observed that higher the density, lower the H/C ratio. Interestingly, the values of density achieved for amphoteric molecule (A) are consistently below than those evaluated for asphaltene model (B), which represents differences associated with molecular topological characteristics like connectivity, locations of chain, and ring size

6.7 Effect of the poly-aromatic nuclei size

Poly-aromatic nuclei size is considered as one of the major differences among the molecules. However, the molecular weight, H/C ratio, and content of heteroatom are the same in both the models. Therefore, it is supposedly possible that density differences might be, at least, moderately ascribed to differences in ring sizes of poly-aromatic compounds. Poly-aromatic rings including amphoteric model are significantly smaller than the asphaltene model being used. Study of various structural modification effects on molecular calculated densities: two more structures were studied containing poly-aromatic rings, relatively small in size. Athabasca asphaltene corresponds to the first structure, while the second structure to an isolated asphaltene extracted from a combination of Arabian crude oil. These structures were acquired from ruthenium ion-catalyzed oxidation. According to these structures, density values were estimated as 1.03 g/cm3 for Athabasca and 1.00 g/cm3 for the Arabian mixture. However, the experimental density of Athabasca asphaltenes, in references, was found to be 1.16 g/cm3. On the contrary, average structures density results with designated heteroatoms (Table 1) differ from 1.06 to 1.17 g/cm3. Bigger poly-aromatic rings are present in these structures when compared with Arabian and Athabasca asphaltenes. By comparing both sets, the values show the existence of bigger poly-aromatic nuclei which tends to increase the structure densities

6.8 Effect of the connectivity

Asphaltene from Athabasca and Arabian mixture were treated as samples. Four molecules were extracted by splitting both molecules. Afterward, the calculations for both sets were made. Both the set of molecules yields 1.00 g/cm3from using this calculation. The results show no significant density differences for the molecules considered as a whole (1.00–1.03 g/cm3) or the parts of the set in the evaluations (1.00 g/cm3)

.

6.9 Effect of heteroatoms

Considering a few molecules here, the calculations of densities were done for both assigned and unassigned heteroatoms. The comparison in Fig. 6.6 shows that the addition of heteroatoms to the structure of molecule results in a minor rise in the trend for the calculated density. Consequently, this effect may be associated with the introduction of heavy atoms in the molecule and increasing the molecular inter-actions. Certainly, this final feature is related directly to a location inside the molecule and the functionality type.

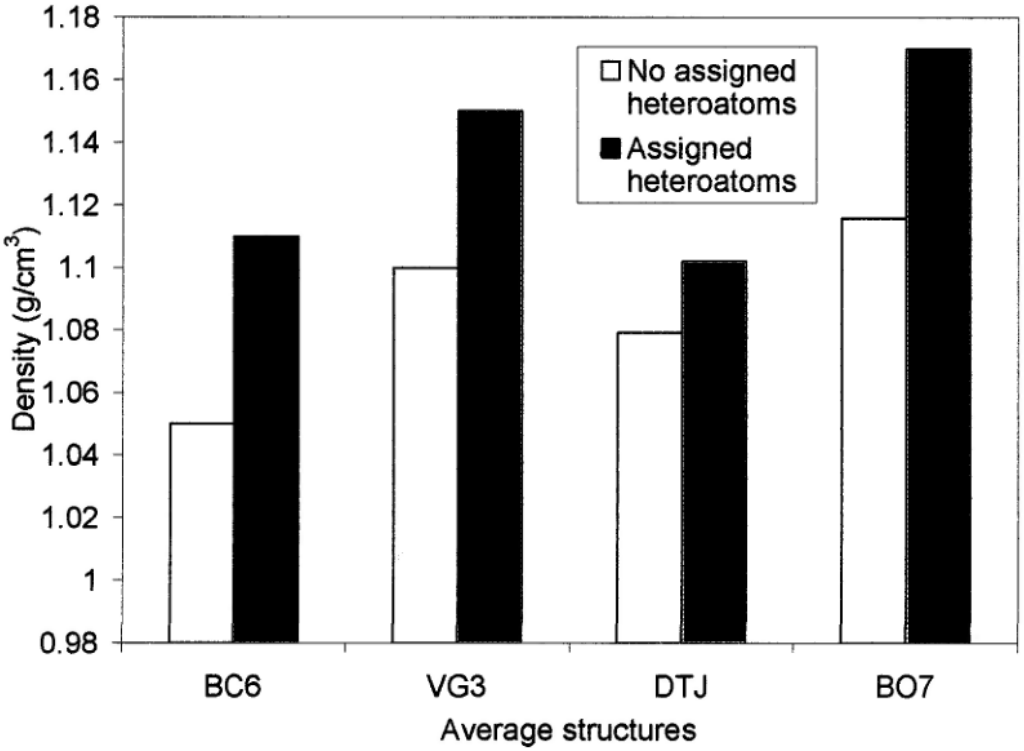

Figure 6-6: Effect of Heteroatoms on density (calculated)

6.10 Molecular dynamics comparison with group contribution technique employed to calculate poly-aromatic density

Currently, a new technique is devised for molar volume calculation of hydrocarbons consisting of condensed hydrocarbons of poly-aromatic. The application of this technique has successfully explained the molar volume of those heavy hydrocarbons which behave as a liquid with sticky nature or crystalline solid at 298 K. The results obtained clearly indicate excellent behaviour compared to other similar results

According to researchers, this recent group contribution method is appropriate in poly-aromatic hydrocarbons case with up to number seven aromatic rings. It is also used to calculate asphaltene density. The suggested technique uses basic structural data to produce the molecule molar volume as

a total individual group of structural improvements that build the molecule. The provided hydrocarbon of molar volume according to this technique is denoted by Vm:

$$Vm=32.8+16.3Nt-39.6Nar-19.6Nnr+2.8Nac+8.6Nai \quad \text{Eq 6.2}$$

Where Nt, Nar, Nnr, Nac, and Nai represent the carbon total number, aromatic rings number, naphthenic rings number, aromatic conjunction atoms number, and the number car-bons in aromatic inner, respectively.

The comparison among two sets of densities calculated by group contribution technique and molecular dynamics is shown. In case of similar results yielded by experiments and calculations, the solid line represents the dropping point. As observed, the values of densities produced by the method of group contribution are higher than the molecular simulation method, however, still below the experimental values. The technique involving group contribution which dominates the technique involving molecular dynamics is because of the development of group contribution method on a broad range of various molecules. Therefore, in certain aspects, the results obtained illustrate an average of isomers that the technique cannot differentiate. For example, Eq. (2) can-not distinguish among molecules with a similar amount of aliphatic chains and different aromatic locations or among molecules with a similar amount of aliphatic carbons but altered chain lengths. However, different calculated densities can be achieved by different isomers when the molecular dynamics technique is employed. In addition, for every calculation, only one molecule was treated. This provides a natural convenience for a technique like a group contribution technique, in which various molecules are averaged over a significant number. Expectations for improved calculated densities are made by introducing additional molecules. For example, a mixture of various molecules describes an asphaltene sample

The calculated densities can be further improved in two ways: first, partly removing the effect of various isomers; second, improvement in packing can be made by the existence of various sizes of molecules in similar volume. An essential part is played by the last effect for correlation of low calculated densities in the current work by applying molecular dynamics. New progress in discovering these hypotheses is made. As shown in Fig. 6.7, the calculated values of both sets correlate well with the correlation coefficient (0.848). This illustrates that the graphical description and molecular parameters provide qualitative correct information. Thus, information acquired predicts trends in the values of density including alternative thermodynamic properties. Currently, it is obvious from the results that calculation of precise values of properties cannot be done by average structures for asphaltenes by simulations of the molecule.

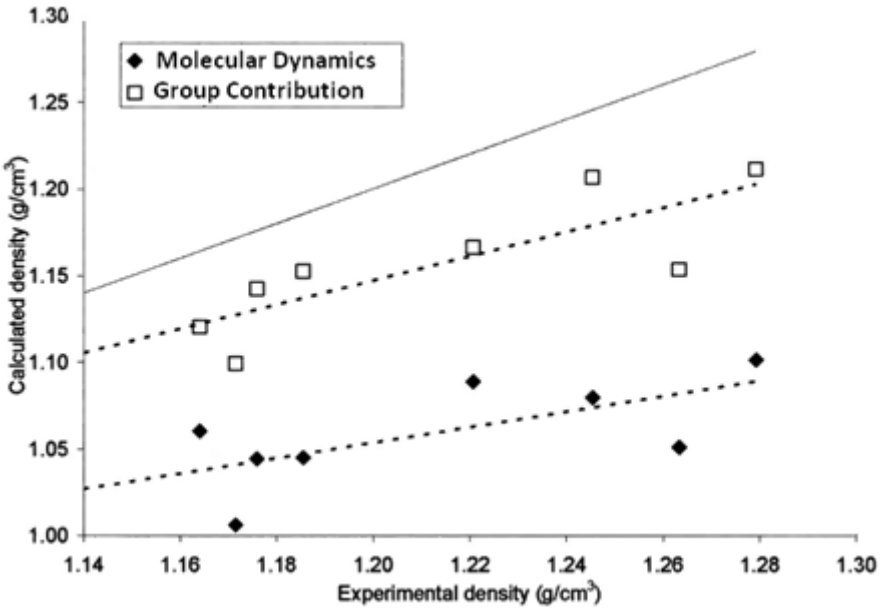

Figure 6-7: Comparison between experimental and calculated densities through molecular modelling

Furthermore, the molecular dynamic simulations can be developed as a tool to improve average structure method by fitting the calculated properties. Moreover, simulations for molecular dynamics need improvement in an average structure in terms of testing various isomers and adjustment of calculated to experimental properties. Consequently, density is considered a potential parameter for adjusting its experimental determination which is easy and dependent on molecular structural characteristics

Group contribution technique was found to provide better results than that of molecular simulations that carried out. Nonetheless, it is essential to note that, in a few standard pressure–temperature conditions, each group contribution produces only one value of a specific property. Contrarily, if an optimized method is introduced for developing molecular simulations for average structures, a broad range of thermo-physical properties can be determined under different conditions. This present study is one step towards the development of an advanced methodology to link thermo-physical properties and molecular structure of asphaltene

It was seen that group contribution technique is a relatively better technique than the molecular simulation method that is being used as it gives improved results. Yet it is important to know that certain perimeters like pressure and temperature gives only one value for each contribution. On the other hand, if the same process is used for optimized method, the current simulation method can give many thermo-physical properties each with a separate condition of temperature and pressure. This is an important leap towards the advancement of the technology in understanding the physical properties of the structure of the asphaltenes.

6.11 Conclusion

Higher densities, lower H/C ratios, and high aromaticities are attributed to asphaltenes from crude oil of unstable nature and deposits, as compared with stable crude oil asphaltenes. The results indicated that the chemical data supplied by average structures and molecular parameters show the essential accuracy that can be used to calculate the densities qualitatively. Asphaltene density estimation,

treating average structures through simulations of molecular dynamics, though liable to huge errors, still provides results that have the precise range and qualitatively accurate. Furthermore, the asphaltene average structure affected the modification of density by this technique and thus proves to be a significant tool to enhance the representation of a condensed structure. The low ratio and large rings of condensed poly-aromatic are associated with the highest densities yielded by the average structure of asphaltenes. Using molecular dynamics, the large variations established between calculated and experimental densities can be mostly ascribed to the particular molecule to define asphaltene which results in poor packing leading to lower densities. To enhance the linking between experimental and calculated densities, a calculation based on group contribution was examined. Finally, a significant role of asphaltene density on asphaltene solubility was observed

CHAPTER 7 *Novel perspective for scaling equations of asphaltene precipitation within an Australian crude oil*

7.1 Introduction

Asphaltene precipitation models, based on study of Mohammadi et al. (M. Mohammadi, Safari, Ghasemi, Daryasafar, & Sedighi, 2019) are classified into five main groups, including 'association equation of state (EoS)' based models, 'scaling laws, 'activity coefficient' based models and 'colloidal/micellization' models.

The advanced equation of state models have been developed based on the models of Ting et al. (David Ting et al., 2003), Wu et al.(Wu et al., 1998), Andersen et al(Simon I Andersen & Speight, 1999)., Buenrostro-Gonzalez et al.(Buenrostro-Gonzalez et al., 2004), Tabatabaei-Nejad and Chacón-Patiño et al.(Chacón-Patiño, Rowland, & Rodgers, 2017) and Dehghani and Sefti(Dehghani, Sefti, Ameri, & Kaveh, 2008), Nikookar et al.(Nikookar, Pazuki, & Masoudi, 2005) and the developed PR and SRK EoS's. A more applicable form of Flory -Huggins equation was developed later by Mohammadi and Richon(A. H. Mohammadi & Richon, 2007). A new thermodynamic model for asphaltene deposition was recently developed in which the Flory- Huggins solution theory is combined with the chemical theory of association solution.

In this modelling approach, precipitation process is known to be reversible. The Hirschberg model is based on the assumption that asphaltene is the only precipitating phase, while Cimino et al.(Cimino et al., 1995) model is based on the assumption that non-asphaltene components are also present in the precipitating phase. Scaling equations-based models have been much attended during the last two decades.

The simplicity of scaling models is that asphaltene properties are not required for the modelling. The first scaling equation was developed by Rassamdana et al. (Rassamdana et al., 1996) at constant temperature with exponents Z and Z'. The effect of composition and temperature was studied by Hu and Guo (Guo et al., 2006) to predict the onset and amount of the precipitated asphaltene.

This method was applied for core flooding experiments and the amount of precipitated asphaltene was measured. Rassamdana et al.(Rassamdana et al., 1996) equation was modified, and a new scaling equation was developed by Soulgani et al.(Soulgani, Jamialahmadi, Rashtchian, & Tohidi, 2009) for live oil at many temperatures and pressures. Moreover, the model was optimized by adding some physical properties including onset pressure, critical temperature and bubble point pressure. Manshad et al.(Manshad & Edalat, 2008) model was developed by including temperature, pressure, dilution ratio and molecular weight to determine the onset of asphaltene precipitation and total amount of it by using many solvents.

Over the last decades, artificial neural networks have been developed, which require large sets of data to develop a model with many adjustable parameters. Deficiencies of these models include uncertainties and over fitting and under fitting of data. Least square support vector machine (LSSVM) is another technique for solving complex and nonlinear problems with more accurate results in comparison to other existing intelligent methods. Hemmati-Sarapardeh et al. (Ameli, Hemmati-Sarapardeh, Dabir, & Mohammadi, 2016) recently applied this method to predict the amount of asphaltene precipitation during natural depletion.

This study will discuss models based on asphaltene precipitation titration data; models based on asphaltene precipitation during natural depletion of reservoir; and quality of the previous experimental data.

7.2 The scaling equation

Modelling asphaltene precipitation using PC-SAFT (the P=perturbed-C=chain S=statistical-A=associating F=fluid T=theory) and the analysis of SARA (S=Saturate, A=Aromatic, R=Resin and A=Asphaltene) of crude oil has been in continuous development through the recent years (Gonzalez et al. (Gonzalez, Vargas, Hirasaki, & Chapman, 2008); Pannapala et al.(Panuganti, Vargas, & Chapman, 2013); Tavakkoli et al.(Tavakkoli, Panuganti, Taghikhani, Pishvaie, & Chapman, 2014)).
Generally, these developments followed exactly the same lumping procedure but differed in the methodology for parameter estimation. Because SARA analysis can be used to characterize the STO (stock-tank oil), this characterization procedure is known as the SARA-b aced method. The description of the SARA-based method in this section follows the most recent development as implemented by Punnapala and Vargas (Panuganti et al., 2013)for mono-disperse asphaltenes and Tavakkoli et al. (Tavakkoli et al., 2014)for poly-disperse asphaltenes. The two approaches differ only in the characterization of the asphaltenes pseudo-fraction.
However, in order to predict the phase behaviour of asphaltenes, experimental results are not sufficient on their own . The extensive controlled experimentation on crude oil while trying to keep the similar reservoir conditions adds to the cost and makes such research impossible due to financial constraints. The models proposed by researchers for asphaltene deposition have been divided into two general groups' i.e. Thermodynamic models and solid colloidal models.

7.3 Thermodynamic Model

The thermodynamic approach comprises of the solubility parameter models e.g., Perturbed-chain statistical associating fluid theory (PC-SAFT) and Cubic-Plus-Association (CPA) (Li & Firoozabadi, 2010) .
According to the thermodynamic approach, asphaltene molecules are assumed to be initially dissolved in the oil phase similar to the solution of a polydisperse polymer in a solvent (Forte & Taylor, 2015). Asphaltenes' polydispersity is a result of the broad size distribution of asphaltene molecules in crude oils. This means that the thermodynamic properties of asphaltenes fractions (having different molecular weights) will depend upon their respective molecular weight. Thus, in order to calculate the phase behaviour (i.e., phase–equilibrium) of an asphaltenes-oil system, the chemical potentials of the many asphaltenes fractions (with different molecular weights) have to be calculated using a suitable EoS (e.g., SAFT) as described by McMillan-Mayer theory (Forte & Taylor, 2015). Thus, asphaltenes precipitation can be treated as an equilibrium phase separation process in which a separate solid asphaltenes phase is formed from the continuous solution (asphaltenes-oil) when temperature, pressure or/and continuous phase composition attain certain critical values (Fig.6.1. Variation of asphaltene precipitation). A great number of publications have followed the above mentioned general thermodynamic approach to foresee the phase behaviour of asphaltenes in model oil systems or in crude oil, namely, the onset of asphaltenes precipitation and deposition, the mass fraction of deposited asphaltenes, the effect of different miscible solvents, etc. in terms of temperature, pressure and oil composition (Barreira, Reis, Nunes, Filipakis, & Lucas, 2018; Chaisoontornyotin, Haji-Akbari, Fogler, & Hoepfner, 2016; Sabet et al., 2019) .

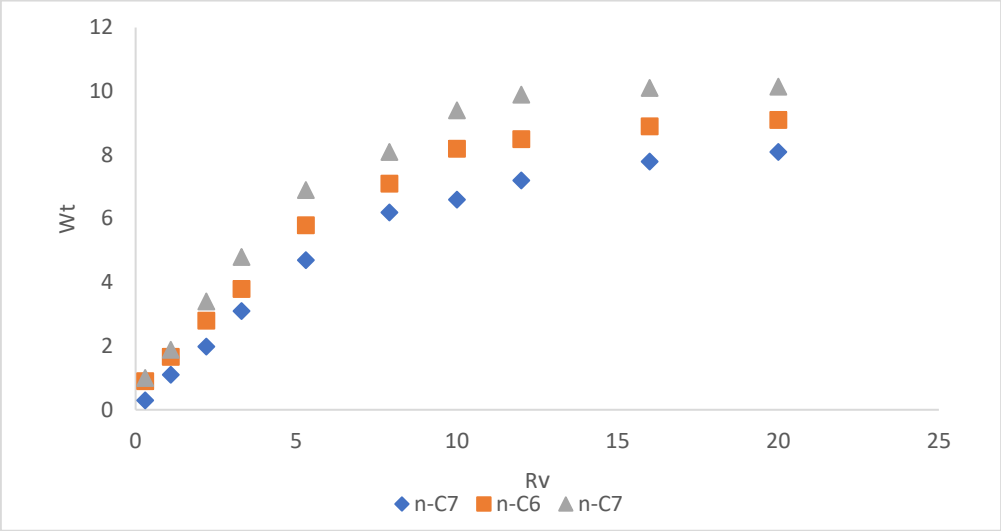

Figure 7-1: Variation of asphaltene precipitation

7.4 The solid colloidal model

The solid colloidal model assumes that asphaltenes present in the crude is present as suspended solid particles in the stable form. Stabilization of the suspended asphaltenes clusters is assumed to be due to the presence of resins that are adsorbed on the exterior of the asphaltene nanoparticles. The stabilizing resins act as a repulsive barrier between the suspended asphaltenes nanoparticles preventing them from aggregating in the crude oil. Primary precipitation and flocculation start when the resin concentration in the crude oil is reduced below a critical value (critical resin concentration – CRC). Similarly, to EOS studies on asphaltenes, colloidal science has been successfully applied to describe the colloidal character of asphaltenes as well (L.-l. Zhang, Yang, Yang, & Que, 2016).

7.5 Experimental methods and procedures

For the purpose of the formulation of the quantitative analysis of asphaltenes and the precipitation titration data, many methods have been proposed, however, the scaling equations are most popular due to the minimal requirement for the asphaltene and crude oil properties. Research in this field where Asoodeh et al.(Asoodeh, Gholami, & Bagheripour, 2014) developed a new scaling equation for the prediction of asphaltene precipitation using hybrid genetic algorithm-pattern search tool. Genetic algorithm (GA) is an optimization tool, which has been applied in many fields of science and engineering.

The study has found that previous practice for developing the scaling equations for asphaltene precipitation work only for dead oils. The method employed was titration using standard alkane solvents. The method is dissimilar from the asphaltene precipitation behaviour in the oil during production from the well and thus cannot replicate the process. This difference in asphaltene precipitation mechanism increases when pressure changes are involved particularly during gas injection in the reservoir for enhanced oil recovery. Furthermore, the models incorporate a few numbers of properties such as solvent to oil ratio, molecular weight, and density under isothermal conditions. These models omit some of the other important parameters including bubble point, presence of resin in oil, gas to oil ratio and lower/upper onset pressures which directly influences the behaviour of asphaltene precipitation in the reservoir oil.

In order to incorporate the parameters, two new variables (x and y) are defined using titration data and then deriving the equation implying a third-order polynomial function as follows: (Nikookar et al., 2008)

$$x = \frac{R_v}{T^{C_1} M_w^z}$$
$$y = \frac{W_t}{x^{C_2} R_v^{z1}} \quad \text{Eq. 7.1}$$

Where, R_v is solvent to oil dilution ratio; T is temperature, Mw is molecular weight of solvent, W_t is mass of asphaltene precipitated and Z, C_1, C_2, and Z are modifiable factors for attaining the best fit between the scaling equation model and titration data. A subsequent equation relates the variable x and y as follows:

$$y = B_0 + B_1 x + B_2 x^2 + B_3 x^3 \quad \text{Eq. 7.2}$$

Where $B_0, B_1, B_2\ and\ B_3$ are scaling coefficients.

This equation can be optimized by adjusting the values of Z, C_1, C_2, Z_0, B_0, B_1, B_2 and B_3. The optimization was achieved using a hybrid GA-pattern search technique. This technique extracts the best suitable values of these coefficients. The next section covers detailed procedure for applying this technique.

7.6 Hybrid genetic algorithm (GA)-pattern search tool

Genetic Algorithm is a tool based on stochastic optimization for solving the problems in many fields. Following are the steps for carrying out the hybrid GA pattern search.

1. The first step is to define a fitness factor (FF) where the task is to find the global minimum
2. The second step involves the generation of chromosome like solutions for the fitness factor.
3. These solutions are evaluated, and fitness score is assigned
4. The solutions are ranked according to their fitness scores.
5. The top ranked chromosomes are selected.
6. Using many genetic operators on the top ranked chromosomes, a more appropriate chromosomes are generated.
7. The steps from 3 to 6 are repeated until desired chromosomes are found.

To develop a new scaling equation, the values of constant parameters should be modified. To do this, a hybrid GA-pattern model was developed to obtain the best values. To define the eight constants based on the "divide-and-conquer" principle, the problem was broken into smaller parts and each part was solved separately. Using the first fitness function, the values of Z, C1, C2 and Z' were obtained using the following equations:

$$C = \frac{\sum_{i=1}^{N}(x_i - x)(y_i - y)}{(L-1)S_x S_y}$$
$$FF1 = \frac{1}{1+|C|} \quad \text{Eq. 7.3}$$

Here, C denotes the correction coefficient, FF1 is the first fitness function, L represents the number of data points and S denotes the standard deviation in x, y directions.

7.7 Results and discussions

It was found that the introduction of first fitness factor to the genetic algorithm produces the values of Z, C1, C2 and Z' in such a way that the factor x and y have highest correlation constant. If the value of correlation constant is = 1, the optimized value of fitness factor will be 0.5. The variables x and y were defined by the run of genetic algorithm pattern search tool:

$$x = \frac{R_v}{T^{2.56553227} M_{\cdot}^{z0.27289830}}$$

$$y = \frac{W_t}{x^{-0.0046515} R^{-0.63839854}} \quad \text{Eq. 7.4}$$

The next step introduces a second fitness factor to the genetic algorithm pattern search tool. This step provides the values for mining coefficients i.e. $B_0, B_1, B_2 \; and \; B_3$

$$FF2 = \frac{1}{L}\sum_{j=1}^{L}\left(y_j - B_o + B_1 x_j + B_2 x_j^2 + B_3 x_j^3\right)^2 \quad \text{Eq. 7.5}$$

The following third order polynomial was produced by running the fitness factor-2 on the genetic algorithm pattern search tool

$$y = -5.8818148 + 285529891x + 2886048795x^2 + (-3.95e + 19x^3) \quad \text{Eq. 7.6}$$

The precipitating solvent, normally n-heptane, is added to the crude oils until flocculation occurs. The amount of n-heptane obtained for precipitation is then plotted against the concentration of the solutions A straight line is obtained from which Heithaus parameters are calculated (Guzmán et al.,2017). One of the parameters is P value. It is the quantitative measure of overall solubility of asphaltenes and maltenes. This P value also distinguishes between the solution type and gel type asphaltenes. This parameter can be optimized. The Table 7.1 shows the extracted values of the parameters obtained using Hybrid GA-PS technique.

Table 7. 1: Values of correlation parameters for the proposed scaling model.

Parameters	**$P \leq P_b$**	**$P \geq P_b$**
B	−6.89	0.606
Z	0.76	2.3
Z`	0.32	0.32
Z``	0.90	0.79
A	0.326	−0.07

Table 7.1 shows the suppositions for the projected scaling model. The results in the table show that exponents Z and Z'' are dependent on the crude oil properties while the Z' is a universal constant and has a value of 0.32. When these equations were exposed to the experimental data, it was found that the optimum values of Z and Z'' were in the range of 0.76 to 2.3 and 0.79 to 0.90 respectively.

Lastly, the experimental measured values were compared with the predicted values obtained from genetic algorithm pattern search tool. Fig 7.2 shows that there is a close match between measured and predicted values.

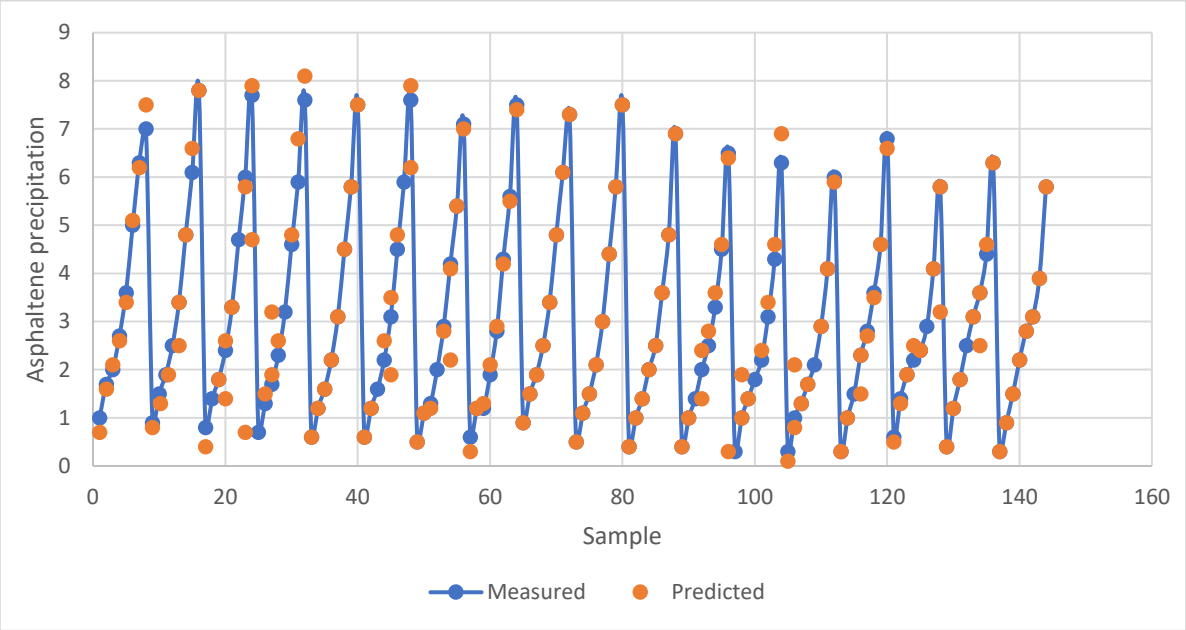

Figure 7-2: Comparison between predicted and measured values for asphaltene precipitation

7.8 Conclusion

In this study, asphaltene precipitation models were reviewed using different scaling equations. These equations do not require asphaltene properties inputs and have simple mathematical formulations. All the proposed scaling equations have been reviewed and the priority of them has been discussed over each other. In the category of asphaltene titration data, before developing the support vector machines, genetic algorithm-based scaling equations resulted in the best results in terms of R2. After developing the support vector machine, better results were obtained in comparison to the previously developed techniques.

It was concluded from the study that:

1. The genetic algorithm pattern search provides a convenient, reliable and economical alternative to the tedious statistical analysis by implying the scaling equations and optimizing its parameters.
2. The use of genetic algorithms coupled with pattern search technique helps in optimization task using divide and conquer formula.
3. It can be concluded from fig. 7.2 that the predicted results from genetic algorithm and the measured data closely match. Thus, the application of scaling equations based on genetic algorithm accurately predict the asphaltene behavior, hence saving on cost and time.

CHAPTER 8 *Investigation of CO_2 injection impact on asphaltene precipitation in an Australian oil well.*

Enhanced oil recovery (EOR) methods used in petroleun reservoirs include CO_2 and water flooding (Gabrienko, Martyanov, & Kazarian, 2016). A large quantity of residual oil can be recovered from reservoirs using this procedure. When CO_2 comes in contact with oil it changes the oil's properties which can cause problems such as wax deposition and asphaltene precipitation .

8.1 Data and Methodology

When the CO_2 gas is injected into the reservoir, there is a change in pressure, temperature and oil composition. These conditions are considered here in order to develop the model. The framework involves the direct calculation of molar volumes and solubility parameters for asphaltene.
A model for asphaltene precipitation is presented in light of the polymer arrangement model. The polymer solution can act as asphaltene precipitation, and disintegration forms in oil compared with different models.

$$\emptyset a(max) = exp\left[\frac{MVa}{MVl} - 1 - \frac{MVa}{RT}\ (\delta A - \delta l\ )^2\right] \qquad \text{Eq. 8.1}$$

Where,

$\emptyset a$ = maximum volume fraction of dissolved asphaltene in the liquid phase
MVa= molar volume of asphaltene a
R = universal gas constant
T = temperature
δa= solubility parameter of asphaltene
δb = solubility parameter of liquid.

Another equation is used to calculate the weight fraction W_{AF}.

$$V_{AF=}\frac{VA}{VTL} = \frac{\frac{WA}{\rho A}}{\frac{WTL}{\rho L}} = \frac{WA}{WTL}\left[\frac{\rho l}{\rho A}\right] = WAF\left[\frac{\rho L}{\rho A}\right] \qquad \text{Eq. 8.2}$$

Where,

WA = weight of precipitated asphaltene
Wtal = maximum weight of asphaltene in liquid
Wal = weight of asphaltene in liquid after flooding
Wtl = total weight of liquid.

The volume fraction is calculated as:

Where,

$\rho A =$ density of asphaltene
$\rho l =$ density of liquid
VA = volume of asphaltene precipitated
VTL = total volume of liquid.

To find the total weight:

$$W_{TL} = (V_{TL} - V_{TL} \text{ x } V_{AL})\ rho_A + W_{AL} \qquad \text{Eq. 8.3}$$

Where,

V_{AL} = volume fraction of dissolved asphaltene in liquid

W_{AL} = weight of asphaltene remaining in liquid.

To find the percentage weight of the asphaltene precipitated:

$$\% W_{TL} = \left[\frac{WTAL-WAL}{(VTL-VTL\ x\ VAL)\rho A+WAL}\right] x\ 100 \qquad \text{Eq. 8.4}$$

The weight percentage of asphaltene precipitated is in the form of model parameter:

$$Wmodel = \frac{WTAL-WAL}{\left|VTL-VTL\ x \exp\frac{MVA}{MVL}-1-\frac{MVA}{RT}(\delta A-\delta L)^2\right| x\ \rho A+WAL} \qquad \text{Eq. 8.5}$$

Where, Density of asphaltene, which is 1.28 gram/cm3, is a constant value

Wmodel = weight in percent of asphaltene precipitated

WTAL = asphaltene in liquid maximum weight

WAL = weight of asphaltene in liquid

VTL = total volume of liquid

MVA = molar volume of asphaltene

MVL = molar volume of liquid

δA = solubility parameter of asphaltene

δL = solubility parameter of liquid

R = universal gas constant

T = temperature in kelvin

ρA = density of asphaltene.

The solubility parameter of asphaltene is:

δA = 20.04 X (1 – 1.07 x 10-3 x T)

The solubility parameter of the fluid is the focus of this study, as this parameter is recognised as an inward durable density parameter (CED), which is known as the molar inner vitality of vaporisation of unadulterated fluid ($\Delta Uvap$) separated by its molar volume (MVl):

$$\delta l = CED½ = \sqrt{\frac{\Delta Uvap}{MVl}} \qquad \text{Eq. 8.6}$$

To find $\Delta Uvap$, which is the molar internal energy of vaporisation of pure liquid equation, we use:

$$\Delta Uvap\left(\frac{J}{mol}\right) = -14820 + 99.2\ x\ Tb + 0.084\ x\ Tb \qquad \text{Eq. 8.7}$$

A change is required in accordance with the solubility parameter of the fluid; thus, the model provides a unique answer for a particular oil test. Thus, α and β are presented as tuning parameters, and the molar volume of CO_2 ($MVCO_2$) is integrated into the condition to address the effect of CO_2 infusion. The solubility parameter equation is given by:

$$\delta L = \alpha\ x \sqrt{\frac{\Delta Uvap}{MVl}}\ x \exp\left[(\frac{MVco2}{MVl})\beta\right] \qquad \text{Eq. 8.8}$$

α and β can be determined using an experimental method or regression analysis.

8.2 Procedure for obtaining data

The initial crude-oil property data was taken from the literature and then recombined with CO_2 in the investigation conditions. By changing the estimations of the mol. % CO_2, another recombined data set was created. In this study, PVT-sim using CMG WinProp is used to create the PVT properties required in the calculation such as the weight, temperature and organisation changes.

The following two conditions must be fulfilled and discussed:

Term 1: Change two parameters (temperature and pressure) with a particular mixture.

Term 2: Change in composition.

The parameters are density of liquid, the molar volume of liquid, molar volume, temperature, total weight of liquid and total weight of asphaltene.

In order to understand the tuning parameters, the fitting procedure of the model is considered in an iterative way (Fig. 8.1). The cycle procedure stops when there are fewer remaining errors than the meeting criteria (ε). At the point when the iterations end, the best occurrence of the tuning parameters is found, and the delegate model is prepared to use in the model. Before the experimental model is used, the greater part of the PVT properties should be created at many pressures and temperatures. By simulating blends of pressures and temperatures, the weight percent of the encouraged asphaltene can be assessed in a wide range of working conditions to obtain an enhanced understanding of asphaltene conduct.

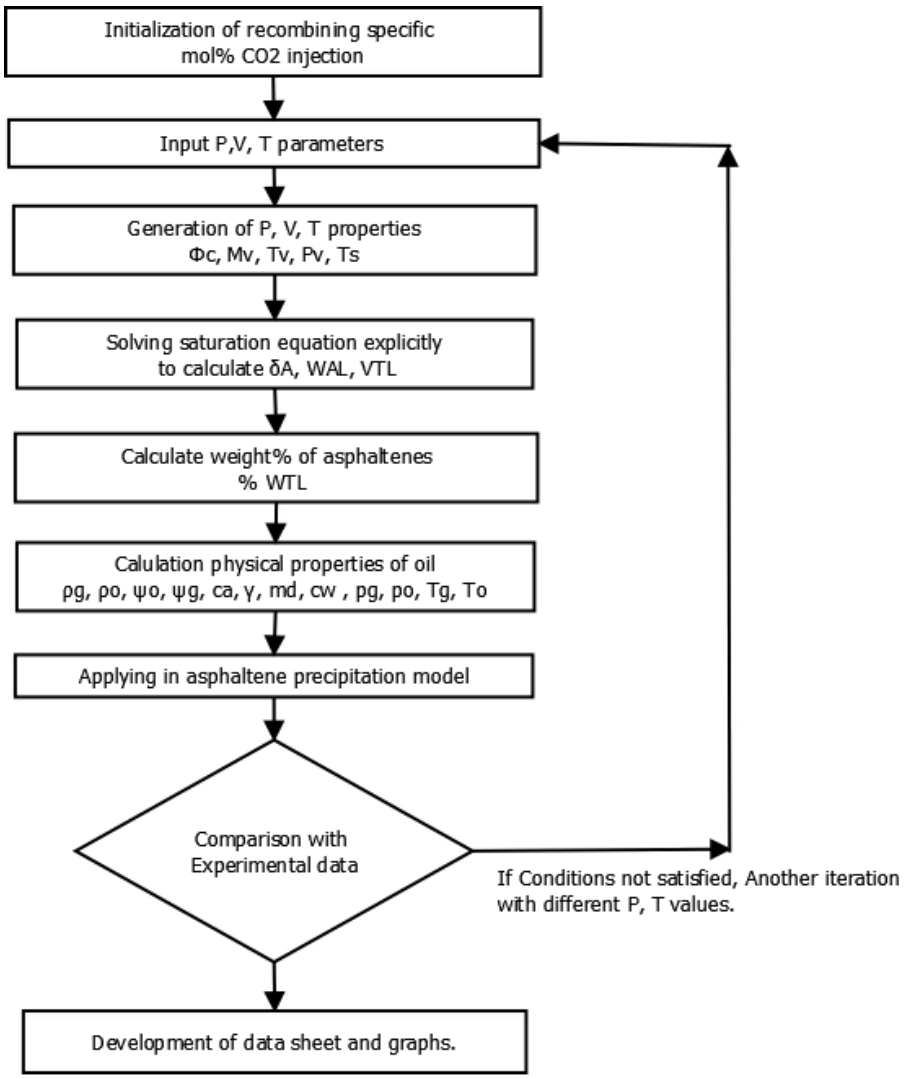

Figure. 8-1: Procedure flow chart.

The legend for figure 8.1 is shown below:

Symbol	Description	Symbol	Description
P	Pressure	σA	solubility parameter of asphaltene
V	Volume	WAL	Weight of asphaltenes in liquid
T	Temperature	VTL	Total volume of liquid
ϕ_c	Sephericity of asphaltene molecule	ψ_o and ψ_g	oil and gas mass influx terms
M_v	Molar volume	ρ_g and ρ_o	oil and gas mass densities
T_v	Specific temperature	γ	flocculation of solid particles from the reservoir
P_v	Specific pressure	c_w	wax concentration in the crude oil
T_s	Specific time	Ca	Asphaltene concentration in crude

From the calculations, asphaltene density is considered as being constant (1.28 g/cm3) when pressure, temperature recorders are connected. In a specific oil sample, the molar volume of asphaltene remains consistent at all pressures and temperatures.

8.3 Experiment or simulation data

Some of the test results are used to create the model. Data have been collected and provided estimations of asphaltenes with different concentrations of CO_2 injection, which are used in this study.

Table 8. 1: Simulations in different studies.

Study	Pressure	Temperature
X	150	99–100
Y	150	65–66

A recombination of oil with CO_2 is performed using PVT-sim to create the modified oil system for each mol. % of CO_2 injected. The recombined oil data was obtained from many literary works(Hadi, Jachim, & Abbas, 2016; Long, Guo, Chao, & Guo 2016; sreedhar & Sebastien, 2016). The following tables, 8.2 – 8.5, first demonstrate the oil composition of X and Y individually. Further, the following tables present the test results of the weight percent of precipitated asphaltene amid CO_2 injections for X and Y respectively.

Table 8. 2: Oil composition with X data, without injection of CO2

Component	Mol. (%)	Atomic mass
N2	0.246	28
CO2	4.039	44
C1	24.381	16
C2	3.185	30
C3	4.17	44
i-c4	0.636	58
n-c4	1.479	58
i-c5	0.8	72
n-c5	0.9	72

Table 8. 3: Oil composition with Y data, without the injection of CO2.

Component	Mol. (%)	Atomic mass	Density
N_2	0.9	44	-
CO_2	0.16	28	-
C_1	24	16	-
C_2	0.7	30	-
C_3	3.2	44	-
i-C_4	0.64	58.12	-
n-C_4	2.7	58.12	-
i-C_5	0.52	72	-
n-C_5	1.06	72	-
C_6	0.7	86.17	0.66
C_7	0.58	91.26	0.73
C_8	1.8	104	0.76
C_9	2.3	119	0.78
C_{10}	0.82	175	0.79
C_{11+}	52.91	442	0.92
Resin	4.89	850	1

Table 8. 4: Experiment results of weight.

% mol. injected	% mol. of CO_2	Weight (%)
2.4	4..3	0.78
11.50	10.14	4.5
18.98	14.27	7.05
25.21	17.17	8.6
30.48	19.31	9.7
35.05	20.97	10.78
42.5	23.39	11.10
46.00	24.38	11.26
48.7	25.1	11.31

Table 8. 5: Experiment results of weight.

Mol. of % CO_2 injected	Mol. of % CO_2 liquid	Weight (%)
51.5	32.25	0.06
63.8	35.87	0.23
71.6	37.7	0.35
80.2	39.4	0.42

8.4 Composition simulation

The ECLIPSE appliation was used to construct a block that is 7,500 ft. long, 1,000 ft. wide and 50 ft. thick. It is situated at 4,000 ft. depth. The simulated block has a measurement of 15 x 1 x (1D even), where a CO_2 injector is situated at the left edge of the square and the other side is the producer (Fig. 8.2).

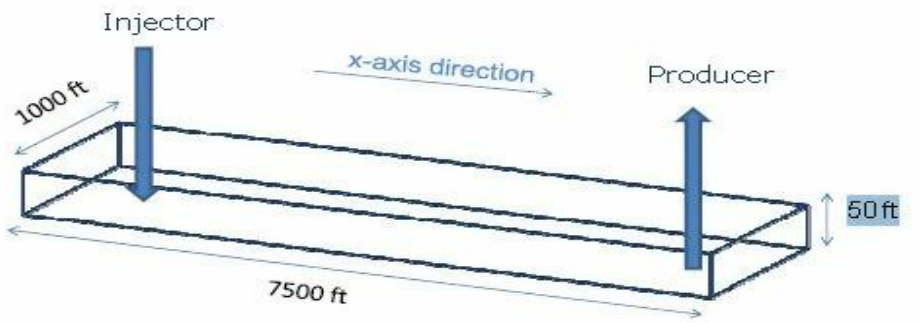

Figure 8-2: Block of simulated reservoir.

The block is partitioned into 15 portions with a square length of 50 ft. at the first and last three pieces while 800 ft. in the middle. The starting equivalent pressure (Pi) is 4,000 psia. Gas–oil contact is situated at 2,000 ft. and oil–water contact is at 4,060 ft. Absolute permeability is 500 md and partial porosity is 0.1. Underlying oil saturation is 0.84. Repository rock compressibility is set to 3.5 10^{-6} psi. Table 8.6 lists the reservoir information used in the simulator

Table 8. 6: Reservoir parameter.

Standard	Value
Absolute porosity	0.1
Permeability	500 md
d_{go}	2,000 ft.
d_{woc}	4,060 ft.
S_{oil}	0.84
P_i	4000 psi
Reservoir liquid	Oil

In this study, a stored liquid has eight particles with no proximity of CO_2 in the blend. Further, the blend at first contains 2% asphaltene. All PVT properties and the composition of liquids are illustrated in Table 8.7.

Table 8. 7: PVT properties.

Composition	Zi	Mw	T_{crit}	P_{Crit}	Z_{crit}	ACF
CO2	0	44.10	547.5	1069	0.27	0.22
C1	0.5	16.04	343	667	0.29	0.013
C3	0.03	44.1	665.7	616.3	0.22	0.15
C6	0.07	80.18	913.4	436.9	0.264	0.301
C10	0.2	149.29	1111	304	0.25	0.48
C15	0.1	206	1270	200	0.24	0.65
C20	0.08	282	1380	162	0.235	0.85
Asphaltene	0.02	282	1380	162	0.23	0.85

The relative permeability curves are shown in Figs. 8.3. – 8.5

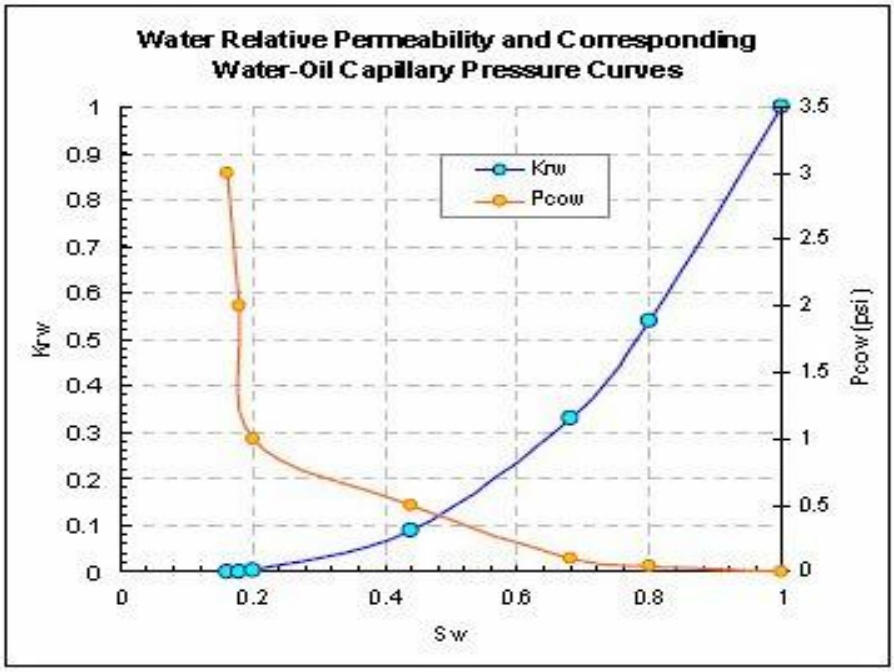

Figure 8-3: Water oil capillary v. pressure.

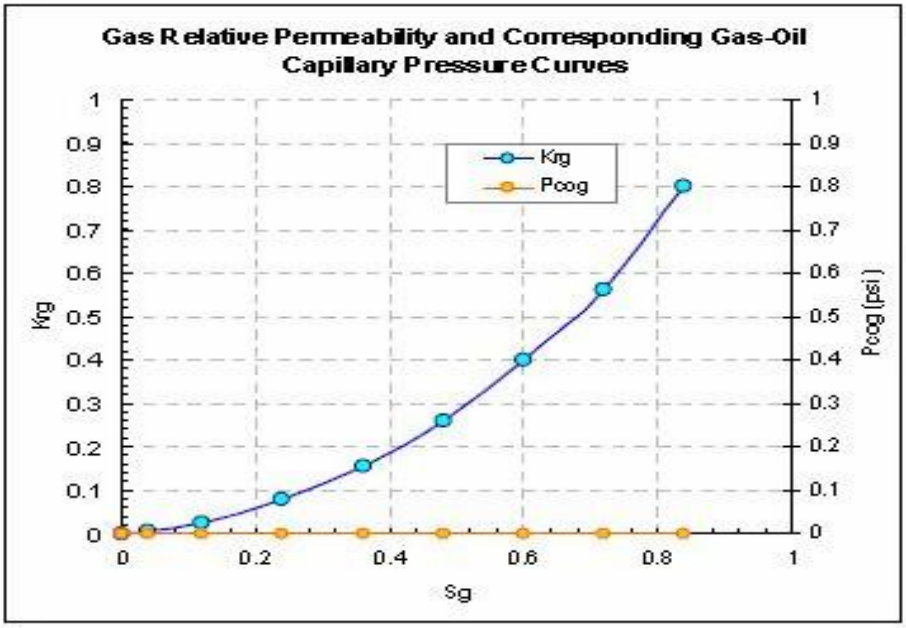

Figure. 8-4: Gas Relative Permeability V. pressure

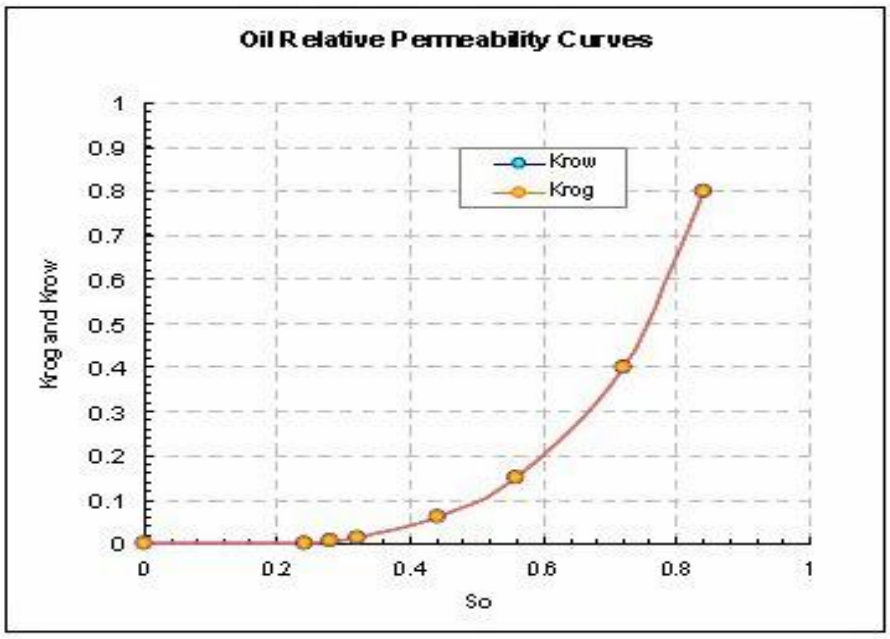

Figure 8-5: Oil relative permeability curve.

Table 8.8 shows the demonstrated rates, which is a component of the adsorption and entrainment rates. Table 8.9 presents the constraint taken for the CO_2 injection. Table 8.10 presents the bottom-hole pressure for injection and for production.

Table 8.8: Asphaltene dissociation rate

Procedure	Time (hours)
CO_2 to asphaltene	4
Asphaltene to CO_2	0.04

Table 8. 9: Constraint taken for injection and production.

Average production	Liquid injection	CO_2 injection
3,500	25,000	15,000

Table 8. 10: Constraint for injection.

BHP of injection	BHP for production
4,400 psia	500 psia

8.5 Results and discussion

The data were checked for model validation. An alteration or tuning procedure was made for better delivery so that the model can be used to determine the amount of the precipitated asphaltene. The model's approval depends on the iterative system of the tuning parameters α and β. In a non-linear regression, the coordination of these parameters depends on the coordination of the anticipated qualities to the trial results and is represented by an error sum of squares (SSE). SSE is used to assess how well the model condition fits the test experiment data. It deals with the total of the squared deviations of real qualities from anticipated qualities, as shown in the below equation:

$$\text{SSE} == \sum_{i=1}^{n} [(Wexp - Wmodel)]^2 \qquad \text{Eq. 8.9}$$

Using this technique for calculation, which is trial and error to estimate SSE value, a Gauss-Newton iIterative method is used to find an approximate SSE value.

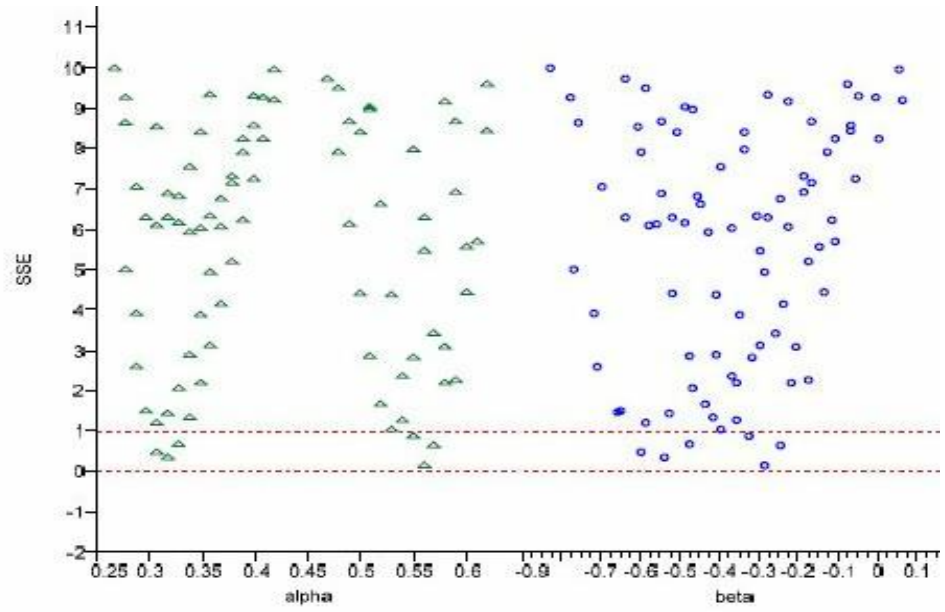

Figure 8 8-6: SSE v. α and ϐ by X.

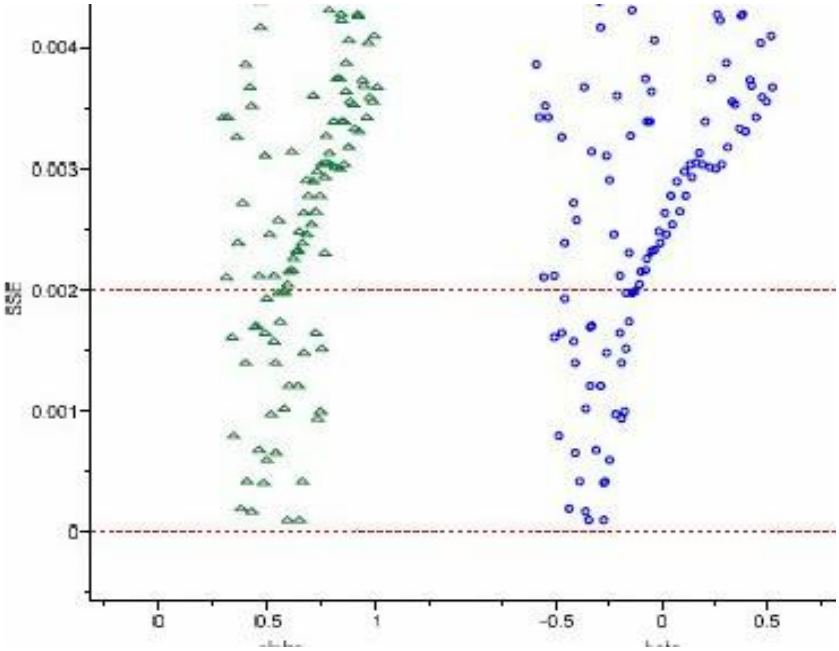

Figure 88-7: SSE v. α and β by Y.

Table 8. 11: Parameters of α and β by X and Y.

X parameters			Y parameters		
α	β	SSE	α	β	SSE
0.296482	-0.65829	1.483285	0.346734	-0.48744	0.000794
0.296482	-0.64824	1.488981	0.376884	-0.43719	0.000191
0.306533	-0.59799	0.492866	0.537688	-0.40704	0.000656
0.316583	-0.53769	0.335558	0.407035	-0.38693	0.000419
0.316583	-0.52764	1.446041	0.427136	-0.35678	0.00017
0.326633	0.47739	0.682229	0.58794	-0.34673	0.000104

The α, β and SSE results are presented in Table 8.12.

Table 8. 12: Most suitable parameters.

X	Y	SSE
α= .3104753	α= 0.40162921	0.0019135886
β= - 0.570452	β= -0.39722664	$1.24x\ 10^{-07}$

8.6 Conclusion

The asphaltene deposition rate is a function of temperature and pressure and the crude oil composition. The results show that the presence of light components, like CO_2, can considerably increase the asphaltene deposition in the wellbore. CO_2 destabilizes asphaltene in the phase envelope

and increases both the bubble point pressure and the asphaltene onset pressure. Consequently, once CO_2 is mixed with an asphaltenic crude oil, it lowers the deposition sites in the wellbore to bottom-hole, where the pressure is higher.

The ability of asphaltene precipitation prediction was confirmed from a material science perspective. When pressure is reduced at above bubble point pressure, the asphaltene content in oil will decrease, and the quantity of the slightest solvent substance of asphaltene will remain in oil at bubble point pressure. In declining pressures, below bubble point, the asphaltene is resorbed into the oil. The experimental data results showed that asphaltene deposition varies with displacement, which is caused by the miscibility of CO_2 flooding. The equation used for the Flory–Huggins polymer solution was further developed for asphaltene precipitation modelling. In summary, the experiment and the simulation process of CO_2 flooding showed that no deposition of asphaltene was present at the injection point.

8.7 Future work

A 3D reservoir model can be used in future studies for obtaining a better perspective of asphaltene precipitation due to CO_2 injection. This proposed model may display and explain full asphaltene behaviour.

We will further investigate asphaltene precipitation onsets and yield information measured for oil mixes acquired from multiple unrefined and refined oils.

CHAPTER 9 : *Asphaltene precipitation and deposition prediction and mitigation through the use of neural networks*

9.1 Introduction

In this research we used Artificial Neural Networks (ANN) for predicting asphaltenes deposition due to crude oil flow variations, using a prediction/genetic algorithm. Neural networks (NNs) are computational models, inspired by brain structure, mechanisms and functions which could have been used for regression and classification purposes (Lipton, Berkowitz, & Elkan, 2015). In order to increase the prediction accuracy for asphaltenes deposition, a fuzzy approach was deployed. Many studies have shown that the mechanisms of asphaltene deposition are not a clearly understood phenomenon. A fuzzy logic approach is more feasible for developing models used to predict asphaltene precipitation and deposition (Asoodeh et al., 2014; Bělohlávek, Dauben, & Klir, 2017). The major advantage of fuzzy based neural network is that it generates a fuzzy cognitive map i.e. dynamic state machine with fuzzy states. These fuzzy states can be used to preprocess the data in fuzzy systems. Furthermore a fuzzy based neural network has the capability to learn new relationships with discrete input creating refined fuzzy rules in turn producing a more efficient fuzzy adaptive system. The prediction of the rate of asphaltenes deposition in the crude oil and compositions of various crude oil were examined. This research uses 5 samples for predicting asphaltenes deposition in crude oil. By testing and training data sets, performance was evaluated. Analysis of the simulated results demonstrate that using fuzzy based prediction/genetic approach improves the prediction level with minimized Bit Error Rate (BER).

9.2 Factors influencing asphaltenes deposition

The evaluation of asphaltenes precipitation and deposition of asphaltenes are described in three stages (Elochukwu, Attarhamed, & Joukarborazjany, 2013):

a) Asphaltenes precipitation occurs when the solid particles form a distinctive phase as they come out of solution. The particles of asphaltenes coming out of solution at this stage are small in size.

b) The small particles of asphaltenes aggregates or clump together to form larger size solid particles. This stage is known as the flocculation stage.

c) Due to the large size of the asphaltenes particles, the crude oil can no longer support it, and thus the particles settle out on solid surfaces. This stage is known as deposition.

Asphaltene is usually present in the suspended state under the conditions of normal reservoir temperature and pressure. The factors of temperature, pressure and composition of crude oil determine the flocculation behavior of asphaltenes. Changes in any of the factors can lead to an instability of asphaltenes solubility causing its precipitation, eventually dropping the production and may lead to formation damage.

Several models (Almehaideb, 2004; Kor and Kharrat, 2016; Lei et al., 2010) have been developed to predict asphaltenes precipitation. However, the majority are focused on asphaltenes precipitation

issues that are specific to the deposition or recovery deposition on production facilities (Zahedi et al., 2009). Another study focused on the behavior of asphaltenes during CO_2 flooding using an experimental approach. More recently mathematical relationships were developed to predict asphaltenes precipitation induced by CO_2 injection. An important conclusion was that asphaltenes starts to flocculate when the CO_2 concentration reaches a threshold value and precipitation increases rapidly with the injection of more CO_2. Further increase in CO_2 concentration over a certain level leads to a decrease in asphaltenes precipitation. The paramaeters incorporated in the study were pressure, temperature, specific gravity of crude oil, oil compositon and solvent molecular weight (Manshad, Rostami, Rezaei, & Hosseini, 2015).

9.3 The mathematical model

The mathematical model developed in this paper is based on fuzzy logic. This provides a completely different approach towards the model development (Bělohlávek, Dauben, & Klir, 2017). In the fuzzy based model, the major benefit is that the researcher can concentrate on problem solving rather than trying to model the system, unaware of the fact that model can either be developed or not.

There are three fundamental steps are used for refinement of the mathematical model which estimates the amount of asphaltenes precipitation (Hertz, 2018).

The first step involves the stochastic optimization of the neural network using hybrid genetic pattern search approach (Moradi & Gholampour, 2016).

In the second step, a stochastic optimization was performed to tune the mean and range of input membership functions in the fuzzy logic model.

For the third step a hybrid genetic algorithm is used for extracting optimal values of membership functions used in fuzzy clusters. Finally, optimized elements with committee machine were assembled for the benefit of both optimized fuzzy logic and neural network.

Stochastic optimization is necessary because of severe randomness present in the input data. This optimization technique can minimize or maximize the objective function when random input data is present. The purpose of membership functions in fuzzy logic control is to define the degree of inputs. In other words it is a graphical representation of fuzzy sets (Ahmadi et al., 2017). The need for this step is because spread of membership functions will not be optimized manually.

9.4 Genetic algorithm for prediction

The genetic algorithm (GA) is a globally accepted optimization method (Kurkova, Steele, Neruda, & Karny, 2013), which starts with a random population of chromosome-like elements and evolves towards obtaining better solutions by applying genetic operations. The genetic algorithm evaluates the global minimum of fitness function (a function which its global minimum is desired). Subsequently, the function is resolved through a minimum of the rearranged functions as well as the desired points of original function are similar. Evaluation of each chromosome (solution) produces the corresponding fitness score which in turn is used for selection procedure and forming the succeeding population after applying genetic operations. This process continues until the desired chromosomes are achieved. For better performance of the genetic algorithm, pattern search techniques are integrated with GA. This

means, after each generation, all chromosomes are improved using pattern search method. In the pattern search method, the algorithm searches a set of points, called a mesh, around the current chromosome. Mesh network has been found through current chromosome to a scalar multiple of a set of vectors called a pattern (Asoodeh and Bagheripour, 2013). After evaluation of all the points according to the fitness function, the best solution in the mesh is substituted by current chromosome. There are several optimization methods available such as adaptive random search, Powell Direst search method, random exploration with shrinkage, dynamic hill climbing algorithm, population based incremental learning algorithms etc. (Chen, Elliot, & Smith, 2018). The studies have shown that genetic algorithm coupled with several other techniques such as Niching can be used efficiently to mitigate the noisy functions in the prediction algorithms. With other models, the "bump problem" is hard to tackle for most of the optimization methods (Kramer, 2017). In the current study niching technique is used with genetic algorithm to mitigate the noisy functions and "bump problem"

9.5 Stochastically optimized neural networks

Stochastically optimized neural networks can extract the implicit dependency of input/output data space through the specific architecture of their processing elements, called neurons. More details on the neural network can be found in several publications (Asoodeh, 2013; Khazaeni and Mohaghegh, 2011). Neural network with back-propagation learning algorithm is highly at risk of sticking in local minima. In other words, it is very probable that a trained neural network does not mean all implicit information available in input/output data space due to sticking in local minima. Therefore, the need for a surrogate algorithm for the training of neural network is required. For this purpose, hybrid genetic algorithm-pattern search technique is used. The hybrid genetic algorithm pattern search has several advantages in fuzzified artificial neural network model development. One of the advantage is that it can efficiently be used in case of discountinous objective functions (Beg & Islam, 2016). It can also be used for discrete, integer design and continous variables. The hybrid genetic algorithm pattern search helps in minimizing the risk to converge to a local optimum. This is because of simultaneous processing of input data (Xu et al., 2016). The pattern search method is efficient compared to other genetic algorithm tehcniques because the number of iterations are reduced.

9.6 Solution procedures for the model

In order to predict the deposition of asphaltenes 5 samples of crude oil were considered. In the selected samples composites and deposition of asphaltenes in crude oil were evaluated for the temperature ranges from 293K to 338K with a sample time interval of 15K. The analysis of 5 samples of crude oil revealed different compositions at different temperature range for different dilution ratio. The identified chemical composites in the 5 samples of crude oil were hexane, heptane, nonane, decane, pentane, octane, and dodecane. The analysis of the collected sample for the specific period of time was carried out by considering atmospheric conditions. In the existing model, analysis was carried out by evaluating the relationship between input and output variables using clustering algorithms. The data point in these algorithms exists in the space defined by its attributes and by the relative distance to all other data points in the analysis.

9.7 Oil composition and mechanics of asphaltene precipitation

Some studies have demonstrated that an increase in temperature increases asphaltenes precipitation (Gabrienko et al., 2015). In a dataset of this study, a reverse relationship was observed between asphaltenes precipitation and temperature. An increase in the carbon number of the paraffinic precipitant will minimize asphaltenes precipitation, while the increase in dilution ratio (ratio of solvent volume to weight of crude oil) increases the asphaltenes yield (Gabrienko et al., 2015). Therefore, dilution ratio, the molecular weight of solvent, and the temperature are used as an input data, and the corresponding amounts of precipitated asphaltenes are used as output.A simple way to determine the paraffinic or aromatic nature of crude oil is based on the ratio of hydrogen to carbon atoms (H/C). As crude oil becomes denser, there are more aromatic rings with less hydrogen i.e. the H/C ratio becomes low. Normally, H/C ratio of resins is from 1.3 to 1.6 and 1 to 1.3 for asphaltenes (Bělohlávek et al., 2017).

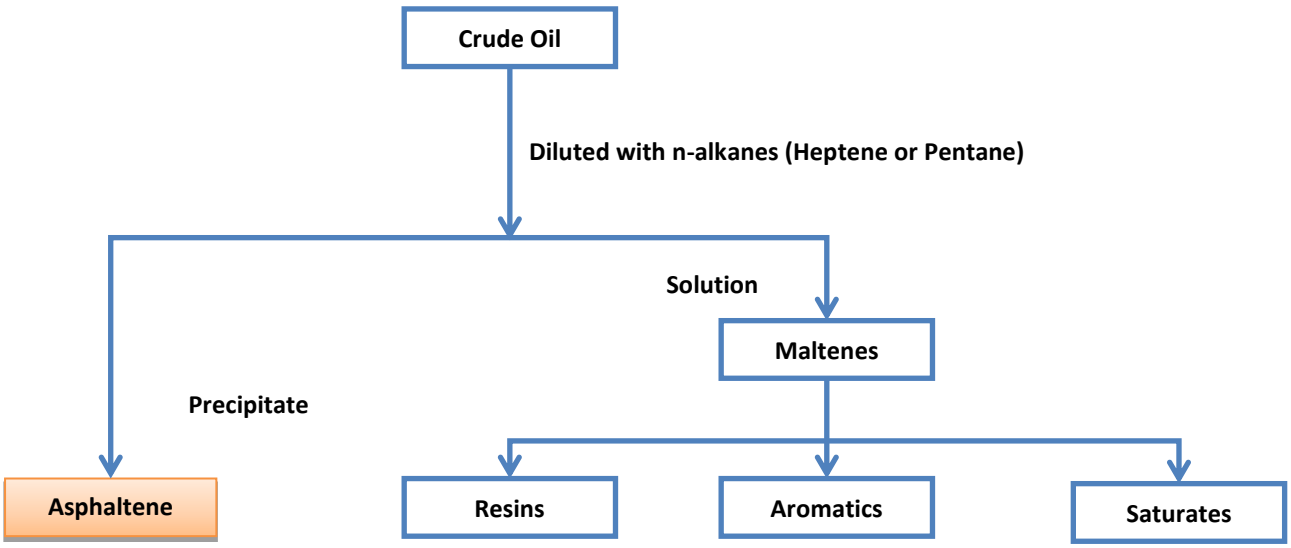

Figure 99-1: Mechanism of asphaltenes precipitation (Kashefi et al., 2017)

9.8 Crude oil composition and reporting methods

Crude oil is a mixture of millions of different hydrocarbon compounds and varies in composition depending on their geological location. Many reporting methods for crude composition are applied such as elemental and hydrocarbon content based. However, SARA-separation (saturates, aromatic, resins, asphaltenes) provides a distinctive classification on the basis of solubility and polarity properties .

Saturates are also known as aliphatic molecules which consist of nonpolar hydrocarbons both straight and branched chain alkanes along with some cycloalkanes. The closed chain structural derivatives of benzene are referred to as aromatics. Aromatics are common in the crude oil and are further classified as mono-aromatic, di-aromatic or tri-aromatics depending upon the number of aromatic rings present in the molecule. Resins are defined under the solubility class as the fraction insoluble in propane but soluble in light alkanes, for instance, pentane and heptane. Resins consist of polar molecules containing sulphur, nitrogen, and oxygen.
Asphaltenes are the fraction present in crude oil characterized by their solubility in toluene and benzene while precipitating in light alkanes. The composition of asphaltenes is a large proportion of polar atoms (S, N, O) and also organometallic constituents such as nickel, vanadium and iron. The structure of asphaltenes is a polycyclic aromatic cluster with varying alkyl chains.

9.9 Artificial neural network (ANN) and prediction of precipitation

For a rough approximation with a simplified simulation of the processed data, ANN has evolved which uses biological neuron network system for prediction and processing of collected data. The key aspect of ANN is creating the effective parameters for data processing with the learning and testing, convergence, generalization, data representation and interpretation. The simplest practical implication of ANNs was in 1950's when Frank Rosenblatt and his assistants demonstrated the capability of this technique in pattern recognition. Subsequently ANNs were improved and applied in various disciplines such as aerospace, automotive, defense, transportation, telecommunications, electronics, entertainment, manufacturing, finance, medical, and petroleum. But the challenge with the conventional ANN model is that it locked at a local optimum point and produces multiple optimum points. Another disadvantage is the convergence rate of BP-ANN (Back Propagation – Artificial Neural Network) which is slower. Most of the system parameters in the BP-ANN are determined through trial and error technique (Saduf, 2013). Therefore, there is always a difference between them and the optimized (best) ones that cause some errors in the model outputs.

To predict asphaltenes deposition in crude oil, data was collected from previously analyzed five samples from the oil producing company. The data from existing literature was entered into the ANN system and evaluated for prediction values by means of training and testing data sets. The mean square error of the network (MSE) is expressed by Equation 8.1:

$$MSE = \frac{1}{2}\sum_{k=1}^{G}\ \sum_{j=1}^{m}[y_j(k) - T_j(k)]^2 \qquad \text{Eq. 9.1}$$

Where, m - number of output nodes,
G - number of training samples,
$Y_j(k)$ - expected output,
$T_j(k)$ - actual output.

Data used in this study was split into training and validation data sets. The motivation of training a network obtains an optimum set of connection weights.

9.10 Genetic algorithm and predicting deposition

The asphaltenes prediction in crude oil is performed by an adaptive heuristic search algorithm, the genetic algorithms which are premised on ideas of natural selection and genetic. The design of genetic

algorithms simulates processes in the natural system that are necessary for evolution. As such they represent an intelligent exploitation of a random search within a defined search space to solve a problem. The genetic algorithm not only provides an alternative method for solving the problem, but it also consistently outperforms other traditional methods in most of the problems alike (Kashefi, Lotfollahi, & Shahrabadi, 2017). To predict the deposition level in the crude oil reservoir using collected data, the best fitness value for the collected data is evaluated. The basic steps involved in prediction are as illustrated in Figure 9.2, below:

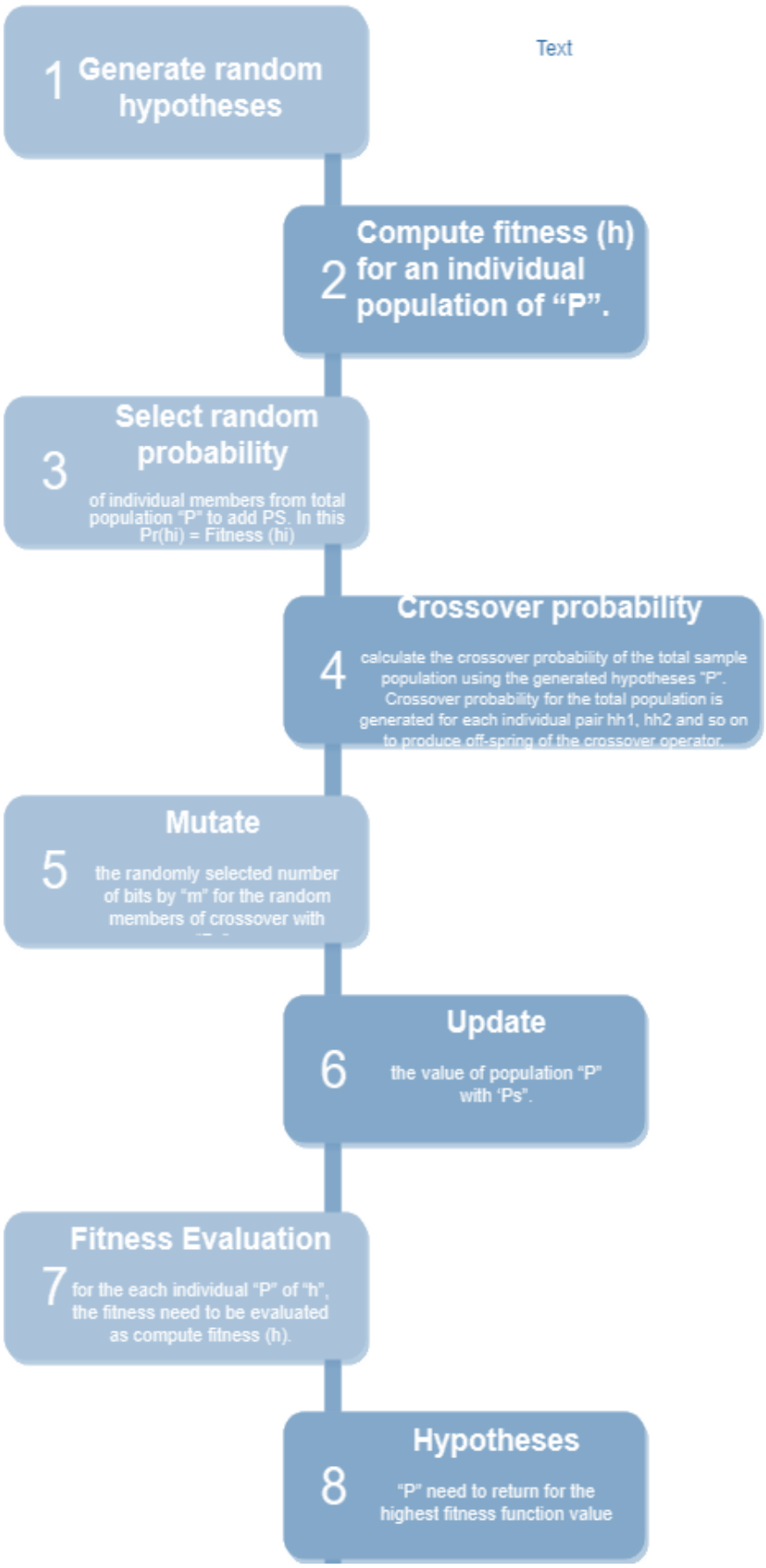

Figure 9-2 Flowchart for prediction of asphaltene deposition levels in crude oil

The analysis is carried out in an artificial neural network by the selection of an appropriate sample. Data for estimating asphaltenes prediction is conducted in an artificial neural network using various compositions of crude oil. In this review, five samples are used for evaluating the asphaltenes deposition percentage using fuzzy based ANN. The data sets considered in this research for predicting asphaltenes deposition in crude oil is evaluated by selecting five samples.

All the variables involved in asphaltenes precipitation were combined in the two variables which are shown in Equation 8.2 below:

$$X = \frac{R}{M^2} \text{ and } Y = \frac{W}{R^2} \qquad \text{Eq. 92}$$

where, X and Y are two adjustable parameters which must be carefully tuned to obtain the best fit of the experimental data. The initial population is generated randomly with the population of "P". This size was selected after examination of many population sizes. In addition, mean 5-fold cross-validated normalized mean square error is used as the fitness function with the Equation 8.3:

$$= \frac{1}{5}\sum_{k=1}^{5} NMSE_k \qquad \text{Eq. 9.3}$$

Where,

$$NMSE = \frac{\sum_{i=1}^{n}(d_i - p_i)^2}{\sum_{i=1}^{n}(d_i - \bar{d}_i)^2} \qquad \text{Eq. 9.4.}$$

k - the number of cross-validation fold

di- desired (actual) value

pi- predicted value

di - mean of the desired values

N is the total number of data samples in the validation dataset for each fold.

For the prediction of asphaltenes deposition, the parameters shown in Table 9.1 were used for analysis in crude oil. The analysis of collected data was carried by using following 5 samples for performance measurement.

Table 9. 1: Crude oil samples components

S.No	Components	Sample 1	Sample 2	Sample 3	Sample 4	Sample 5
1	H_2S	1.87	0.00	0.00	2.54	6.37
2	N_2	0.31	0.30	0.30	0.37	1.41
3	CO_2	3.37	0.93	1.83	4.65	3.95
4	C_1	43.59	18.91	22.7	22.62	41.95
5	C_2	8.58	7.20	8.24	8.51	8.74
6	C_3	6.27	5.21	6.14	4.45	5.21
7	iC_4	1.64	1.11	1.19	0.81	1.33
8	nC_4	4.89	2.93	3.61	3.21	2.12
9	iC_5	2.20	1.05	1.38	0.97	1.83
10	nC_5	2.49	1.14	1.59	1.30	2.56
11	C_6	1.91	5.44	6.95	6.07	2.41
12	C_7	0.89	4.11	4.10	2.96	2.28
13	C_8	3.01	3.43	3.88	3.49	3.39
14	C_9	2.05	3.07	2.49	2.23	2.75
15	C_{10}	1.84	2.95	4.03	1.87	2.04
16	C_{11}	1.39	2.59	2.85	3.72	2.11
17	C_{12+}	13.71	39.62	28.74	30.23	9.55

9.11 Results and discussion

The data series were configured into two categories (i.e. training and testing sets to implement artificial neural network (ANN) modelling). In general, about 75–80% of the data is assigned to the training phase and remaining to the testing phase (George, Osinga, Lavie, & Scott, 2016). For instance, out of total 371 experimental case data sets, data points used for training were 276 (74.4%) and for testing were 95 (25.6%) whilst implying a smart technique for precipitation test runs. Moreover, for training of ANN for deposition prediction a total of 110 data sets were used for training and 35 for testing making a total of 145 data sets (Zendehboudi et al., 2014). The data sets used in the connectionist model (computer modelling approach for processing any information based on architecture of the brain) for the static experimental case totalled 371, of which 290 were taken from the literatures and 81 from the current study (Zendehboudi et al., 2014). On the other hand, the ANN systems used to predict asphaltenes deposition during the dynamic tests applied 145 data points points taken from other studies. In the current study, various ANN structures with different numbers of hidden layers and neurons (in each layer) are examined to attain the optimized network such that the asphaltenes precipitation/deposition were estimated with acceptable precision in a reasonable time. A back-propagation algorithm was employed in all the connectionist (or ANN) modelling runs to find the results when the mean squared error (MSE) is minimized over training and testing stages.

The back-propagation algorithm is used in every connectionist (or ANN) modelling runs which assists in finding results when the mean squared error (MSE) is minimized over training and testing stages, shown in Table 9.2.

Table 9. 2: Training, Validation and testing values

	Samples	MSE	R
Training	11	$2.74500e^{-1}$	$4.78688e^{-1}$
Validation	3	$1.07590e^{0}$	$1.02397e^{-1}$
Testing	3	$4.51152e^{-1}$	$-8.76110e^{-1}$

Different numbers of neurons (4, 5, 6, 7, 8, 9, 10, 11 and 12) are tested for the ANN networks. Based on statistical parameters (e.g., R^2 and MSE), the optimum number of hidden neurons determined were 10 (as shown in Fig. 9.3).

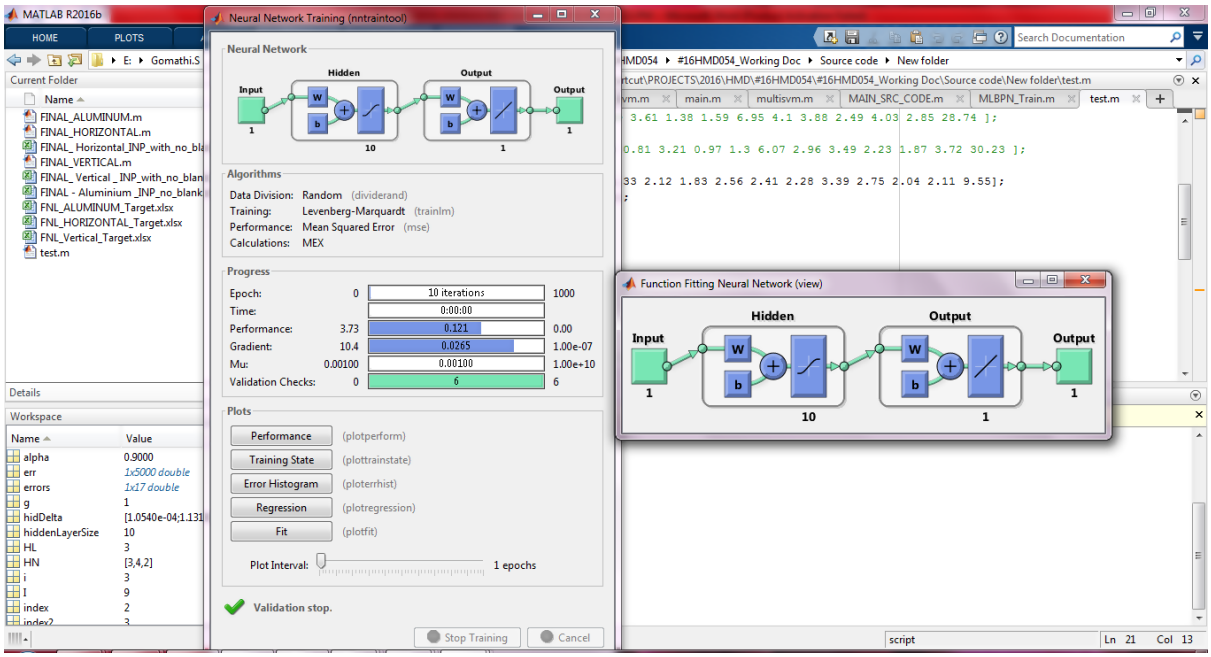

Figure 9-3: Experimental setup with results

It is important to note that having more neurons in the network increases the processing time in ANN modelling, leading to data overfitting using a higher number of neurons may improve the network performance, inconsiderably.

Figs. 9.4a through 9.4e demonstrate a comparison between the calculated and real amounts of asphaltenes precipitated over the training and testing stages for the whole ANN systems including BP-ANN, PSO-ANN (Particle Swarm Optimization-ANN), and ICA-ANN (Imperialist Competitive Algorithm-ANN). From the results, the predictive performance of ANN-PSO and ANN-ICA is nearly the same but much better than that of BP-ANN in terms of accuracy. The statistical criteria such as mean squared error (MSE) and maximum absolute percentage error (MAAPE), minimum absolute percentage error (MIAPE), and correlation coefficient (R2) are used to evaluate the performance of the BP-ANN, PSO-ANN, and ICA-ANN models for selected samples as presented in Table 1. The data for both asphaltenes precipitation and deposition are included in the table, as well. The results listed in Table 4 reveal that

the hybrid ANN system using ICA algorithm exhibits an excellent predictive performance in terms of both convergence rate and global optimality. The PSO-ANN holds the second rank in terms of predictive performance. However, fairly high error percentages at some conditions are obtained while utilizing BP-ANN when predicting the amount of precipitated asphaltenes. It can be concluded that all models employed exhibit lower accuracy in forecasting target conditions in case of dynamic asphaltenes deposition as compared to the static, since a higher number of variables are involved in the former case, and more uncertainties come into play in the predictive models.

For comparative analysis of the above methods, the prediction capability of ANN-ICA and ANN-PSO is more reliable than BP-ANN. The following criteria are used when the evaluation of the performance is carried out given in the table 8.2. Moreover, the asphaltenes precipitation as well as deposition data is given.

- mean squared error (MSE)
- maximum absolute percentage error (MAAPE)
- minimum absolute percentage error (MIAPE)
- correlation coefficient (R2).

For better performance particularly in convergence rate and global optimality, the hybrid ANN system is employed by the use of ICA algorithm. For the prediction analysis accuracy, PSO-ANN is next to ICA-ANN. On the other hand, P-ANN can result in some percentage of error while making prediction about the amount of asphaltenes precipitation. When the number of variable involved in the process are large, the accuracy decreases. This is because the tested conditions are dynamic rather than static. This makes the modelling uncertain and forecasting becomes difficult.

9.12 Simulating asphaltenes deposition in a sample of light oil

In this part, the simulation study of asphaltenes deposition in the light oil sample data was carried out by simulating flooding the core with different mole fractions of CO_2 data sets. The test trials covered a wide range of temperatures. A cell with a diameter of 10 cm and length of 30 cm was set for the simulation of asphaltenes deposition. The volume data sets of oil varies between 50 cm^3 and 300 cm^3, depending on the type of production process. Fig. 9.3 demonstrates the simulation setup which consists of a core cell and data sets for pressure, temperature, and a displacement pressure. After using data sets for saturation process, we input CO_2 data to simulate CO_2 injection then record the outcome flow rate. During CO_2 injection phase, the pressure difference between the input and output is controlled by a separate pressure function to reach desired outcome. Thus, we must simulate the pressure drop along the porous medium length to remain unchanged during injection phase. When oil flow rate was not being recorded in the system, the core pressure was slightly reduced. As soon as the core pressure approached zero then, the simulation stops. In addition, we input a temperature data of 150°C, then we calculate the amount of asphaltenes deposited on the core cell by calculating the difference between the mass of the dried core (without applying temperature) prior to saturation process and after CO_2 injection. Fig. 9.4(a) shows the prediction of asphaltenes on crude oil deposition for Mu value (a constant that designates the amount of weights changed on each iteration. Its value lies between 10^{-6} to 0.1) of 0.0001. This provides the prediction rate of 101 for the studied samples with the different periods of time.

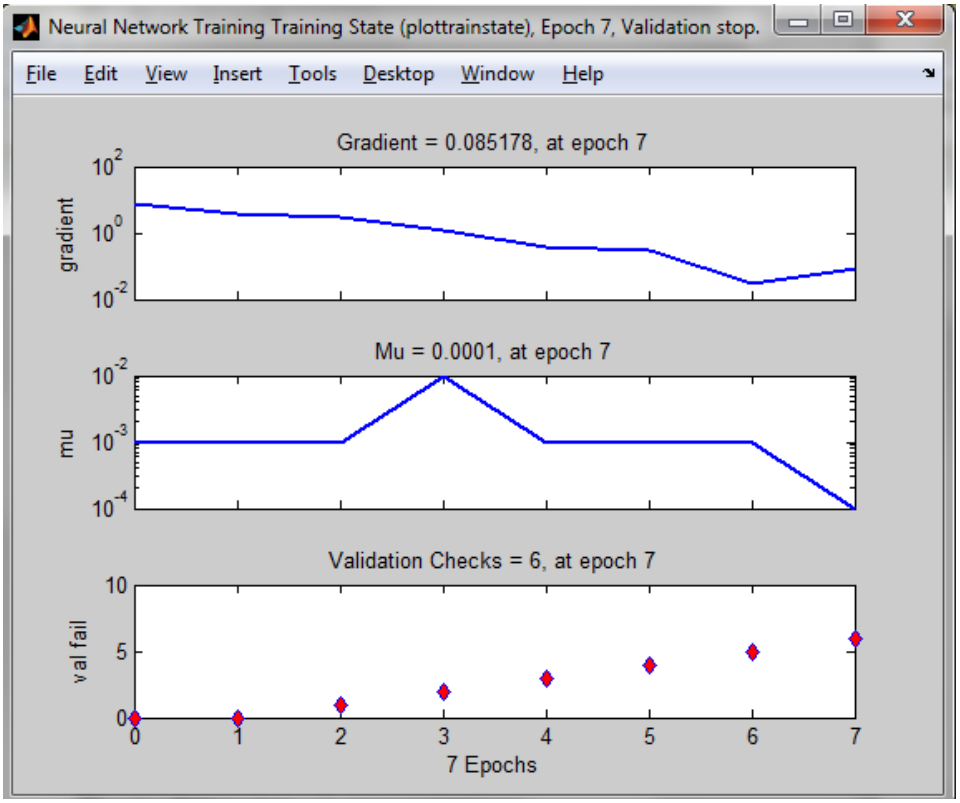

Figure 9-4(a): Prediction of asphaltenes for sample 1

Fig. 8.4(b) provides the prediction value of asphaltenes deposition of sample 2 which has the gradient value of 0.065462.

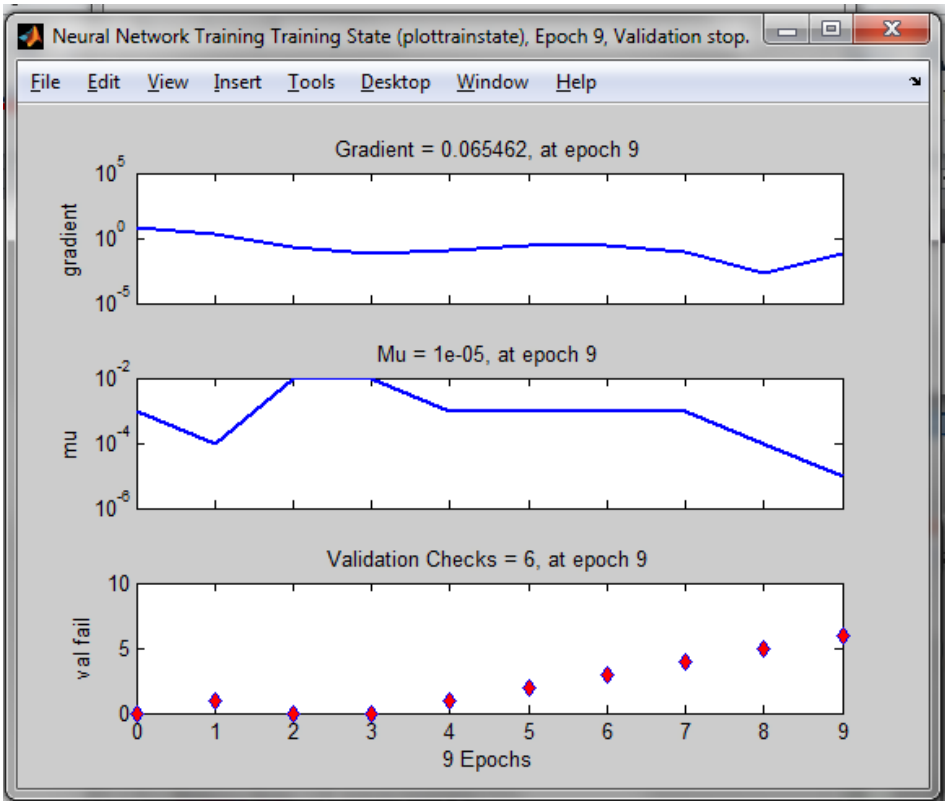

Figure 9.4(b). Prediction of asphaltenes for sample 2

In Figs. 9.4(c), 9.4(d), and 9.4(e), the samples considered were analysed with a gradient value of 0.070105, 0.01899 and 0.017478 respectively for total of 5 samples.

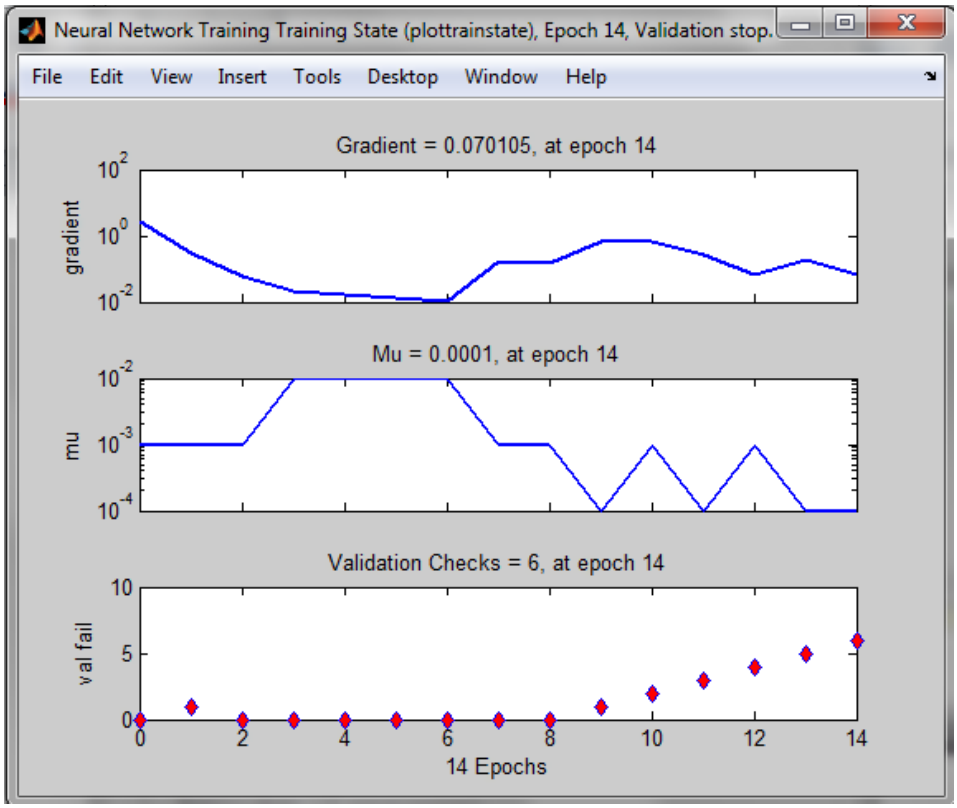

Figure 9.4(c). Prediction of asphaltenes for sample 3

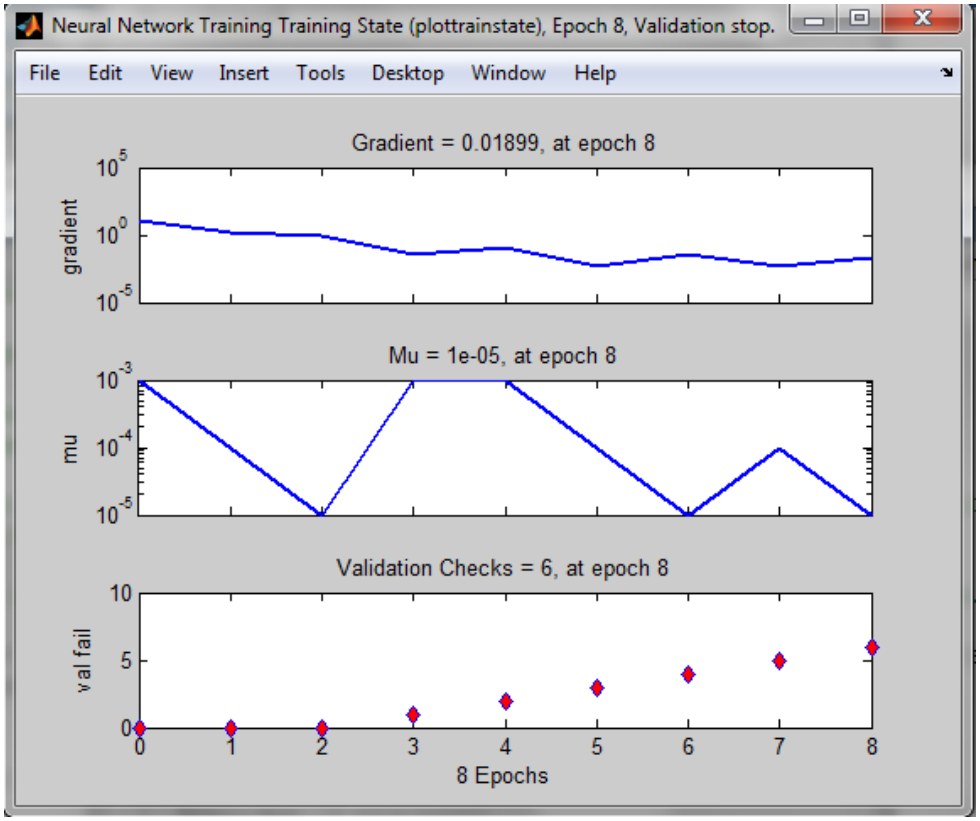

Figure 9.4(d). Prediction of asphaltenes for sample 4

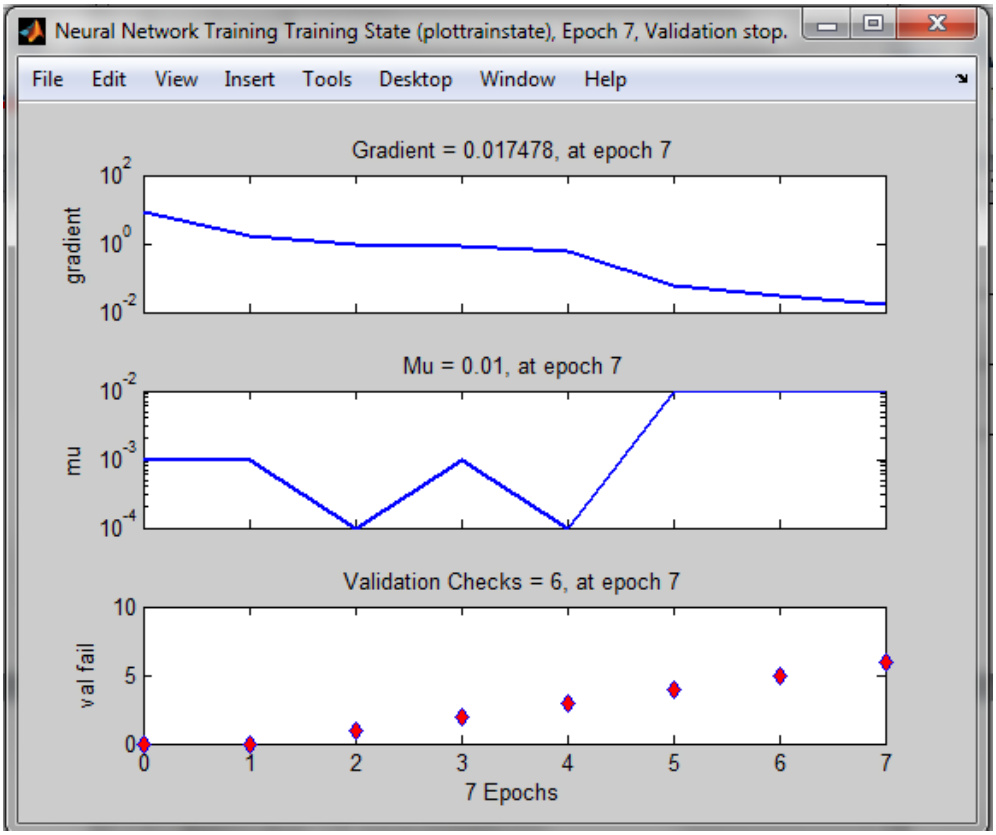

Figure 9.4(e). Prediction of asphaltenes for sample 5

9.13 Performance of fuzzy logic model

At the first stage of this study, a fuzzy inference system was constructed to estimate asphaltenes amounts using the Takagi and Sugeno model (Asoodeh, Gholami, & Bagheripour, 2014). The optimal number of fuzzy rules was obtained through trial and error.

The different values for clustering radii were assigned and performance corresponding to each clustering radius was evaluated. The model with the highest performance was chosen as an optimal model. The optimal value of clustering radius defines an optimal number of fuzzy rules.

Results showed that specification of one clustering radius produces the best model by estimating precipitated asphaltenes amounts. To assess the reliability of the fuzzy model, test data was used, and the corresponding precipitated asphaltenes amount was predicted. This prediction was made using the concept of the correlation coefficient. In the next step, a three-layered neural network with back propagation learning algorithm was constructed. The optimal number of hidden neurons was assigned through trial and error process.

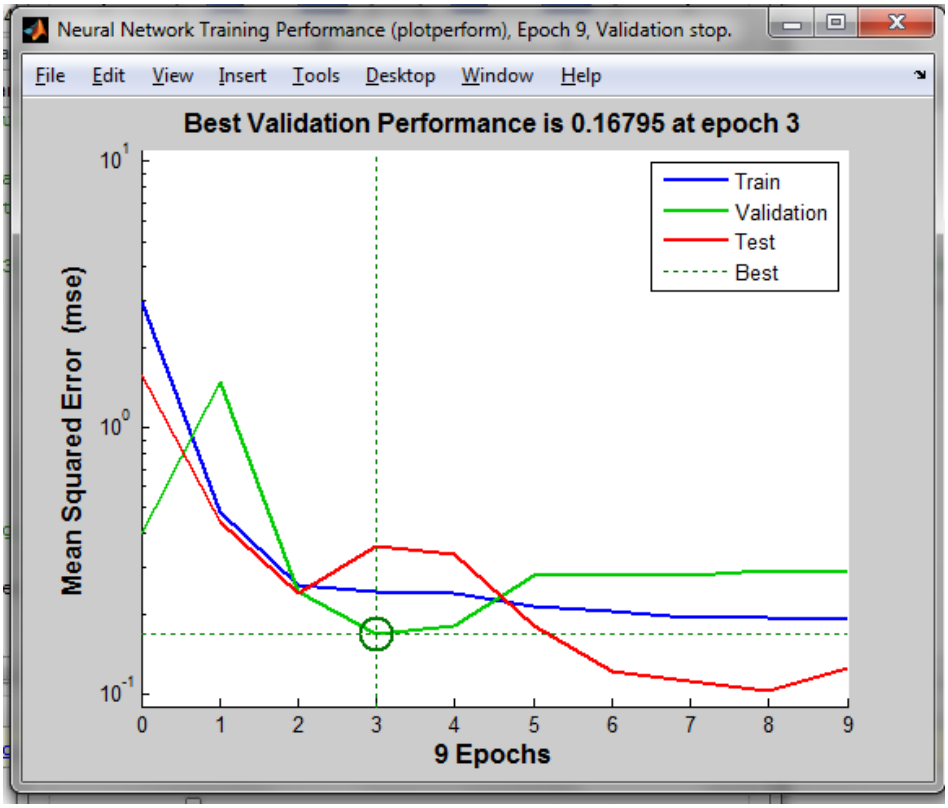

Figure 9. 5(a): MSE for Sample 2

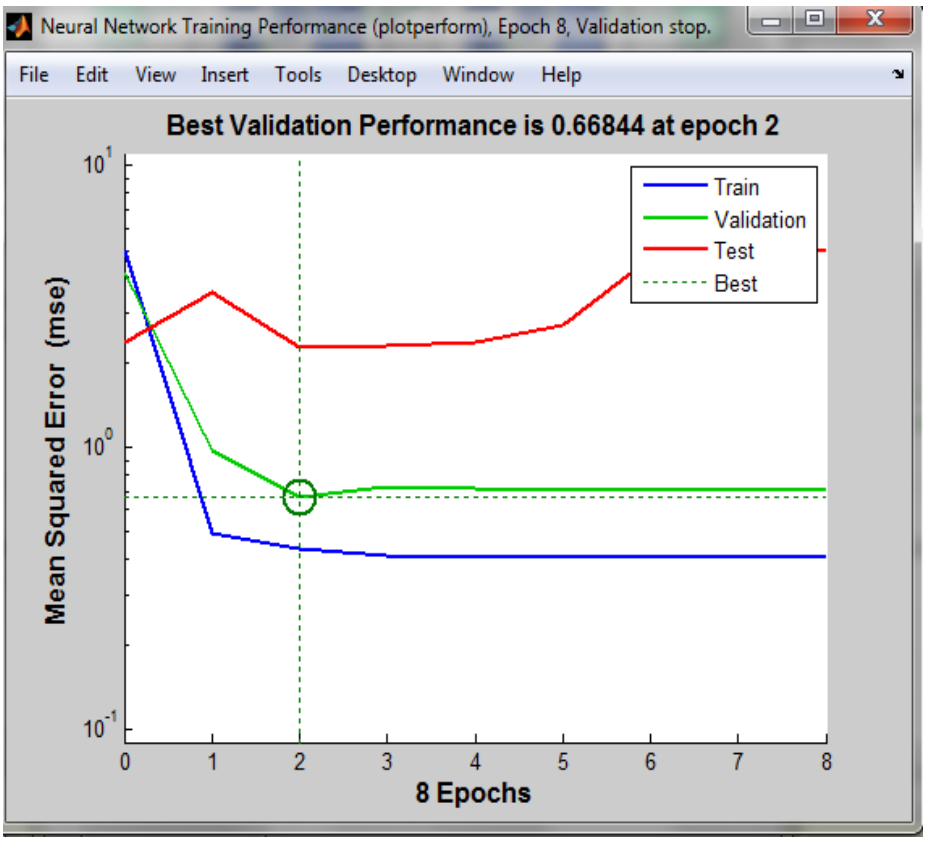

Figure 9-5(b). MSE for Sample

The neural network is then trained by Levenberg–Marquardt training function. The training process ceases in the 8th iteration (epochs) of back-propagation algorithm. Back-propagation algorithm has identified this point as a global minimum. Different parameters play significant roles in the occurrence of over-fitting in a neural network such as the number of data point, number of hidden layers, number of hidden nodes, type of training function, etc. In situations where a number of data points are not as much as desired it is possible to prevent over-fitting by regulating other mentioned parameters. The probability of over-fitting was controlled by setting the appropriate regulations in this model. The performance of neural network was evaluated by inputting the experimental data into the model which helped in prediction of the amount of asphaltenes.

9.14 Conclusions

In this study, prediction of asphaltenes formation was evaluated by developing a model based on genetic algorithms and Artificial Neural Network (ANN). Specifically, the asphaltene deposition in crude oils having different compositions was evaluated using the predictive models. The study points out various discrepancies associated with previous asphaltene prediction models such as limitations occurred due to incorporation of molecular weights and exclusion of simulation conditions. These discussions critically analyzed the challenging issues in prediction modeling of precipitation/deposition processes occurring in crude oil reservoirs. Techniques also have been discussed which used genetic or evolutionary algorithms for dynamic tests to simulate the production process and statistical experiments for sensitivity analysis in asphaltenes deposition prediction. Performance evaluation of current developed model was tested by inputting the data from various experiment and industrial sources. It can be concluded that the prediction algorithm improved once the data were analyzed at various gradient values by first training the ANN algorithm. Similarly, it can be concluded that the fuzzy logic model, trained using the Takagi and Sugeno model, produces reliable results for asphaltenes precipitation. The best validation performance was evaluated by plotting epochs against MSE producing reliable test results using ANN. The significance of the developed genetic algorithm based on ANN is that it can be combined with available asphaltenes precipitation simulation software by inputting the data conditions of experiments to lower the uncertainties and, increase prediction performance and modeling capabilities.

CHAPTER 10 *Conclusion and recommendations from this research*

10.1 Conclusions:

Two-fluid model provided for practical and precise modelling of multiphase flow problems. It is the most appropriate method suitable for both co-current and counter-current flows. These models are capable of considering the physics in detail. Though, the con to this model is that it is quite costly computationally. Therefore, another model "drift-flux model" can be used in its place by tuning for the slippage ratio. Drift-flux models are actually most suitable for the dispersed flows. For avoiding problems regarding stability in numeric calculations, approaches of mathematical regularization are vital for two-fluid models. Also, the sturdiness and time of computation of two-fluid models requires discretization algorithms.

The most crucial element for simulation of continuity of flow in wellbore is modelling the equilibrium condition and phase behaviour of the hydrocarbon solutions. The probability of hindrance in flow can be quantified by correct calculation of phase envelope of hydrocarbon fluids. In current module of phase behaviour, we utilized cubic EOS. When, working with cubic EOS, procedures of fluid characterization and proper tuning are necessary to capture the asphaltenes precipitation.

In this study we attained quite fine agreement for settings at which validity of deposition models is not challenged. Moreover, the comparison in this study described that models in earlier sections are appropriate for deposition of asphaltene in gas as well as oil flow streams. The deposition rate of asphaltene effectively reduces by either reducing the temperature of tubing surface or by increasing the velocity. From these facts we can infer that when expansion increases the velocity or there is decrease in temperature due to thermal gradient in the wellbore system, the rate of deposition of asphaltenes decreases remarkably.

The results of simulation analysis showed that the depth where pressure is near bubble point pressure has maximum rate of asphaltene deposition. Moreover, over that depth, stability of asphaltene is achieved as it is dissolved in crude oil also the lighter hydrocarbons burst out from oil at that point. Deposition rate of asphaltene along with being related to pressure and temperature also depends upon composition of crude oil. It was indicated by the results that the deposition of asphaltene in wellbore is enhanced by the occurrence of lighter molecules i.e., CO2. Carbon dioxide is responsible for increasing bubble point and onset pressure as well as it causes destabilization of asphaltene in phase envelope. Therefore, mixing of CO2 with asphaltene, significantly reduces the sites of deposition in wellbore to bottom-hole because of higher pressure. A collective model of reservoir and wellbore is needed when problems in continuity of flow in wellbore and reservoir area are modelled. The results of simulation analysis showed that the problem of asphaltene deposition is more persistent in wellbore when compared to the reservoir. With pressure going below onset pressure, the damaging effects of asphaltene in reservoir begin to reveal. The asphaltenes once precipitated undergo flocculation in reservoir and inflict many problems in well's bottom section.

Lastly, the remediation of deposition problems of asphaltene in wellbore was discussed. It was found by simulation analysis that changing temperature and pressure can effectively eliminate the

asphaltene deposition problem. Asphaltene's thermodynamic equilibrium can be affected by well's operation condition and molecule's dynamic transportation. The deposits of asphaltene shrink and are transported to bottom of well by reducing the surface pressure of well below bubble-point pressure

10.2 Recommendations

Following recommendation are presented to further the scope of research in this area:

As the components of asphaltene in the crude mainly consists of polar components, there are significant molecular forces in the polar components structural sites. This make the research on asphaltene components more complicated resulting into difficult research. To successfully predict the asphaltene precipitation at variable temperatures and pressures, the cubic state equation was used.

The use of standalone wellbore model was very important in this research. As understanding of the effect of light components of the oil was important in asphaltene deposition, this model was used to find better results. To better understand the impact of carbon dioxide on the asphaltene deposition, the dynamic simulation of carbon dioxide was used. Due to limitation of the simulation process, it was required to develop a more complex simulation process to study the impact of carbon dioxide injected on the asphaltene precipitation in the wellbore. In addition to the carbon dioxide flooding with the water injection, it was also studied with other fluid options available including gas in the simulation process.

To solve this issue, method of solvent circulation can be used. This is discussed in the chapters of this research. To reduce or completely remove the blockage of the wellbore by asphaltene, aromatic compounds and de-asphalted oils can be used. These solvents can be injected in the production wells from the top. This can also be simulated by thermodynamic modelling. The solvent phase can be studied in the modelling and its impact with the crude oil when it is injected in the wellbore. In future research works, annulus flow path can be studied for solvents to inject in the wellbore. While working on modelling for this research, it is important to keep in consideration the impact of temperature on the tubing and annulus. This annulus flow model will be equally beneficial for similar processes like gas lift process.

In the wellbore model, the only trajectory is of the flow line having multiple angles. The wellbore in the present model does not have multiple junctions. There is a space for improvement in these models to increase the branches and junctions. This can be used in multilateral wells, the in the surface gathering systems and such other platforms.

A comprehensive surface facility network can be obtained in case of realistic modelling of crude reservoir by exploiting presently available options.

Finally, we recommend developing analytical solutions for flow rate decline curves and pressure transient models during asphaltene deposition in the wellbore. These models can be used as

diagnostic tools for detecting flow assurance problems in the wellbore without full simulation of the wellbore flow.

APPENDIX A - Development and explanation of flow equations applied in the research and input data for reservoir flow modelling

The fluid flow model for a wellbore is well established for single-phase flow with limited applications in gas reservoirs or gas pipelines. Introducing the second phase as a concurrent or counter-current gas/liquid flow leads to flow models computationally more challenging and time consuming.

The following discussions relate to numbers of equations utilised within various sections of the mathematical modelling research, discussed in this thesis, relating to the prediction of asphaltene behaviour under various conditions of single and multiphase fluid flow.

Single **p***hase* **f***low* **e***quations*

Single-phase flow can occur in the gas production wells, water injection wells, or superheated steam injection wells at certain conditions where condensation or evaporation of the continuous phase has not occurred. Although single-phase flow in the entire system may not be maintained, formulation of single-phase models can be useful for our development purposes and further extensions to multiphase flow codes. In addition, single-phase models can be used for multiphase flow simulations with some multiple precautions, if the mixture of the phases can be assumed homogenous.

My model is capable of using single-phase model for injection wells and production wells. Usually this module is applied to well test analysis for single-phase pressure drawdown and buildup tests.

The governing equations in single-phase flow model consist of one mass conservation equation and one momentum conservation equation. Derivation of general balance equations for single-phase flow are discussed.

However, incorporating the basic assumption for one-dimensional models and neglecting the turbulence effect, the balance equations in single-phase flow becomes

$$\frac{\partial \rho}{\partial t} + \frac{1}{A}\frac{\partial A\rho u}{\partial x} = \dot{\psi},$$

$$\frac{\partial \rho u}{\partial t} + \frac{\partial \rho u^2}{\partial x} + \left(144.0 g_C\right)\frac{\partial P}{\partial x} + \rho g \sin\theta + \frac{\tau \pi D}{A} = 0,$$

where ρ is the density of the fluid, u is the actual velocity, P is the pressure, T is the wall shear stress, D is the diameter of the pipe, A is the cross section of the pipe, $\dot{\psi}$ is the source/sink term in mass influx, and 144.0gc is the field unit conversion factor. To obtain the flow variable, these equations are solved along with appropriate wall-phase shear friction equations and state relations that will be presented.

Multiphase flow

Multiphase flow can occur in many occasions during oil production and transportation in hydrocarbon reservoirs. In the past few decades, development of robust multiphase flow models for hydrocarbon transportation has been aggressively expanded by many researchers and commercial developers in the petroleum industry. Accurate modelling of multiphase flow in the wells can be advantageous not only for production optimization but also for flow line designs.

$$\frac{\partial(\rho_o\alpha_o)}{\partial t}+\frac{1}{A}\frac{\partial(A\rho_o\alpha_o u_o)}{\partial x}=\dot{\psi}_o-\Gamma_g,$$
$$\frac{\partial(\rho_g\alpha_g)}{\partial t}+\frac{1}{A}\frac{\partial(A\rho_g\alpha_g u_g)}{\partial x}=\dot{\psi}_g+\Gamma_g,$$

Although multiphase flow models can yield better approximation of the flow variables, the complexity of the models has added some restrictions to full applications of these models. For instance, most of the multiphase flow models for the wellbores have been developed in 1D along the well trajectory and cross-sectional average schemes have been used to represent the fluids in the flow line. In fact, a full 3D model for the wellbore can be very computationally time-consuming and inefficient for a set of simulation studies. Hence, for development purposes of multiphase flow in the wellbore, we need to make some assumptions listed as follows:

One-dimensional flow is assumed along the trajectory of the well in horizontal, deviated, and vertical inclinations. This assumption is reasonable for the wellbores and pipelines with small diameter. Considering a long well in the order of 1000 ft with a small diameter in the order of 1 ft, one-dimensional assumption for the flow path is reasonable.

- Eulerian time and spatial averaging are applied.

- The liquid phase consists of oil/water mixture. In case water exists in the flow, liquid properties are calculated by volumetric and mass averaging between water and oil. This assumption is valid when the slippage between oil and water is negligible. For the
- cases that oil viscosity is not very large no slip assumption is reasonable for the liquid
- mixture. However, for heavy oil systems the oil/water slippage should be considered.

- For the three-phase flow cases, oil and water slippage is included using a drift-flux
- correlation for the liquid mixture.

- In addition to source or sink mass flow rate, another term is also considered which is
- calculated by well indices values for each phase.

Mass conservation equations

Since oil and gas phases are a mixture of hydrocarbon components, we derive our mass conservation equations from mass conservation of hydrocarbon components. Afterward, we can sum up the mass conservation of components in each hydrocarbon phase to obtain the mass conservation of hydrocarbon phases.

Assuming, k to be the hydrocarbon component in the gas and oil phase, the mass

conservation of component k becomes

$$\frac{\partial\left(\hat{\rho}_o\alpha_o x_k+\hat{\rho}_g\alpha_g y_k\right)}{\partial t}+\frac{1}{A}\frac{\partial\left(A\hat{\rho}_o\alpha_o u_o x_k+A\hat{\rho}_g\alpha_g u_g y_k\right)}{\partial x}=\dot{\psi}_{ok}+\dot{\psi}_{gk},\ k=1,\ \ldots,\ nc$$

$\hat{\rho}_o$ and $\hat{\rho}_g$ are the molar density of oil and gas phases, α_o and α_g are the volume fractions of oil and gas, x_k and y_k are the compositions of component k in the oil and gas phases,

$$\frac{\partial\sum_{k=1}^{nc}\left(\hat{\rho}_o\alpha_o x_k+\hat{\rho}_g\alpha_g y_k\right)}{\partial t}+\frac{1}{A}\frac{\partial\sum_{k=1}^{nc}A\left(\hat{\rho}_o\alpha_o u_o x_k+\hat{\rho}_g\alpha_g u_g y_k\right)}{\partial x}=\sum_{k=1}^{nc}\dot{\psi}_{ok}+\dot{\psi}_{gk},$$

$$\frac{\partial\left(\hat{\rho}_o\alpha_o+\hat{\rho}_g\alpha_g\right)}{\partial t}+\frac{1}{A}\frac{\partial\left(A\hat{\rho}_o\alpha_o u_o+A\hat{\rho}_g\alpha_g u_g\right)}{\partial x}=\dot{\psi}_o+\dot{\psi}_g.$$

If we split equation into Oil and Gas phases, we will have the below equations:

where Rg is the interphase mass transfer term between oil and gas, $\dot{\psi}_o$ and $\dot{\psi}_o$g are oil and gas mass influx terms and ρ_o and ρ_g are oil and gas mass density. As can be seen, this can be converted by reducing the component-based mass conservation equation to the phase based mass conservation equation. Along with an appropriate definition of interphase mass transfer term, these equations can decrease the number of primary unknowns in our system of equations.

Momentum conservation equation assuming a homogenous approach

One of the simplest approaches to calculate the velocity of phases in the multiphase flow model is using momentum equation for the mixture of fluids. In this method, we assume the entire fluid moving with the same velocity, no slippage and the momentum interactions exerted to the bulk of fluid

$$u_g=u_o=u_w=u_m.$$

Hence, in a homogenous model, we combine the mixture properties and solve the momentum equation for the bulk of the fluid to obtain um.

$$\frac{\partial\left(\rho_m u_m\right)}{\partial t}+\frac{\partial\left(\rho_m u_m^2\right)}{\partial x}+\left(144.0g_c\right)\frac{\partial P}{\partial x}+\rho_m g\sin\theta+\frac{\tau_m\pi D}{A}=0.$$

In Equation above ρ_m is the mixture density which is calculated by volumetric averaging:

$$\rho_m=\rho_g\alpha_g+\rho_o\alpha_o+\rho_w\alpha_w$$

Momentum conservation equation with drift-flux approach

In the drift-flux modelling approach, the slippage of phases can be included in the velocity calculations using the model proposed by Ishii (1997)

$$u_g = C_0 J + V_d.$$

In previous Equation J is volumetric average velocity of the bulk, Vd is the drift velocity and C0 is the profile parameter (or distribution coefficient). Therefore, once we are able to calculate the volumetric average velocity of the bulk from the momentum equation, we can calculate the velocity of gas from previous Equation. Using average velocity equation, we can calculate the liquid velocity as well.
Referring to previous Equation, considering phase velocity slippage, the momentum equation is reformulated as follows:

$$\frac{\partial(\rho_m u_m)}{\partial t} + \frac{\partial\left(\rho_g \alpha_g u_g^2 + \rho_o \alpha_o u_o^2 + \rho_w \alpha_w u_w^2\right)}{\partial x} + \left(144.0 g_c\right)\frac{\partial P}{\partial x} + \rho_m g \sin\theta + \frac{\tau_m \pi D}{A} = 0.$$

Since velocities of gas, oil and water are no longer equal to the average velocity of the bulk fluid; the momentum equation becomes a function of phase velocities and mass average velocity, um,

$$u_m = \frac{\rho_g \alpha_g u_g + \rho_o \alpha_o u_o + \rho_w \alpha_w u_w}{\rho_m}.$$

Furthermore, in the drift-flux model proposed by Ishii (1997), volumetric average velocity is used; hence, to be able to use um in drift-flux correlation, certain modification is required. In addition, to extend the drift-flux model to calculate gas, oil, and water velocities, two pairs of systems (first, liquid and gas and second, oil and water) are considered. Hence, the mixture average velocity is used to calculate the liquid and gas velocities and the liquid average velocity is used to obtain oil and water velocities. With a correct definition of profile parameters and drift velocities for each system; the gas, liquid, oil, and water velocities are defined as follows:

$$u_g = C_1^{gl} u_m + v d_1^{gl},$$
$$u_l = C_2^{gl} u_m + v d_2^{gl},$$
$$u_o = C_1^{ow} u_m + v d_1^{ow},$$
$$u_w = C_2^{ow} u_m + v d_2^{ow}.$$

Momentum conservation equations with two-fluid approach

The momentum conservation equations of gas and liquid phases in non-stratified flow becomes

$$\frac{\partial\left(\alpha_g \rho_g u_g\right)}{\partial t} + \frac{\partial\left(\alpha_g \rho_g u_g^2\right)}{\partial x} + \left(144.0 g_c\right)\alpha_g \frac{\partial P}{\partial x} + \alpha_g \rho_g B_x +$$
$$\alpha_g \rho_g u_g FWG - \Gamma_g u_{gi} + \alpha_g \rho_g \left(u_g - u_l\right) FIG = 0,$$
$$\frac{\partial\left(\alpha_l \rho_l u_l\right)}{\partial t} + \frac{\partial\left(\alpha_l \rho_l u_l^2\right)}{\partial x} + \left(144.0 g_c\right)\alpha_l \frac{\partial P}{\partial x} + \alpha_l \rho_l B_x +$$
$$\alpha_l \rho_l u_l FWL + \Gamma_g u_{li} + \alpha_l \rho_l \left(u_l - u_g\right) FIL = 0.$$

$$\alpha_g \rho_g \frac{\partial u_g}{\partial t} + \alpha_g \rho_g \frac{\partial u_g^2}{2\partial x} + (144.0 g_c)\alpha_g \frac{\partial P}{\partial x} + \alpha_g \rho_g B_x +$$
$$\alpha_g \rho_g u_g FWG + \Gamma_g (u_g - u_{gi}) + \dot{\psi}_g u_g + \alpha_g \rho_g \left(u_g - u_l\right) FIG = 0,$$
$$\alpha_l \rho_l \frac{\partial u_l}{\partial t} + \alpha_l \rho_l \frac{\partial u_l^2}{2\partial x} + (144.0 g_c)\alpha_l \frac{\partial P}{\partial x} + \alpha_l \rho_l B_x +$$
$$\alpha_l \rho_l u_l FWL - \Gamma_g (u_l - u_{li}) + \dot{\psi}_l u_l + \alpha_l \rho_l \left(u_l - u_g\right) FIL = 0.$$

$$u_{gi} = u_{li} = u_i,$$
$$\alpha_g \rho_g FIG = \alpha_l \rho_l FIL = \alpha_l \rho_l \alpha_g \rho_g FI,$$

Characteristic Roots of Multiphase Flow Equations

To analyze the characteristic roots of the different modelling approaches, the equations, above, were solved for each modelling approach. We discussed the regions where characteristic roots may become imaginary. In the homogenous model we have:

$$\frac{\partial(\rho_m)}{\partial t} + \frac{\partial(\rho_m u_m)}{\partial x} = \dot{\psi}_l + \dot{\psi}_g,$$
$$\frac{\partial(\rho_m u_m)}{\partial t} + \frac{\partial\left(\rho_m u_m^2\right)}{\partial x} + (144.0 g_c)\frac{\partial P}{\partial x} = -\rho_m g \sin\theta - \frac{\tau_m \pi D}{A}.$$

Replacing the density derivative with pressure derivative, using the definition of fluid mixture compressibility, we obtain

$$\frac{\partial(\rho_m)}{\partial t} = \frac{\partial(\rho_m)}{\partial P}\frac{\partial P}{\partial t},$$
$$\frac{\partial(\rho_m)}{\partial x} = \frac{\partial(\rho_m)}{\partial P}\frac{\partial P}{\partial x},$$
$$C_m = \frac{\partial(\rho_m)}{\partial P}$$
$$C_m \frac{\partial P}{\partial t} + u_m C_m \frac{\partial P}{\partial x} + \rho_m \frac{\partial u_m}{\partial x} = \dot{\psi}_l + \dot{\psi}_g$$
$$u_m C_m \frac{\partial P}{\partial t} + \rho_m \frac{\partial u_m}{\partial t} + 2\rho_m u_m \frac{\partial u_m}{\partial x} + C_m u_m^2 \frac{\partial P}{\partial x} + (144.0 g_c)\frac{\partial P}{\partial x} = -\rho_m g \sin\theta - \frac{\tau_m \pi D}{A}$$

Assuming

$$U = [u_m, P]^T,$$
$$[A] = \begin{bmatrix} 0 & C_m \\ \rho_m & u_m C_m \end{bmatrix},$$
$$[B] = \begin{bmatrix} \rho_m & u_m C_m \\ 2\rho_m u_m & u_m^2 C_m + 1 \end{bmatrix},$$

The characteristic roots of the homogenous model become

$$\begin{vmatrix} -\rho_m & C_m\lambda - u_m C_m \\ \rho_m\lambda - 2\rho_m u_m & u_m C_m\lambda - u_m^2 C_m - 1 \end{vmatrix} = 0 \rightarrow \lambda = u_m \pm \sqrt{\frac{1}{C_m}}.$$

As can be seen, the characteristic roots of the homogenous model are always real. Hence, the homogenous model is always hyperbolic. In the same manner, we can analyse the characteristic roots of the drift-flux model.

Regularization of non-hyperbolic equations

The first approach for mathematical regularization is hyperbolization of the model by adding some ad hoc terms to the momentum equations. In this method, some physical phenomena (i.e. surface tension, viscosity effect, interfacial pressure) can be considered in the model to move the characteristic roots from complex zone to real zone. For example, Drew et al. (Arnold, Drew, & Lahey Jr, 1990) added virtual mass terms to the right-hand side of the momentum equations which had time and space derivatives of the variables.

Furthermore, No and Kazimi (No & Kazimi, 1981) discussed this model to characterize the virtual mass coefficient range to obtain real roots for the characteristic equation and reasonable error growth amplitude.

Song and Ishii(Song & Ishii, 2000) used some empirical parameters as momentum flux parameters to avoid the non-hyperbolic condition of two-fluid model. Some other researchers also added two-pressure model for gas and liquid (Pauchon & Banerjee, 1986; Ström, Sasic, Jareteg, & Demazière, 2015).

$$F^V = -C^{vm}\alpha_l\alpha_g\rho_m\left[\frac{\partial\left(u_l - u_g\right)}{\partial t} + u_g\frac{\partial u_l}{\partial x} - u_l\frac{\partial u_g}{\partial x}\right].$$

Flow regime detection

One of the most important steps in the multiphase flow modelling is correct flow pattern determination. Since the dominant flow regime characterizes the flow equation, the accuracy of the simulation results is very much affected by the flow pattern detection algorithms. In addition, since the momentum equations are changed for the force balance terms in different flow regimes, the transition of the flow patterns can also add a source of discontinuity and numerical convergence issues in the equations. In this section, we are going to discuss on some robust algorithms for flow regime detection and flow transition smoothing that we have adopted for our model development.

Constitutive relations

The constitutive models are the equations we apply for correlations of phasic velocities in the drift-flux models and for interphase drag forces in the two-fluid models. These relations are required in the momentum equations to grant a closure to the system of equations.

Drift-flux model

The slippage between two fluids results from the non-uniform profile of velocity and buoyancy forces between the phases. This phenomenon can be modelled for a mixture of gas and liquid by a mathematical equation (Shi et al., 2005) as follows:

$$u_g = C_{0gl} u_m + V d_{gl},$$
$$u_l = \left(\frac{1-\alpha_g C_{0gl}}{1-\alpha_g} \right) u_m - \left(\frac{\alpha_g}{1-\alpha_g} \right) V d_{gl}.$$

Phasic wall friction

In the momentum equations, there are wall friction terms (FWL and FWG) that contribute the interaction of wall with the fluids. Defining a correct mathematical model for these terms is crucial since they significantly contribute to pressure drop at high flow rates. Wall friction terms are function of wall roughness, velocity of phases, and surface contact of fluids with wall. To calculate wall friction terms, first we define a two-phase wall friction term. Afterward, we split it to friction forces of liquid and gas phases by a partitioning factor.

$$\left(\frac{dP}{dl} \right)_{2\Phi} = \frac{1}{2D} \left(f_l \rho_l (\alpha_l u_l)^2 + C \left[f_l \rho_l (\alpha_l u_l)^2 f_g \rho_g (\alpha_g u_g)^2 \right]^{0.5} + f_g \rho_g (\alpha_g u_g)^2 \right)$$

Interphase mass transfer

Interphase mass transfer R g is another undetermined term in mass conservation equations. This parameter defines the amount of gas that can evaporate or condensate between hydrocarbon gas and liquid system. control volume of a liquid and gas system that can exchange mass. Since the amount of gas that is exchanged between the phases depends on pressure and temperature variations in the control volume, R g is computed as a function of pressure and temperature.

$$\Gamma_g = -\frac{\rho_{gsc}}{5.615 B_o} \left[\begin{array}{l} \left(\frac{\partial R_s}{\partial P} \right) \frac{\partial P}{\partial t} \alpha_o + \left(\frac{\partial R_s}{\partial P} \right) \frac{\partial P}{\partial x} (u_o \alpha_o) + \\ \left(\frac{\partial R_s}{\partial T} \right) \frac{\partial T}{\partial t} \alpha_o + \left(\frac{\partial R_s}{\partial T} \right) \frac{\partial T}{\partial x} (u_o \alpha_o) \end{array} \right],$$

Wellbore heat transfer models

we study the process of heat transfer between wellbore and the surrounding (ambience), solving the coupled wellbore/surrounding energy equations. With the energy equation for the ambient and the wellbore taken into account, more accurate results are obtained for fluid temperature. In addition, since temperature affects the fluids' properties, a better approximation of temperature can yield a better approximation of flow rates and pressure.

Energy equation in the wellbore

Although in reality the flowing liquid and gas temperatures are not equal, for the sake of simplicity we assume they are identical in our application. Accordingly, the energy equation that we solve to obtain fluid temperature in wellbore is the total energy conservation:

$$\frac{\partial\left[\alpha_o\rho_o\left(\bar{h}_o+\frac{u_o^2}{2g_cJ_c}\right)\right]}{\partial t}+\frac{\partial\left[\alpha_g\rho_g\left(\bar{h}_g+\frac{u_g^2}{2g_cJ_c}\right)\right]}{\partial t}+\frac{\partial\left[\alpha_w\rho_w\left(\bar{h}_w+\frac{u_w^2}{2g_cJ_c}\right)\right]}{\partial t}+$$

$$\frac{1}{A}\frac{\partial\left[A\alpha_o\rho_o u_o\left(\bar{h}_o+\frac{u_o^2}{2g_cJ_c}\right)\right]}{\partial x}+\frac{1}{A}\frac{\partial\left[A\alpha_g\rho_g u_g\left(\bar{h}_g+\frac{u_g^2}{2g_cJ_c}\right)\right]}{\partial x}+\frac{1}{A}\frac{\partial\left[A\alpha_w\rho_w u_w\left(\bar{h}_w+\frac{u_w^2}{2g_cJ_c}\right)\right]}{\partial x}-$$

$$\dot{H}_w-\dot{H}_o-\dot{H}_g+\alpha_w\rho_w\frac{u_w}{g_cJ_c}g\sin\theta+\alpha_o\rho_o\frac{u_o}{g_cJ_c}g\sin\theta+\alpha_g\rho_g\frac{u_g}{g_cJ_c}g\sin\theta+$$

$$\frac{\dot{Q}_{loss}}{A}=0.$$

Wellbore heat loss model

$$\frac{1}{U_{to}}=\frac{r_{to}}{r_{ti}h_{to}}+\frac{r_{to}\ln(r_{to}/r_{ti})}{k_t}+\frac{r_{to}\ln(r_{ins}/r_{to})}{k_{ins}}+\frac{r_{to}}{r_{ins}(h_c+h_r)}+\frac{r_{to}\ln(r_{co}/r_{ci})}{k_{cas}}+$$

$$\frac{r_{to}\ln(r_{wb}/r_{co})}{k_{cem}}.$$

Wellbore Models Numerical Solutions

$$\frac{\partial(\rho_w\alpha_w)}{\partial t}+\frac{1}{A}\frac{\partial A(\rho_w\alpha_w u_w)}{\partial x}=\dot{\psi}_w,$$

$$\frac{\partial\left(\rho_g\alpha_g-\rho_o\alpha_o-\rho_w\alpha_w\right)}{\partial t}+\frac{1}{A}\frac{\partial A\left(\rho_g\alpha_g u_g-\rho_o\alpha_o u_o-\rho_w\alpha_w u_w\right)}{\partial x}=2\Gamma_g+\dot{\psi}_g-\dot{\psi}_o-\dot{\psi}_w,$$

$$\frac{\partial\left(\rho_g\alpha_g+\rho_o\alpha_o+\rho_w\alpha_w\right)}{\partial t}+\frac{1}{A}\frac{\partial A\left(\rho_g\alpha_g u_g+\rho_o\alpha_o u_o+\rho_w\alpha_w u_w\right)}{\partial x}=\dot{\psi}_g+\dot{\psi}_o+\dot{\psi}_w,$$

$$\frac{\partial u_g}{\partial t}-\frac{\partial u_l}{\partial t}+\frac{\partial u_g^2}{2\partial x}-\frac{\partial u_l^2}{2\partial x}=-(144.0g_c)\left(\frac{1}{\rho_g}-\frac{1}{\rho_l}\right)\frac{\partial P}{\partial x}-\frac{\rho_m}{\rho_g\rho_l}\left(\rho_l-\rho_g\right)B_y\frac{\partial y}{\partial x}-u_gFWG+$$

$$u_lFWL-\Gamma_g\left(\frac{\alpha_l\rho_l u_g+\alpha_g\rho_g u_l-\rho_m u_i}{\alpha_g\rho_g\alpha_l\rho_l}\right)-\left(\frac{\dot{\psi}_g u_g}{\alpha_g\rho_g}-\frac{\dot{\psi}_l u_l}{\alpha_l\rho_l}\right)-\rho_m(u_g-u_l)FI-$$

$$\frac{C^{vm}\rho_m}{\rho_g\rho_l}\frac{\partial\left(u_g-u_l\right)}{\partial t},$$

$$\alpha_g\rho_g\frac{\partial u_g}{\partial t}+\alpha_l\rho_l\frac{\partial u_l}{\partial t}+\alpha_g\rho_g\frac{\partial u_g^2}{2\partial x}+\alpha_l\rho_l\frac{\partial u_l^2}{2\partial x}=-(144.0g_c)\frac{\partial P}{\partial x}-\rho_mB_x-$$

$$\alpha_g\rho_g u_gFWG-\alpha_l\rho_l u_lFWL-\Gamma_g(u_g-u_l)-\dot{\psi}_g u_g-\dot{\psi}_l u_l,$$

$$\frac{\partial\left[\alpha_g\rho_g\left(\bar{h}_g+\frac{u_g^2}{2g_cJ_c}\right)\right]}{\partial t}+\frac{\partial\left[\alpha_o\rho_o\left(\bar{h}_o+\frac{u_o^2}{2g_cJ_c}\right)\right]}{\partial t}+\frac{\partial\left[\alpha_w\rho_w\left(\bar{h}_w+\frac{u_w^2}{2g_cJ_c}\right)\right]}{\partial t}+$$

$$\frac{1}{A}\frac{\partial\left[A\alpha_g\rho_g u_g\left(\bar{h}_g+\frac{u_g^2}{2g_cJ_c}\right)\right]}{\partial x}+\frac{1}{A}\frac{\partial\left[A\alpha_o\rho_o u_o\left(\bar{h}_o+\frac{u_o^2}{2g_cJ_c}\right)\right]}{\partial x}+\frac{1}{A}\frac{\partial\left[A\alpha_w\rho_w u_w\left(\bar{h}_w+\frac{u_w^2}{2g_cJ_c}\right)\right]}{\partial x}=$$

$$\dot{H}_w+\dot{H}_o+\dot{H}_g-\alpha_g\rho_g\frac{u_g}{g_cJ_c}g\sin\theta-\alpha_o\rho_o\frac{u_o}{g_cJ_c}g\sin\theta-\alpha_w\rho_w\frac{u_w}{g_cJ_c}g\sin\theta-$$

$$\frac{\dot{Q}_{loss}}{A}.$$

Gas and liquid mass conservation difference:

$$V_b\left[\rho_{g,L}^n\left(\tilde{\alpha}_{g,L}^{n+1}-\alpha_{g,L}^n\right)-\rho_{o,L}^n\left(\tilde{\alpha}_{o,L}^{n+1}-\alpha_{o,L}^n\right)-\rho_{w,L}^n\left(\tilde{\alpha}_{w,L}^{n+1}-\alpha_{w,L}^n\right)\right]+$$

$$V_b\left[\alpha_{g,L}^n\left(\tilde{\rho}_{g,L}^{n+1}-\rho_{g,L}^n\right)-\alpha_{o,L}^n\left(\tilde{\rho}_{o,L}^{n+1}-\rho_{o,L}^n\right)-\alpha_{w,L}^n\left(\tilde{\rho}_{w,L}^{n+1}-\rho_{w,L}^n\right)\right]+$$

$$\Delta t\left[\dot{\alpha}_{g,j+1}^n\dot{\rho}_{g,j+1}^n A_{j+1}^n u_{g,j+1}^{n+1}-\dot{\alpha}_{g,j}^n\dot{\rho}_{g,j}^n A_j^n u_{g,j}^{n+1}\right]-$$

$$\Delta t\left[\dot{\alpha}_{o,j+1}^n\dot{\rho}_{o,j+1}^n A_{j+1}^n u_{o,j+1}^{n+1}-\dot{\alpha}_{o,j}^n\dot{\rho}_{o,j}^n A_j^n u_{o,j}^{n+1}\right]-$$

$$\Delta t\left[\dot{\alpha}_{w,j+1}^n\dot{\rho}_{w,j+1}^n A_{j+1}^n u_{w,j+1}^{n+1}-\dot{\alpha}_{w,j}^n\dot{\rho}_{w,j}^n A_j^n u_{w,j}^{n+1}\right]=$$

$$V_b\Delta t\left(2\tilde{\Gamma}_g^{n+1}+\dot{\psi}_{g,L}^n-\dot{\psi}_{o,L}^n-\dot{\psi}_{w,L}^n\right),$$

Gas and liquid mass conservation summation:

$$V_b\left[\rho_{g,L}^n\left(\tilde{\alpha}_{g,L}^{n+1}-\alpha_{g,L}^n\right)+\rho_{o,L}^n\left(\tilde{\alpha}_{o,L}^{n+1}-\alpha_{o,L}^n\right)+\rho_{w,L}^n\left(\tilde{\alpha}_{w,L}^{n+1}-\alpha_{w,L}^n\right)\right]+$$

$$V_b\left[\alpha_{g,L}^n\left(\tilde{\rho}_{g,L}^{n+1}-\rho_{g,L}^n\right)+\alpha_{o,L}^n\left(\tilde{\rho}_{o,L}^{n+1}-\rho_{o,L}^n\right)+\alpha_{w,L}^n\left(\tilde{\rho}_{w,L}^{n+1}-\rho_{w,L}^n\right)\right]+$$

$$\Delta t\left[\dot{\alpha}_{g,j+1}^n\dot{\rho}_{g,j+1}^n A_{j+1}^n u_{g,j+1}^{n+1}-\dot{\alpha}_{g,j}^n\dot{\rho}_{g,j}^n A_j^n u_{g,j}^{n+1}\right]+$$

$$\Delta t\left[\dot{\alpha}_{o,j+1}^n\dot{\rho}_{o,j+1}^n A_{j+1}^n u_{o,j+1}^{n+1}-\dot{\alpha}_{o,j}^n\dot{\rho}_{o,j}^n A_j^n u_{o,j}^{n+1}\right]+$$

$$\Delta t\left[\dot{\alpha}_{w,j+1}^n\dot{\rho}_{w,j+1}^n A_{j+1}^n u_{w,j+1}^{n+1}-\dot{\alpha}_{w,j}^n\dot{\rho}_{w,j}^n A_j^n u_{w,j}^{n+1}\right]=$$

$$V_b\Delta t\left(\dot{\psi}_{g,L}^n+\dot{\psi}_{o,L}^n+\dot{\psi}_{w,L}^n\right),$$

Gas and liquid momentum conservation difference:

$$\Delta x_j\left(1+\frac{C^{vm}\rho_m^2}{\rho_g\rho_l}\right)_j^n\left[\left(u_{g,j}^{n+1}-u_{g,j}^n\right)-\left(u_{l,j}^{n+1}-u_{l,j}^n\right)\right]+$$

$$\frac{\Delta t}{2}\left[\left(\frac{\dot{\alpha}_g\dot{\rho}_g}{\alpha_g\rho_g}\right)_j^n\left((u_g^2)_L^n-(u_g^2)_K^n\right)-\left(\frac{\dot{\alpha}_l\dot{\rho}_l}{\alpha_l\rho_l}\right)_j^n\left((u_l^2)_L^n-(u_l^2)_K^n\right)\right]-$$

$$\frac{\Delta t}{2}\left[\left(\frac{\dot{\alpha}_g\dot{\rho}_g}{\alpha_g\rho_g}\right)_j^n VISG_j^n-\left(\frac{\dot{\alpha}_l\dot{\rho}_l}{\alpha_l\rho_l}\right)_j^n VISL_j^n\right]=$$

$$-\Delta t\left(144.0g_c\right)\left(\frac{\rho_l-\rho_g}{\rho_l\rho_g}\right)_j^n\left(P_L^{n+1}-P_K^{n+1}\right)-\Delta t\Delta x_j FWG_j^n u_{g,j}^{n+1}+\Delta t\Delta x_j FWL_j^n u_{l,j}^{n+1}$$

$$+\Delta t\Delta x_j\left(\frac{\Gamma_g}{\alpha_g\rho_g\alpha_l\rho_l}\right)_j^n\left(\rho_{m,j}^n u_{i,j}^{n+1}-\alpha_{l,j}^n\rho_{l,j}^n u_{g,j}^{n+1}-\alpha_{g,j}^n\rho_{g,j}^n u_{l,j}^{n+1}\right)$$

$$+\Delta t\Delta x_j f_{x,j}^n\left(\frac{1}{\alpha_g\rho_g}+\frac{1}{\alpha_l\rho_l}\right)_j^n\left(fwg_j^n u_{g,j}^{n+1}-fwl_j^n u_{l,j}^{n+1}\right)$$

$$-\Delta t\Delta x_j\left(\rho_m FI\right)_j^n\left[\left(1+f_x(C_{1gl}-1)\right)_j^n u_{g,j}^{n+1}-\left(1+f_x(C_{0gl}-1)\right)_j^n u_{l,j}^{n+1}\right]$$

$$-\Delta t\left(\frac{\rho_m}{\rho_g\rho_l}\right)_j^n\left(\rho_l-\rho_g\right)_j^n B_y\left(y_L^n-y_K^n\right)$$

Discretization method for drift-flux model

As for the two-fluid model, a staggered gridding is used for discretization of drift flux model. The mixture velocity vector is calculated at the junction and the pressure, temperature, and phasic volume fractions are calculated in the centre of the grid block. The discretised equations in the drift-flux model consist of water mass conservation, liquid mass conservation, mixture mass conservation, mixture momentum conservation and mixture energy conservation. The final forms of those equations are:

$$\frac{\partial\left(\rho_w\alpha_w\right)}{\partial t}+\frac{1}{A}\frac{\partial A\left(\rho_w\alpha_w u_w\right)}{\partial x}=\psi_w,$$

$$\frac{\partial\left(\rho_o\alpha_o+\rho_w\alpha_w\right)}{\partial t}+\frac{1}{A}\frac{\partial A\left(\rho_o\alpha_o u_o+\rho_w\alpha_w u_w\right)}{\partial x}=-\Gamma_g+\psi_o+\psi_w,$$

$$\frac{\partial\left(\rho_g\alpha_g+\rho_o\alpha_o+\rho_w\alpha_w\right)}{\partial t}+\frac{1}{A}\frac{\partial A\left(\rho_g\alpha_g u_g+\rho_o\alpha_o u_o+\rho_w\alpha_w u_w\right)}{\partial x}=\psi_g+\psi_o+\psi_w,$$

$$\frac{\partial\left(\rho_m u_m\right)}{\partial t}+\frac{\partial\left(\rho_g\alpha_g u_g^2+\rho_o\alpha_o u_o^2+\rho_w\alpha_w u_w^2\right)}{\partial x}=-\left(144.0g_c\right)\frac{\partial P}{\partial x}-\rho_m g\sin\theta-\frac{\tau_m\pi D}{A},$$

$$\frac{\partial\left[\alpha_g\rho_g\left(\bar{h}_g+\frac{u_g^2}{2g_cJ_c}\right)\right]}{\partial t}+\frac{\partial\left[\alpha_o\rho_o\left(\bar{h}_o+\frac{u_o^2}{2g_cJ_c}\right)\right]}{\partial t}+\frac{\partial\left[\alpha_w\rho_w\left(\bar{h}_w+\frac{u_w^2}{2g_cJ_c}\right)\right]}{\partial t}+$$

$$\frac{1}{A}\frac{\partial\left[A\alpha_g\rho_g u_g\left(\bar{h}_g+\frac{u_g^2}{2g_cJ_c}\right)\right]}{\partial x}+\frac{1}{A}\frac{\partial\left[A\alpha_o\rho_o u_o\left(\bar{h}_o+\frac{u_o^2}{2g_cJ_c}\right)\right]}{\partial x}+\frac{1}{A}\frac{\partial\left[A\alpha_w\rho_w u_w\left(\bar{h}_w+\frac{u_w^2}{2g_cJ_c}\right)\right]}{\partial x}=$$

$$\dot{H}_w + \dot{H}_o + \dot{H}_g - \alpha_g \rho_g \frac{u_g}{g_c J_c} g\sin\theta - \alpha_o \rho_o \frac{u_o}{g_c J_c} g\sin\theta - \alpha_w \rho_w \frac{u_w}{g_c J_c} g\sin\theta - \frac{Q_{loss}}{A}.$$

Water Mass Conservation

$$V_b\left[\rho_{w,L}^{n+1}\alpha_{w,L}^{n+1} - \rho_{w,L}^{n}\alpha_{w,L}^{n}\right] +$$
$$\Delta t\left[\alpha_{w,j}^{n+1}\rho_{w,j}^{n+1}A_j^n u_{w,j}^{n+1} - \alpha_{w,j-1}^{n+1}\rho_{w,j-1}^{n+1}A_{j-1}^n u_{w,j-1}^{n+1}\right] = V_b \Delta t \dot{\psi}_{w,L}^{n+1}.$$

Liquid Mass Conservation

$$V_b\left[\left(\rho_{o,L}^{n+1}\alpha_{o,L}^{n+1} - \rho_{o,L}^{n}\alpha_{o,L}^{n}\right) + \left(\rho_{w,L}^{n+1}\alpha_{w,L}^{n+1} - \rho_{w,L}^{n}\alpha_{w,L}^{n}\right)\right] +$$
$$\Delta t\left[\alpha_{o,j}^{n+1}\rho_{o,j}^{n+1}A_j^n u_{o,j}^{n+1} - \alpha_{o,j-1}^{n+1}\rho_{o,j-1}^{n+1}A_{j-1}^n u_{o,j-1}^{n+1}\right] +$$
$$\Delta t\left[\alpha_{w,j}^{n+1}\rho_{w,j}^{n+1}A_j^n u_{w,j}^{n+1} - \alpha_{w,j-1}^{n+1}\rho_{w,j-1}^{n+1}A_{j-1}^n u_{w,j-1}^{n+1}\right] =$$
$$V_b \Delta t\left(-\Gamma_g^{n+1} + \dot{\psi}_{o,L}^{n+1} + \dot{\psi}_{w,L}^{n+1}\right).$$

Mixture Mass Conservation

$$V_b\left[\left(\rho_{g,L}^{n+1}\alpha_{g,L}^{n+1} - \rho_{g,L}^{n}\alpha_{g,L}^{n}\right) + \left(\rho_{o,L}^{n+1}\alpha_{o,L}^{n+1} - \rho_{o,L}^{n}\alpha_{o,L}^{n}\right) + \left(\rho_{w,L}^{n+1}\alpha_{w,L}^{n+1} - \rho_{w,L}^{n}\alpha_{w,L}^{n}\right)\right] +$$
$$\Delta t\left[\alpha_{g,j}^{n+1}\rho_{g,j}^{n+1}A_j^n u_{g,j}^{n+1} - \alpha_{g,j-1}^{n+1}\rho_{g,j-1}^{n+1}A_{j-1}^n u_{g,j-1}^{n+1}\right] +$$

Fully implicit approach

Fully implicit approach has been used to solve the drift-flux flow models.

We first solve the transport equation and then update the temperature, if thermal modelling was involved.

In the Newton method, we solved the mass balance and momentum balance equations by constructing a Jacobian matrix, J , and a residual vector, R , with primary variables: mixture average velocity, pressure, liquid volume fraction, and water volume fraction.

$$J = \begin{bmatrix}
\frac{\partial f_{1,1}}{\partial u_{m,1}} & \frac{\partial f_{1,1}}{\partial P_1} & \frac{\partial f_{1,1}}{\partial \alpha_{l,1}} & \frac{\partial f_{1,1}}{\partial \alpha_{w,1}} & \cdots & \frac{\partial f_{1,1}}{\partial u_{m,N}} & \frac{\partial f_{1,1}}{\partial P_N} & \frac{\partial f_{1,1}}{\partial \alpha_{l,N}} & \frac{\partial f_{1,1}}{\partial \alpha_{w,N}} \\
\frac{\partial f_{2,1}}{\partial u_{m,1}} & \frac{\partial f_{2,1}}{\partial P_1} & \frac{\partial f_{2,1}}{\partial \alpha_{l,1}} & \frac{\partial f_{2,1}}{\partial \alpha_{w,1}} & \cdots & \frac{\partial f_{2,1}}{\partial u_{m,N}} & \frac{\partial f_{2,1}}{\partial P_N} & \frac{\partial f_{2,1}}{\partial \alpha_{l,N}} & \frac{\partial f_{2,1}}{\partial \alpha_{w,N}} \\
\frac{\partial f_{3,1}}{\partial u_{m,1}} & \frac{\partial f_{3,1}}{\partial P_1} & \frac{\partial f_{3,1}}{\partial \alpha_{l,1}} & \frac{\partial f_{3,1}}{\partial \alpha_{w,1}} & \cdots & \frac{\partial f_{3,1}}{\partial u_{m,N}} & \frac{\partial f_{3,1}}{\partial P_N} & \frac{\partial f_{3,1}}{\partial \alpha_{l,N}} & \frac{\partial f_{3,1}}{\partial \alpha_{w,N}} \\
\frac{\partial f_{4,1}}{\partial u_{m,1}} & \frac{\partial f_{4,1}}{\partial P_1} & \frac{\partial f_{4,1}}{\partial \alpha_{l,1}} & \frac{\partial f_{4,1}}{\partial \alpha_{w,1}} & \cdots & \frac{\partial f_{4,1}}{\partial u_{m,N}} & \frac{\partial f_{4,1}}{\partial P_N} & \frac{\partial f_{4,1}}{\partial \alpha_{l,N}} & \frac{\partial f_{4,1}}{\partial \alpha_{w,N}} \\
\cdots & \cdots & \cdots & \cdots & \cdots & \cdots & \cdots & \cdots & \cdots \\
\frac{\partial f_{1,N}}{\partial u_{m,1}} & \frac{\partial f_{1,N}}{\partial P_1} & \frac{\partial f_{1,N}}{\partial \alpha_{l,1}} & \frac{\partial f_{1,N}}{\partial \alpha_{w,1}} & \cdots & \frac{\partial f_{1,N}}{\partial u_{m,N}} & \frac{\partial f_{1,N}}{\partial P_N} & \frac{\partial f_{1,N}}{\partial \alpha_{l,N}} & \frac{\partial f_{1,1}}{\partial \alpha_{w,N}} \\
\frac{\partial f_{2,N}}{\partial u_{m,1}} & \frac{\partial f_{2,N}}{\partial P_1} & \frac{\partial f_{2,N}}{\partial \alpha_{l,1}} & \frac{\partial f_{2,N}}{\partial \alpha_{w,1}} & \cdots & \frac{\partial f_{2,N}}{\partial u_{m,N}} & \frac{\partial f_{2,N}}{\partial P_N} & \frac{\partial f_{2,N}}{\partial \alpha_{l,N}} & \frac{\partial f_{2,1}}{\partial \alpha_{w,N}} \\
\frac{\partial f_{3,N}}{\partial u_{m,1}} & \frac{\partial f_{3,N}}{\partial P_1} & \frac{\partial f_{3,N}}{\partial \alpha_{l,1}} & \frac{\partial f_{3,N}}{\partial \alpha_{w,1}} & \cdots & \frac{\partial f_{3,N}}{\partial u_{m,N}} & \frac{\partial f_{3,N}}{\partial P_N} & \frac{\partial f_{3,N}}{\partial \alpha_{l,N}} & \frac{\partial f_{3,1}}{\partial \alpha_{w,N}} \\
\frac{\partial f_{4,N}}{\partial u_{m,1}} & \frac{\partial f_{4,N}}{\partial P_1} & \frac{\partial f_{4,N}}{\partial \alpha_{l,1}} & \frac{\partial f_{4,N}}{\partial \alpha_{w,1}} & \cdots & \frac{\partial f_{4,N}}{\partial u_{m,N}} & \frac{\partial f_{4,N}}{\partial P_N} & \frac{\partial f_{4,N}}{\partial \alpha_{l,N}} & \frac{\partial f_{4,1}}{\partial \alpha_{w,N}}
\end{bmatrix},$$

$$R = \begin{bmatrix} f_{1,1} \\ f_{2,1} \\ f_{3,1} \\ f_{4,1} \\ \dots \\ f_{1,N} \\ f_{2,N} \\ f_{3,N} \\ f_{4,N} \end{bmatrix}.$$

Input parameters for gas/oil/ water three-phase flow simulation

Well Data		**Reservoir and Fluid Data**	
Well MD	2000 ft	Net pay zone	150 ft
Well TVD	2000 ft	Reservoir pressure	2000 psi
Max grid size	50.0 ft	Reservoir temperature	180 °F
Ambient temperature at top	60 °F	Oil API	30
Ambient temperature at bottom	180 °F	Oil bubble point pressure	2000 psi
Total heat transfer coefficient	1.0 Btu/ft^2-hr-°F	Gas specific gravity	0.6
Tubing ID	0.229 ft	Water specific gravity	1.0
Oil productivity index	0.1 ft^3/psi-ft-day	Gas heat capacity	0.55 Btu/lbm-°F
Water productivity index	0.1 ft^3/psi-ft-day	Oil heat capacity	0.45 Btu/lbm-°F
Gas productivity index	1.0 ft^3/psi-ft-day	Water heat capacity	1.0 Btu/lbm-°F
Wellhead pressure	1000 psi		

Input parameters for gas/water two-phase flow simulation in PROSPER, OLGA & Petrel

Well Data		**Fluid Data**	
Well MD	5000 ft	Gas specific gravity	0.7
Well TVD	5000 ft	Water specific gravity	0.98
Max grid size	50 ft	Gas heat capacity	0.55 Btu/lbm-°F
Ambient temperature at top	71 °F	Water heat capacity	1.0 Btu/lbm-°F
Ambient temperature at bottom	141 °F		
Total heat transfer coefficient	0.5 Btu/ft^2-hr-°F		
Tubing ID	0.25 ft		
Water mass injection	1 lb/sec		
Gas mass injection	1 lb/sec		
Wellhead pressure	500 psi		

Input parameters for the gas-lift simulation in OLGA and PROSPER

Well Data		Reservoir and Fluid Data	
Well MD	7000 ft	Net pay zone	100 ft
Well TVD	7000 ft	Reservoir pressure	2350 psi
Tubing ID	0.229 ft	Reservoir temperature	155.9 F
Tubing OD	0.29166 ft	Oil API	35.072
Casing ID	1.56 ft	Oil bubble point pressure	14.696 psi
Casing OD	1.66 ft	Gas specific gravity	0.55
Wellbore hole size	1.7498 ft	Oil heat capacity	0.45 Btu/lbm-°F
Well productivity index	0.02 STB/ psi-ft-day	Gas heat capacity	0.40 Btu/lbm-°F
Wellhead pressure	150 psi	Oil thermal conductivity	0.45 Btu/hr-ft-°F
Gas injection depth	4100 ft	Gas thermal conductivity	0.55 Btu/hr-ft-°F

REFERENCES

Ahmadi, S., Amiribakhtiar, M. S., Gholami, A., & Bahrami, N. (2017). Upgrading fuzzy logic by GA-PS to determine asphaltene stability in crude oil. Egyptian journal of petroleum, 26(2), 505-510.

Ahmed, T. (2013). Equations of state and PVT analysis: Elsevier.

Akbarzadeh, K., Alboudwarej, H., Svrcek, W. Y., & Yarranton, H. W. (2005). A generalized regular solution model for asphaltene precipitation from n-alkane diluted heavy oils and bitumens. Fluid Phase Equilibria, 232(1-2), 159-170.

Al-Maamari, R. S., & Buckley, J. S. (2003). Asphaltene precipitation and alteration of wetting: the potential for wettability changes during oil production. SPE Reservoir Evaluation & Engineering, 6(04), 210-214.

Al-Sahhaf, T. A., Fahim, M. A., & Elkilani, A. S. (2002). Retardation of asphaltene precipitation by addition of toluene, resins, deasphalted oil and surfactants. Fluid phase equilibria, 194, 1045-1057.

Ali, M., Dahraj, N. U., & Haider, S. A. (2015). Study of Asphaltene Precipitation during CO2 Injection in Light Oil Reservoirs. Paper presented at the SPE/PAPG Pakistan section Annual Technical Conference.

Alian, S. S., Omar, A. A., Alta'ee, A. F., & Hani, I. (2011). Study of Asphaltene Precipitation induced formation Damage during CO 2 Injection for a Malaysian light oil. World Academy of Science, Engineering and Technology.

Alkafeef, S. F. (2001). An investigation of the stability of colloidal asphaltene in petroleum reservoirs. Paper presented at the SPE International Symposium on Oilfield Chemistry.

Alkafeef, S. F., Al-Medhadi, F., & Al-Shammari, A. D. (2003). A simplified method to predict and prevent asphaltene deposition in oilwell tubings: field case. Paper presented at the SPE Annual Technical Conference and Exhibition.

Almehaideb, R. A. (2004). Asphaltene precipitation and deposition in the near wellbore region: a modelling approach. Journal of Petroleum Science and Engineering, 42(2-4), 157-170.

Ameli, F., Hemmati-Sarapardeh, A., Dabir, B., & Mohammadi, A. H. (2016). Determination of asphaltene precipitation conditions during natural depletion of oil reservoirs: A robust compositional approach. Fluid Phase Equilibria, 412, 235-248.

Andersen, S. I., & Birdi, K. S. (1991). Aggregation of asphaltenes as determined by calorimetry. Journal of Colloid and Interface Science, 142(2), 497-502.

Andersen, S. I., & Speight, J. G. (1999). Thermodynamic models for asphaltene solubility and precipitation. Journal of Petroleum Science and Engineering, 22(1-3), 53-66.

Andersen, S. I., & Speight, J. G. (2001). Petroleum resins: separation, character, and role in petroleum. Petroleum science and technology, 19(1-2), 1-34.

Andreatta, G., Bostrom, N., & Mullins, O. C. (2005). High-Q ultrasonic determination of the critical nanoaggregate concentration of asphaltenes and the critical micelle concentration of standard surfactants. Langmuir, 21(7), 2728-2736.

Aquino-Olivos, M., Andersen, S. I., & Lira-Galeana, C. (2003). Comparisons between asphaltenes from the dead and live-oil samples of the same crude oils. Petroleum science and technology, 21(5-6), 1017-1041.

Arnold, G., Drew, D., & Lahey Jr, R. (1990). An assessment of multiphase flow models using the second law of thermodynamics. International journal of multiphase flow, 16(3), 481-494.

Arya, A., Liang, X., von Solms, N., & Kontogeorgis, G. M. (2017). Prediction of gas injection effect on asphaltene precipitation onset using the cubic and cubic-plus-association equations of state. Energy & Fuels, 31(3), 3313-3328.

Asoodeh, M., Gholami, A., & Bagheripour, P. (2014). Renovating scaling equation through hybrid genetic algorithm-pattern search tool for asphaltene precipitation modelling. Journal of dispersion science and technology, 35(4), 607-611.

Attar, M. S., Sedaghat, M. H., Kord, S., & Mayahi, H. (2015). Field Development Strategy through Full-Filed Reservoir Simulation Considering Asphaltene Precipitation and Deposition. Paper presented at the SPE reservoir characterisation and simulation conference and exhibition.

Australia, G. (2018).

Applying geoscience to Australia's most important challenges. Retrieved from http://www.ga.gov.au/scientific-topics/energy/resources/petroleum-resources/oil

Azinfar, B., Haddadnia, A., Zirrahi, M., Hassanzadeh, H., & Abedi, J. (2017). Effect of asphaltene on phase behavior and thermophysical properties of solvent/bitumen systems. Journal of Chemical & Engineering Data, 62(1), 547-557.

Barreira, F. R., Reis, L. G., Nunes, R. d. C. P., Filipakis, S. D., & Lucas, E. F. (2018). Asphaltenes Precipitation Onset: Influence of the Addition of a Second Crude Oil or Its Asphaltenes Fractions (C3I and C5I). Energy & Fuels, 32(10), 10391-10397.

Bayat, M., Sattarin, M., & Teymouri, M. (2008). Prediction of asphaltene self-precipitation in dead crude oil. Energy & Fuels, 22(1), 583-586.

Behbahani, T. J., Ghotbi, C., Taghikhani, V., & Shahrabadi, A. (2014). Investigation of asphaltene adsorption in sandstone core sample during CO2 injection: Experimental and modified modelling. Fuel, 133, 63-72.

Bělohlávek, R., Dauben, J. W., & Klir, G. J. (2017). Fuzzy logic and mathematics: a historical perspective: Oxford University Press.

Bissada, K., Szymczyk, E., & Nolte, D. (2003). Enhanced SARA and PIN group-type separations and quantification: Mass balance conservation in crude-oil and condensate characterization (abs.): Galveston Island, Texas, Gulf Coast Conference. Paper presented at the 100th Meeting.

Buch, L., Groenzin, H., Buenrostro-Gonzalez, E., Andersen, S. I., Lira-Galeana, C., & Mullins, O. C. (2003). Molecular size of asphaltene fractions obtained from residuum hydrotreatment☆. Fuel, 82(9), 1075-1084.

Buenrostro-Gonzalez, E., Lira-Galeana, C., Gil-Villegas, A., & Wu, J. (2004). Asphaltene precipitation in crude oils: Theory and experiments. AIChE journal, 50(10), 2552-2570.

Burke, N. E., Hobbs, R. E., & Kashou, S. F. (1990). Measurement and Modelling of Asphaltene Precipitation (includes associated paper 23831). Journal of Petroleum Technology, 42(11), 1,440-441,446.

Burnham, A. K. (2017). Structures of Coal, kerogen, and Asphaltenes. In Global Chemical Kinetics of Fossil Fuels (pp. 75-105): Springer.

Burya, Y. G., Yudin, I. K., Dechabo, V. A., Kosov, V. I., & Anisimov, M. A. (2001). Light-scattering study of petroleum asphaltene aggregation. Applied optics, 40(24), 4028-4035.

Butler, R. M., & Mokrys, I. J. (1991). A new process (VAPEX) for recovering heavy oils using hot water and hydrocarbon vapour. Journal of Canadian Petroleum Technology, 30(01).

Chacón-Patiño, M. L., Rowland, S. M., & Rodgers, R. P. (2017). Advances in asphaltene petroleomics. part 1: asphaltenes are composed of abundant island and archipelago structural motifs. Energy & fuels, 31(12), 13509-13518.

Chaisoontornyotin, W., Haji-Akbari, N., Fogler, H. S., & Hoepfner, M. P. (2016). Combined asphaltene aggregation and deposition investigation. Energy & Fuels, 30(3), 1979-1986.

Chapman, W. G., Gubbins, K. E., Jackson, G., & Radosz, M. (1989). SAFT: Equation-of-state solution model for associating fluids. Fluid Phase Equilibria, 52, 31-38.

Chen, L., Meyer, J., Campbell, T., Canas, J., Betancourt, S. S., Dumont, H., . . . Hall, D. L. (2018). Applicability of simple asphaltene thermodynamics for asphaltene gradients in oilfield reservoirs: The Flory-Huggins-Zuo Equation of State with the Yen-Mullins model. Fuel, 221, 216-232.

Chilingarian, G. V., & Yen, T. F. (1994). Asphaltenes and Asphalts, 1: Elsevier.

Chung, T.-H. (1992). Thermodynamic modelling for organic solid precipitation. Retrieved from

Cimino, R., Correra, S., Del Bianco, A., & Lockhart, T. P. (1995). Solubility and phase behavior of asphaltenes in hydrocarbon media. In asphaltenes (pp. 97-130): Springer.

Clark, J., Hastie, J., Kihlborg, L., Metselaar, R., & Thackeray, M. (1994). Definitions of terms relating to phase transitions of the solid state. Int. Pure Appl. Chem, 66, 577-594.

Cooper, C., Dubin, P., Kayitmazer, A., & Turksen, S. (2005). Polyelectrolyte–protein complexes. Current opinion in colloid & interface science, 10(1-2), 52-78.

Craddock, P. R., Bake, K. D., & Pomerantz, A. E. (2018). Chemical, molecular, and microstructural evolution of kerogen during thermal maturation: case study from the Woodford Shale of Oklahoma. Energy & Fuels, 32(4), 4859-4872.

Darabi, H., Shirdel, M., Kalaei, M. H., & Sepehrnoori, K. (2014). Aspects of modelling asphaltene deposition in a compositional coupled wellbore/reservoir simulator. Paper presented at the SPE Improved Oil Recovery Symposium.

David Ting, P., Hirasaki, G. J., & Chapman, W. G. (2003). Modelling of asphaltene phase behavior with the SAFT equation of state. Petroleum Science and Technology, 21(3-4), 647-661.

De Boer, R., Leerlooyer, K., Eigner, M., & Van Bergen, A. (1995). Screening of crude oils for asphalt precipitation: theory, practice, and the selection of inhibitors. SPE Production & Facilities, 10(01), 55-61.

Dehghani, S. M., Sefti, M. V., Ameri, A., & Kaveh, N. S. (2008). Minimum miscibility pressure prediction based on a hybrid neural genetic algorithm. chemical engineering research and design, 86(2), 173-185.

Diallo, M. S., Strachan, A., Faulon, J.-L., & Goddard III, W. A. (2004). Thermodynamic properties of asphaltenes through computer assisted structure elucidation and atomistic simulations. 1. Bulk Arabian Light asphaltenes. Petroleum science and technology, 22(7-8), 877-899.

Doryani, H., Malayeri, M., & Riazi, M. (2016). Visualization of asphaltene precipitation and deposition in a uniformly patterned glass micromodel. Fuel, 182, 613-622.

Dumont, H., Zuo, J. Y., Mullins, O. C., Garcia, G., Mishra, V. K., Harrison, C., . . . Montesinos, J. (2016). Asphaltene and Saturation Pressure Detection with DFA While Pulling out of Hole on Wireline. Paper presented at the SPWLA 57th Annual Logging Symposium.

Ebrahimi, M., Mousavi-Dehghani, S., Dabir, B., & Shahrabadi, A. (2016). The effect of aromatic solvents on the onset and amount of asphaltene precipitation at reservoir conditions: Experimental and modelling studies. Journal of Molecular Liquids, 223, 119-127.

Eilers, H. (1949). The Colloidal Structure of Asphalt. The Journal of Physical Chemistry, 53(8), 1195-1211.

Elliott, J. R., & Lira, C. T. (1999). Introductory chemical engineering thermodynamics (Vol. 184): Prentice Hall PTR Upper Saddle River, NJ.

Escobedo, J., & Mansoori, G. (1994). Theory of viscosity as a criterion for detection of onset of asphaltene flocculation. Retrieved from

Eskin, D., Ratulowski, J., Akbarzadeh, K., & Andersen, S. (2012). Modelling of asphaltene deposition in a production tubing. AIChE Journal, 58(9), 2936-2948.

Evdokimov, I. N., Eliseev, N. Y., & Akhmetov, B. R. (2003). Initial stages of asphaltene aggregation in dilute crude oil solutions: studies of viscosity and NMR relaxation☆. Fuel, 82(7), 817-823.

Fenistein, D., Barré, L., & Frot, D. (2000). From aggregation to flocculation of asphaltenes, a structural description by radiation scattering techniques. Oil and Gas Science and Technology-Revue de l'IFP-Institut Francais du Petrole, 55(1), 123.

Forte, E., & Taylor, S. E. (2015). Thermodynamic modelling of asphaltene precipitation and related phenomena. Advances in colloid and interface science, 217, 1-12.

Franco, C. A., Montoya, T., Nassar, N. N., Pereira-Almao, P., & Cortés, F. B. (2013). Adsorption and subsequent oxidation of colombian asphaltenes onto nickel and/or palladium oxide supported on fumed silica nanoparticles. Energy & Fuels, 27(12), 7336-7347.

Franco, C. A., Nassar, N. N., Ruiz, M. A., Pereira-Almao, P., & Cortés, F. B. (2013). Nanoparticles for inhibition of asphaltenes damage: adsorption study and displacement test on porous media. Energy & Fuels, 27(6), 2899-2907.

Gabrienko, A. A., Martyanov, O. N., & Kazarian, S. G. (2015). Effect of temperature and composition on the stability of crude oil blends studied with chemical imaging in situ. Energy & Fuels, 29(11), 7114-7123.

Gabrienko, A. A., Martyanov, O. N., & Kazarian, S. G. (2016). Behavior of asphaltenes in crude oil at high-pressure CO2 conditions: In situ attenuated total reflection–fourier transform infrared spectroscopic imaging study. Energy & Fuels, 30(6), 4750-4757.

Ge, Q., Yap, Y., Vargas, F., Zhang, M., & Chai, J. C. (2013). Numerical modelling of asphaltene deposition. Computational Thermal Sciences: An International Journal, 5(2).

Gonzalez, D. L., Vargas, F. M., Hirasaki, G. J., & Chapman, W. G. (2008). Modelling study of CO2-induced asphaltene precipitation. Energy & Fuels, 22(2), 757-762.

Guo, J., Liu, Q., Li, M., Wu, Z., & Christy, A. A. (2006). The effect of alkali on crude oil/water interfacial properties and the stability of crude oil emulsions. Colloids and Surfaces A: Physicochemical and Engineering Aspects, 273(1-3), 213-218.

Gupta, A. K., Bishnoi, P. R., & Kalogerakis, N. (1991). A method for the simultaneous phase equilibria and stability calculations for multiphase reacting and non-reacting systems. Fluid Phase Equilibria, 63(1-2), 65-89.

Hadi, N., Jachim, M., & Abbas, F. (2016). New Three-Phase Multicomponent Compositional Model for Asphaltene Precipitation during CO2 Injection Using CPA-EOS. Energy Fuels, 3306-3319.

Hammami, A., Phelps, C. H., Monger-McClure, T., & Little, T. (2000). Asphaltene precipitation from live oils: An experimental investigation of onset conditions and reversibility. Energy & Fuels, 14(1), 14-18.

Hasan, A., Kabir, C., & Sayarpour, M. (2010). Simplified two-phase flow modelling in wellbores. Journal of Petroleum Science and Engineering, 72(1-2), 42-49.

Hasanvand, M. Z., Ahmadi, M. A., & Behbahani, R. M. (2015). Solving asphaltene precipitation issue in vertical wells via redesigning of production facilities. Petroleum, 1(2), 139-145.

Hirschberg, A., deJong, L. N., Schipper, B., & Meijer, J. (1984). Influence of temperature and pressure on asphaltene flocculation. Society of Petroleum Engineers Journal, 24(03), 283-293.

Hotier, G., & Robin, M. (1983). Effects of different diluents on heavy oil products: measurement, interpretation, and a forecast of asphaltene flocculation. Revue de l'IFP, 38, 101.

Israelachvili, J. N. (1992). Adhesion forces between surfaces in liquids and condensable vapours. Surface Science Reports, 14(3), 109-159.

Jessen, K., Kovscek, A. R., & Orr Jr, F. M. (2005). Increasing CO2 storage in oil recovery. Energy Conversion and Management, 46(2), 293-311.

Juyal, P., Merino-Garcia, D., & Andersen, S. I. (2005). Effect on molecular interactions of chemical alteration of petroleum asphaltenes. I. Energy & fuels, 19(4), 1272-1281.

Kashefi, S., Lotfollahi, M. N., & Shahrabadi, A. (2017). An investigation of asphaltene deposition mechanisms during natural depletion process by a two phase modelling using genetic algorithm technique. Journal of Petroleum Science and Technology, 7(2), 12-20.

KL, H. (2010). Asphalt category analysis and hazard characterization. In. The American Petroleum Institute Petroleum HPV Testing Group, USA, pp 8, 9–12.

Klein, G. C., Kim, S., Rodgers, R. P., Marshall, A. G., Yen, A., & Asomaning, S. (2006). Mass spectral analysis of asphaltenes. I. Compositional differences between pressure-drop and solvent-drop asphaltenes determined by electrospray ionization Fourier transform ion cyclotron resonance mass spectrometry. Energy & Fuels, 20(5), 1965-1972.

Kontogeorgis, G. M., Michelsen, M. L., Folas, G. K., Derawi, S., von Solms, N., & Stenby, E. H. (2006). Ten years with the CPA (Cubic-Plus-Association) equation of state. Part 2. Cross-associating and multicomponent systems. Industrial & Engineering Chemistry Research, 45(14), 4869-4878.

Kontorovich, A., Bogorodskaya, L., Borisova, L., Burshtein, L., Ismagilov, Z., Efimova, O., . . . Sozinov, S. (2019). Geochemistry and catagenetic transformation of kerogen from the bazhenov horizon. Геохимия, 64(6), 585-593.

Koots, J. A., & Speight, J. G. (1975). Relation of petroleum resins to asphaltenes. Fuel, 54(3), 179-184.

Kor, P., & Kharrat, R. (2016). Modelling of asphaltene particle deposition from turbulent oil flow in tubing: Model validation and a parametric study. Petroleum, 2(4), 393-398.

Leontaritis, K., Amaefule, J., & Charles, R. (1994). A systematic approach for the prevention and treatment of formation damage caused by asphaltene deposition. SPE Production & Facilities, 9(03), 157-164.

Leontaritis, K. J., & Mansoori, G. A. (1987). Asphaltene flocculation during oil production and processing: A thermodynamic collodial model. Paper presented at the SPE International Symposium on Oilfield Chemistry.

Leontaritis, K. J., & Mansoori, G. A. (1992). A colloidal model for asphaltene flocculation from petroleum fluids. Iran. J. Sci. Technol, 16(2), 249-267.

Li, Z., & Firoozabadi, A. (2010). Cubic-plus-association equation of state for asphaltene precipitation in live oils. Energy & fuels, 24(5), 2956-2963.

Lipton, Z. C., Berkowitz, J., & Elkan, C. (2015). A critical review of recurrent neural networks for sequence learning. arXiv preprint arXiv:1506.00019.

Long, L. Z., Guo, H. Y., Chao, h. Y., & Guo , h. q. (2016). Study on Colloidal Model of Petroleum Residues through the Attraction Potential between Colloids. International Journal of Analytical Chemistry, 7.

Mamun, C. K. (2005). Free energy of mixing of cross-linked polymer blends. Langmuir, 21(1), 240-250.

Manshad, A. K., & Edalat, M. (2008). Application of continuous polydisperse molecular thermodynamics for modelling asphaltene precipitation in crude oil systems. Energy & fuels, 22(4), 2678-2686.

Manshad, A. K., Rostami, H., Rezaei, H., & Hosseini, S. M. (2015). Application of artificial neural network-particle swarm optimization algorithm for prediction of asphaltene precipitation during gas injection process and comparison with Gaussian process algorithm. Journal of Energy Resources Technology, 137(6).

Masson, J. (2008). Brief review of the chemistry of polyphosphoric acid (PPA) and bitumen. Energy & Fuels, 22(4), 2637-2640.

Merino-Garcia, D., & Andersen, S. I. (2003). Isothermal titration calorimetry and fluorescence spectroscopy study of asphaltene self-association in toluene and interaction with a model resin. Petroleum science and technology, 21(3-4), 507-525.

Merino-Garcia, D., & Andersen, S. I. (2004). Thermodynamic characterization of asphaltene− resin interaction by microcalorimetry. Langmuir, 20(11), 4559-4565.

Mitchell, D., & Speight, J. (1973). Preparation of mineral free asphaltenes. In: Google Patents.

Mofidi, A. M., & Edalat, M. (2006). A simplified thermodynamic modelling procedure for predicting asphaltene precipitation. Fuel, 85(17-18), 2616-2621.

Mohammadi, A. H., & Richon, D. (2007). A monodisperse thermodynamic model for estimating asphaltene precipitation. AIChE journal, 53(11), 2940-2947.

Mohammadi, M., Safari, M., Ghasemi, M., Daryasafar, A., & Sedighi, M. (2019). Asphaltene adsorption using green nanocomposites: Experimental study and adaptive neuro-fuzzy interference system modelling. Journal of Petroleum Science and Engineering, 177, 1103-1113.

Montel, F. (1994). Petroleum thermodynamics. Document Elf Aquitaine.

Moore, W. J. (1983). Basic physical chemistry: Prentice Hall.

Moradi, S., Dabiri, M., Dabir, B., Rashtchian, D., & Emadi, M. (2012). Investigation of asphaltene precipitation in miscible gas injection processes: experimental study and modelling. Brazilian Journal of Chemical Engineering, 29(3), 665-676.

Moradi, S., Rashtchian, D., Ganjeh Ghazvini, M., Emadi, M. A., & Dabir, B. (2012). Experimental investigation and modelling of asphaltene precipitation due to gas injection. Iranian Journal of Chemistry and Chemical Engineering (IJCCE), 31(1), 89-98.

Moschopedis, S. E., & Speight, J. G. (1976). Investigation of hydrogen bonding by oxygen functions in Athabasca bitumen. Fuel, 55(3), 187-192.

Murgich, J. (2002). Intermolecular forces in aggregates of asphaltenes and resins. Petroleum science and technology, 20(9-10), 983-997.

Murgich, J. (2005). Molecular mechanics study of the selectivity in the interaction between some typical resins and asphaltenes. Paper presented at the 6th International Conference on Petroleum Phase Behavior and Fouling.

Murgich, J., Abanero, J. A., & Strausz, O. P. (1999). Molecular recognition in aggregates formed by asphaltene and resin molecules from the Athabasca oil sand. Energy & Fuels, 13(2), 278-286.

Nasrabadi, H., Moortgat, J., & Firoozabadi, A. (2016). New three-phase multicomponent compositional model for asphaltene precipitation during CO2 injection using CPA-EOS. Energy & Fuels, 30(4), 3306-3319.

Nghiem, L., Hassam, M., Nutakki, R., & George, A. (1993). Efficient modelling of asphaltene precipitation. Paper presented at the SPE Annual Technical Conference and Exhibition.

Nikookar, M., Pazuki, G., & Masoudi, R. (2005). A new approach in modelling asphaltene precipitation in heavy oil. SPE97939-MS-P.

Nikookar, M., Pazuki, G., Omidkhah, M., & Sahranavard, L. (2008). Modification of a thermodynamic model and an equation of state for accurate calculation of asphaltene precipitation phase behavior. Fuel, 87(1), 85-91.

No, H. C., & Kazimi, M. S. (1981). The effect of virtual mass on the characteristics and the numerical stability in two-phase flow.

Östlund, J.-A., Löfroth, J.-E., Holmberg, K., & Nyden, M. (2002). Flocculation behavior of asphaltenes in solvent/nonsolvent systems. Journal of colloid and interface science, 253(1), 150-158.

Padding, J., & Louis, A. (2004). Hydrodynamic and Brownian fluctuations in sedimenting suspensions. Physical review letters, 93(22), 220601.

Panuganti, S. R., Vargas, F. M., & Chapman, W. G. (2013). Property scaling relations for nonpolar hydrocarbons. Industrial & Engineering Chemistry Research, 52(23), 8009-8020.

Paricaud, P., Galindo, A., & Jackson, G. (2002). Recent advances in the use of the SAFT approach in describing electrolytes, interfaces, liquid crystals and polymers. Fluid Phase Equilibria, 194, 87-96.

Parkhurst, D. L., & Wissmeier, L. (2015). PhreeqcRM: A reaction module for transport simulators based on the geochemical model PHREEQC. Advances in Water Resources, 83, 176-189.

Patin, S. (2001). Environmental impact of the offshore oil and gas industry. Journal of Environmental Assessment Policy and Management, 3(1).

Pauchon, C., & Banerjee, S. (1986). Interphase momentum interaction effects in the averaged multifield model: Part I: Void propagation in bubbly flows. International journal of multiphase flow, 12(4), 559-573.

Paul Maruska, H., & Rao, B. M. (1987). The role of polar species in the aggregation of asphaltenes. Fuel science & technology international, 5(2), 119-168.

Pedersen, C., & Andersen, S. I. (2000). Dielectric Studies of Asphaltenes in Toluene Solutions. Paper presented at the 2nd International Conference on Petroleum and Gas Phase Behaviour.

Petrusak, R. L., Riestenberg, D. E., Goad, P. L., Schepers, K. C., Pashin, J., Esposito, R. A., & Trautz, R. C. (2009). World class CO2 sequestration potential in saline formations, oil and gas fields, coal, and shale: the US southeast regional carbon sequestration partnership has it all. Paper presented at the SPE International Conference on CO2 Capture, Storage, and Utilization.

Pfeiffer, J. P., & Saal, R. (1940). Asphaltic bitumen as colloid system. The Journal of Physical Chemistry, 44(2), 139-149.

Porte, G., Zhou, H., & Lazzeri, V. (2003). Reversible description of asphaltene colloidal association and precipitation. Langmuir, 19(1), 40-47.

Prausnitz, J., Lichtenthaler, R., & de Azevedo, E. (1999). Intermolecular Forces, Corresponding States and Osmotic Systems. Molecular Thermodynamics of Fluid-Phase Equilibria, 57.

R, A. (2010). Thesis in chemistry. (Msc). collage science-Anbar,

Radhi, H. (2009). Evaluating the potential impact of global warming on the UAE residential buildings–A contribution to reduce the CO2 emissions. Building and Environment, 44(12), 2451-2462.

Rassamdana, H., Dabir, B., Nematy, M., Farhani, M., & Sahimi, M. (1996). Asphalt flocculation and deposition: I. The onset of precipitation. AIChE journal, 42(1), 10-22.

Ravagnani, A. G., Ligero, E., & Suslick, S. (2009). CO2 sequestration through enhanced oil recovery in a mature oil field. Journal of Petroleum Science and Engineering, 65(3-4), 129-138.

Ravey, J., & Stébé, M. (1989). Small angle neutron scattering studies of aqueous gels with fluorinated nonionic surfactants. Physica B: Condensed Matter, 156, 394-397.

Robson, W. J., Sutton, P. A., McCormack, P., Chilcott, N. P., & Rowland, S. J. (2017). Class type separation of the polar and apolar components of petroleum. Analytical chemistry, 89(5), 2919-2927.

Rogacheva, O., Rimaev, R., Gubaidullin, V., & Khakimov, D. (1980). Investigation of the Surface-Activity of the Asphaltenes of Petroleum Residues. In (Vol. 42, pp. 490-493): PLENUM PUBL CORP CONSULTANTS BUREAU, 233 SPRING ST, NEW YORK, NY 10013.

Rogel, E., & Carbognani, L. (2003). Density estimation of asphaltenes using molecular dynamics simulations. Energy & fuels, 17(2), 378-386.

Rogel, E., Leon, O., Torres, G., & Espidel, J. (2000). Aggregation of asphaltenes in organic solvents using surface tension measurements. Fuel, 79(11), 1389-1394.

Roux, J.-N., Broseta, D., & Demé, B. (2001). SANS study of asphaltene aggregation: concentration and solvent quality effects. Langmuir, 17(16), 5085-5092.

Sabet, N., Mohammadi, M., Zirahi, A., Zirrahi, M., Hassanzadeh, H., & Abedi, J. (2019). Effect of Asphaltene Precipitation and Deposition on Miscible Viscous Fingering in Porous Media—High-Resolution Nonlinear Numerical Simulations. Paper presented at the SPE Annual Technical Conference and Exhibition.

Sarma, H. K. (2003). Can we ignore asphaltene in a gas injection project for light-oils? Paper presented at the SPE international improved oil recovery conference in Asia Pacific.

Shaw, D. (1992). Charged interfaces. Introduction to Colloid and Surface Chemistry, 4th ed.; Shaw, DJ, Ed, 174-209.

Shaw, D. J. (1980). Introduction to colloid and surface chemistry: Butterworths.

Shedid, S. A., & Zekri, A. Y. (2006). Formation damage caused by simultaneous sulfur and asphaltene deposition. SPE Production & Operations, 21(01), 58-64.

Shen, Z., & Sheng, J. (2017). Experimental study of permeability reduction and pore size distribution change due to asphaltene deposition during CO2 huff and puff injection in Eagle Ford shale. Asia-Pacific Journal of Chemical Engineering, 12(3), 381-390.

Siffert, B., Eleli-Letsango, J., Jada, A., & Papirer, E. (1994). Experimental determination of the electron donor and acceptor numbers of oxides by zetametry in organic media. Colloids and Surfaces A: Physicochemical and Engineering Aspects, 92(1-2), 107-111.

Sirota, E. B. (2005). Physical structure of asphaltenes. Energy & Fuels, 19(4), 1290-1296.

Soltani Soulgani, B., Rashtchian, D., Tohidi, B., & Jamialahmadi, M. (2010). A novel method for mitigation of asphaltene deposition in the wellstring. Iranian Journal of Chemistry and Chemical Engineering (IJCCE), 29(2), 131-142.

Song, J. H., & Ishii, M. (2000). The well-posedness of incompressible one-dimensional two-fluid model. International Journal of Heat and Mass Transfer, 43(12), 2221-2231.

Soulgani, B. S., Jamialahmadi, M., Rashtchian, D., & Tohidi, B. (2009). A new thermodynamic scale equation for modelling of asphaltene precipitation form live oil. Paper presented at the Canadian International Petroleum Conference.

Speight, J., & Plancher, H. (1991). Molecular models for petroleum asphaltenes and implications for asphalt science and technology. Paper presented at the Proceedings of the International Symposium on the Chemistry of Bitumens.

Speight, J. G. (1994). Chemical and physical studies of petroleum asphaltenes. In Developments in petroleum science (Vol. 40, pp. 7-65): Elsevier.

Speight, J. G. (1999). The chemical and physical structure of petroleum: effects on recovery operations. Journal of Petroleum Science and Engineering, 22(1-3), 3-15.

Speight, J. G., & Moschopedis, S. E. (1981). On the molecular nature of petroleum asphaltenes. In: ACS Publications.

sreedhar, s., & Sebastien, S. (2016). Asphaltene Precipitation Models: A Review. Journal of dispersion science and technology, 1027-1049.

Srivastava, R., & Huang, S. (1997). Laboratory investigation of Weyburn CO2 miscible flooding. Paper presented at the Technical Meeting/Petroleum Conference of The South Saskatchewan Section.

Srivastava, R. K., & Huang, S. S. (1997). Asphaltene deposition during CO2 flooding: a laboratory assessment. Paper presented at the SPE Production Operations Symposium.

Stachowiak, C., Viguié, J.-R., Grolier, J.-P. E., & Rogalski, M. (2005). Effect of n-alkanes on asphaltene structuring in petroleum oils. Langmuir, 21(11), 4824-4829.

Stanely, N. M. (2016). USA Patent No. US9404344 B2.

Ström, H., Sasic, S., Jareteg, K., & Demazière, C. (2015). Behaviour and stability of the two-fluid model for fine-scale simulations of bubbly flow in nuclear reactors. International Journal of Chemical Reactor Engineering, 13(4), 449-459.

Subramanian, S., Simon, S., & Sjöblom, J. (2016). Asphaltene precipitation models: a review. Journal of Dispersion Science and Technology, 37(7), 1027-1049.

Szewczyk, V., & Behar, E. (1999). Compositional model for predicting asphaltenes flocculation. Fluid Phase Equilibria, 158, 459-469.

Taber, J. J., Martin, F., & Seright, R. (1997). EOR screening criteria revisited-Part 1: Introduction to screening criteria and enhanced recovery field projects. SPE reservoir engineering, 12(03), 189-198.

Tavakkoli, M., Panuganti, S. R., Taghikhani, V., Pishvaie, M. R., & Chapman, W. G. (2014). Precipitated asphaltene amount at high-pressure and high-temperature conditions. Energy & Fuels, 28(3), 1596-1610.

Ting, P.-L. D. (2003). Thermodynamic stability and phase behavior of asphaltenes in oil and of other highly asymmetric mixtures.

Tissot, B. P., & Welte, D. H. (1984). Composition of crude oils. In Petroleum Formation and Occurrence (pp. 375-414): Springer.

Vargas, F. M., Gonzalez, D. L., Hirasaki, G. J., & Chapman, W. G. (2009). Modelling asphaltene phase behavior in crude oil systems using the perturbed chain form of the statistical associating fluid theory (PC-SAFT) equation of state. Energy & Fuels, 23(3), 1140-1146.

Verdier, S., & Andersen, S. I. (2003). Determination of isobaric thermal expansivity of organic compounds from 0.1 to 30 MPa at 30 C with an isothermal pressure scanning microcalorimeter. Journal of Chemical & Engineering Data, 48(4), 892-897.

Victorov, A. I., & Firoozabadi, A. (1996). Thermodynamic micellizatin model of asphaltene precipitation from petroleum fluids. AIChE journal, 42(6), 1753-1764.

Villanueva, A., Ho, S., & Zanzotto, L. (2008). Asphalt modification with used lubricating oil. Canadian Journal of Civil Engineering, 35(2), 148-157.

Wang, S., & Civan, F. (2001). Productivity decline of vertical and horizontal wells by asphaltene deposition in petroleum reservoirs. Paper presented at the SPE International Symposium on Oilfield Chemistry.

Wiehe, I. A., Yarranton, H. W., Akbarzadeh, K., Rahimi, P. M., & Teclemariam, A. (2005). The paradox of asphaltene precipitation with normal paraffins. Energy & Fuels, 19(4), 1261-1267.

Wu, J., Prausnitz, J. M., & Firoozabadi, A. (1998). Molecular-thermodynamic framework for asphaltene-oil equilibria. AIChE journal, 44(5), 1188-1199.

Xu, J., Wang, Z., Wang, J., Tan, C., Zhang, L., & Liu, X. (2016). Acoustic-based cutting pattern recognition for shearer through fuzzy C-means and a hybrid optimization algorithm. Applied Sciences, 6(10), 294.

Yarranton, H. W. (2005). Asphaltene self-association. Journal of dispersion science and technology, 26(1), 5-8.

Yousefi, A. A. (2008). The thermal Rheological Behavior Progcolor. 45-55. Retrieved from http://www.ga.gov.au/scientific-topics/energy/resources/petroleum-resources/oil

Zendehboudi, S., Shafiei, A., Bahadori, A., James, L. A., Elkamel, A., & Lohi, A. (2014). Asphaltene precipitation and deposition in oil reservoirs–Technical aspects, experimental and hybrid neural network predictive tools. Chemical Engineering Research and Design, 92(5), 857-875.

Zhang, L.-l., Yang, G.-h., Yang, C.-h., & Que, G.-h. (2016). Study on colloidal model of petroleum residues through the attraction potential between colloids. International Journal of Analytical Chemistry, 2016.

Zhang, S., Zhang, L., Lu, X., Shi, C., Tang, T., Wang, X., . . . Zeng, H. (2018). Adsorption kinetics of asphaltenes at oil/water interface: Effects of concentration and temperature. Fuel, 212, 387-394.

Zirrahi, M., Azinfar, B., Hassanzadeh, H., Abedi, J., Azin, R., & Osfouri, S. (2019). Particles aggregation and fragmentation—A Monte Carlo study. Chemical Physics, 517, 6-12.